Universitat Autònoma de Barcelona

Revealing the role of early immune responses to control MERS-CoV infection in a camelid model

Nigeer Te

Revealing the role of early immune responses to control MERS-CoV infection in a camelid model

Nigeer Te

PhD Thesis

Bellaterra (Barcelona), 2020

Revealing the role of early immune responses to control MERS-CoV infection in a camelid model

Doctoral thesis presented by **Nigeer Te** to obtain the Doctoral degree under the program of Animal Medicine and Health at Faculty of Veterinary medicine from Universitat Autònoma de Barcelona, under the supervision of **Joaquim Segalés**, **Albert Bensaid** and **Júlia Vergara-Alert.**

Bellaterra, 2020

Joaquim Segalés, catedràtic del Departament de Sanitat i d'Anatomia Animals de la Facultat de Veterinària de la Universitat Autònoma de Barcelona i investigador adscrit a l'IRTA-CReSA, Albert Bensaid, investigador de l'IRTA-CReSA i Júlia Vergara-Alert, investigadora de l'IRTA-CReSA,

Certifiquem:

Que la memòria titulada "Revealing the role of early immune responses to control MERS-CoV infection in a camelid model", presentada per Nigeer Te per a l'obtenció del grau de Doctor en Medicina i Sanitat Animals, s'ha realitzat sota la nostra direcció i tutoria, i n'autoritzem la seva presentació a fi de ser avaluada per la comissió corresponent.

I perquè així consti i tingui els efectes que corresponguin, signen el present certificat a Bellaterra (Barcelona), 4 de novembre de 2020.

Dr. Joaquim Segalés	Dr. Albert Bensaid	Dr. Júlia Vergara-Alert	Nigeer Te
Director	Director	Director	Doctorand




This work has been financially supported as part of the Veterinary Biocontained facility Network (VetBioNet) [EU Grant Agreement INFRA-2016-1 N°731014] and the Zoonotic Anticipation and Preparedness Initiative (ZAPI project) [Innovative Medicines initiative (IMI) grant 115760], with contributions from EFPIA partners, both supported by the European commission.

Nigeer Te is a recipient of a Chinese Scholarship Council grant (CSC NO. 201608150108).

Time waits for no one.

Treasure every moment you have.

Acknowledgements

This thesis has definitively been one of the most fantastic parts of my story since I have learned and grown a lot, both personally and professionally. Yet, I would never be able to fulfill my PhD thesis without the huge support that I have received from so many people. I hereby like to express my deepest appreciation to all the people who completed this episode together with me.

I would like to thank my supervisors, Dr. Albert Bensaid, Dr. Joaquim Segalés and Dr Júlia Vergara-Alert for the continuous support and guidance of my PhD study and related research, for their patience, motivation, and immense knowledge. Albert, thanks for initiating me in the research world, for sharing your profound knowledge on immunology and everything you did for the thesis. I learned to be critical about my results, efficient in troubleshooting, and sharp in data interpretation. You have been my inspiration and motivation in the past four years, and every suggestion you gave me at every discussion helped not just the project but also my growing as a researcher. Certainly, the scientific way of thinking that you taught me will be of great value in my future research life. Wish you a happy and healthy life in the future. Quim, I recall the first time we talked through Skype four years ago, when I was strongly impressed by your knowledge and personality. I express my sincere gratitude for giving me the chance to study here in Barcelona and for your excellent supervision. It was a great pleasure to perform necropsies with you and I appreciate for introducing me in the complex and intriguing world of pathological research and sharing your immense knowledge on MERS and SARS-CoV-2 pathobiology. This thesis would not be prepared without your excellent supervision. Julia, I felt in love with CReSA the first day you showed me all the labs, our research team and the important guidance for the research project. You taught me a lot in all the time of research and writing of this thesis. I know it was not always easy to supervise me because I had to learn and adapt a lot. Nonetheless, under your guidance, I am on the track to become a qualified researcher. It has been a real pleasure making this journey with you. Please accept my deepest gratitude for what you did for me.

Jordi Rodon Aldrufeu, my dear friend and lab mate, I am so grateful to your tremendous support, accompany, and enormous enthusiasm throughout the years. Without your help of all the primer design and the experiments, I would never be able to fulfill my

thesis. Indeed, your attitude on research practice with great passions and energies positively inspired me, thanks again for your support. My sincere thanks also go to Mónica Pérez for technical assistance in the histopathological part, for your friendship and support. Mónica, my work in the lab would not have been possible and not have been half as fun without you. Marta Muñoz for teaching me the basic techniques in the lab. Thank you for helping me with my first steps in the lab. Rosa Valle, thanks so much for your contribution and assistance in my work. Special thanks are owed to Dr. Maria Ballester, who guided and taught us how to design the primers and using the Fluidigm technique. Lola Pailler, thanks for your amazing help with the statistics in the MERS paper. Montse Amenós and Joana, thank you guys for guidance on the use of LCM and Fluidigm BioMark microfluidic assay.

I extend my thanks to Jinya Zhang, Miaomiao Wang and Yanli Li. Without you guys, my life in Barcelona would not have been so colorful. I would also like to express my particular appreciation to my rest of Chinese friends, Lei Gan, Yan Wang, Zhongrui Luo, Chenyang Xie, Zhaobin Mu and Yan Huang for making my life enjoyable during the period of my research.

In particular, I am thankful to the China Scholarship Council, which has been providing me the scholarship for covering my living cost during my PhD studies.

My sincere thanks also go to all the office mates for discussions, suggestions, and also for providing a happy atmosphere in the office. Besides, I would like to thank the rest of the people from CReSA for helping me a lot during the past four years and for all the happy and funny times we had together. It is because of all these and other wonderful colleagues that I had a wonderful time in the CReSA. Wish all of you a happy life in the future.

I also express my gratitude to my landlady, Julia Chico-Marco. Julia, you are such a kind person who take cares me a lot since my second year of PhD period. I wish you all the best of happiness and health.

Last but not the least, I would like to thank my parents for inspiring, supporting and encouraging me spiritually throughout my life in general.

TABLE OF CONTENTS

List of abbreviations

aa	amino acid
ABSL3	level-3 biosafety facilities for animals
AD	adaptor
AL	apical lung
AP	alpaca
ARDS	acute respiratory distress syndrome
AZI2	5-azacytidine-induced protein 2
CARD	caspase recruitment domains
CASP	caspase
CCL	chemokine (C-C motif) ligand
CEEA-IRTA	ethical and animal welfare committee of IRTA
CK	chemokine
CL	caudal lung
CoV	Coronavirus
CPE	cytopathic effect
CXCL	C-X-C motif chemokine Ligand
DC	dendritic cells
DMVs	double-membrane vesicles
DNA	deoxyribonucleic acid
dpi	days post inoculation
DPP4	dipeptidyl peptidase-4
ds	double stranded
Epi	Nasal epithelia
ERGIC	endoplasmic reticulum–Golgi intermediate compartment
Fc	fold change
HCoV-EMC	Human coronavirus Erasmus Medical Center
hDPP4	human dipeptidyl peptidase-4
HE	hematoxylin and eosin stain
HR	heptads repeat
IFN	interferon
IFNAR	interferon α/β receptor
IFNLR1	interleukin 28 receptor, alpha subunit
IHC	immunohistochemistry
IL	interleukin
IRAK1	Interleukin-1 receptor-associated kinase1
IRF	interferon Regulatory Factor
ISG	interferon stimulated gene
ISRE	interferon Regulatory Factor
JAK	janus kinase 1
KSA	Kingdom of Saudi Arabia
LB	large bronchus

LCM	laser capture microdissection
LRT	lower respiratory tract
MAVS	mitochondrial antiviral-signaling protein
MDA5	melanoma differentiation-associated protein 5
MERS	Middle East respiratory syndrome
MFPE	methacarn-fixed paraffin-embedded tissue
ML	medial lung
MNNE	MERS-CoV IHC negative nasal epithelial
Mo-DCs	monocyte-derived dendritic cells
MPNE	MERS-CoV IHC positive nasal epithelial
MX1	interferon-induced GTP-binding protein Mx1
MyD88	myeloid differentiation primary response 88
NF-κB	nuclear factor NF-kappa-B
NFKB1	nuclear factor NF-kappa-B p105 subunit
NFKBIA	nuclear factor of kappa light polypeptide gene enhancer in B-cells inhibitor, alpha
NHP	non-human primates
NLRP3	NACHT, LRR and PYD domains-containing protein 3
NKs	natural killer cells
NQ	normalized quantity
NS	nasal swabs
NT	nasal turbinate
nsp	non-structural proteins
nt	nucleotide
OAS1	2'-5'-oligoadenylate synthetase 1
ORF	open reading frame
PACT	protein activator of the IFN-induced protein kinase
PCR	polymerase chain reaction
pDCs	plasmacytoid dendritic cells
PKR	protein kinase R
Plpro	papain like protease
pp1a	polyprotein1a
pp1ab	polyprotein1ab
PRR	pattern recognition receptors
PYCARD	apoptosis-associated speck-like protein containing a CARD
RBD	receptor binding domain
RBM	receptor-binding motif
RER	rough endoplasmic reticulum
RIG1	retinoic acid-inducible gene 1
RLR	RIG like receptor
RNA	ribonucleic acid
RT-qPCR	real-Time quantitative reverse transcription PCR
SARS	severe acute respiratory syndrome

SB	small bronchus
ss	single stranded
STAT	signal transducer and activator of transcription
Sub	submucosa
TAK1	mitogen-activated protein kinase 7
TC	trachea
TF	transcription factor
TIR	toll/interleukin-1 receptor
TLR	toll like receptor
TNF	tumor necrosis factor
TRADD	TNFRSF1A associated via death domain
TRIF	TIR-domain-containing adapter-inducing interferon-β
TRIM25	tripartite motif-containing protein 25
TYK2	tyrosine kinase 2
URT	upper respiratory tract
WHO	World Health Organization
3Clpro	3C-like protease

Abstract

Middle East respiratory syndrome coronavirus (MERS-CoV) is the etiological agent of a respiratory disease able to cause high mortality in humans. Severe cases associated to MERS-CoV infection are the consequence of the diffuse alveolar damage triggered by the pro-inflammatory cytokine storm and impaired interferon (IFN) responses. By contrast, camelids, the main virus reservoir, are asymptomatic MERS-CoV carriers, suggesting a crucial role for innate immune responses in controlling the infection. In study I of this dissertation, we aim to demonstrate this hypothesis by monitoring the transcription of immune response genes in the respiratory tract of MERS-CoV Qatar15/2015 (clade B strain) infected alpacas. Concomitant to the peak of infection, occurring at 2 days post inoculation (dpi), type I and III IFNs were maximally transcribed only in the nasal mucosa of alpacas, provoking the induction of interferon stimulated genes (ISGs) along the whole respiratory tract. Simultaneous to mild focal infiltration of leukocytes in nasal mucosa and submucosa, upregulation of the anti-inflammatory cytokine IL10 and dampened transcription of pro-inflammatory genes under NF-κB control were observed. In the lung, early (1 dpi) transcription of chemokines (CCL2 and CCL3) correlated with a transient accumulation of mainly mononuclear leukocytes. A tight regulation of IFNs in lungs with expression of ISGs and controlled inflammatory responses, might contribute to virus clearance without causing tissue damage. Thus, the nasal mucosa, the main target of MERS-CoV in camelids, is central in driving an efficient innate immune response based on triggering ISGs as well as the dual anti-inflammatory effects of type III IFNs and IL10.

While MERS-CoV strains from the Middle East region are subdivided into two clades (A and B), all the contemporary epidemic viruses belong to clade B. Thus, clade B MERS-CoV strains must display adaptive advantages over clade A in humans/reservoir hosts. Therefore, in study II of this dissertation, we compared an early epidemic clade A strain (EMC/2012) with a clade B strain (Jordan-1/2015) in an alpaca model monitoring virological and immunological parameters. Further, the Jordan-1/2015 strain has a partial amino acid (aa) deletion in the double stranded (ds) RNA binding motif of the open reading frame ORF 4a protein. Animals inoculated with the Jordan-1/2015 strain had higher MERS-CoV replicative capacities in the respiratory tract and larger nasal viral shedding, indicating a better fitness and transmission capability than

its clade A strain counterpart. In the nasal mucosa, the Jordan-1/2015 strain provoked an early IFN response on 1-day post inoculation (dpi), confirming the role of ORF4a as an IFN antagonist in vivo. However, both strains provoked at the peak of infection (on 2 dpi) maximal transcription of ISGs correlating with decreased tissular viral loads observed on 3 dpi. Genome alignment analysis revealed several clade B specific aa substitutions occurring in the replicase and the S protein which could explain a better adaptation of clade B strains in camelid hosts.

Overall, the results exposed in the present thesis highlight the complex interactions between MERS-CoV and host factors through which camelids control the infection in a short period of time. In addition, MERS-CoV strains are still evolving acquiring enhanced replicative fitness as shown in alpacas in the present study. This is reflected in the field by the dominance of MERS-CoV clade B strains over early epidemic clade A strains in humans and camelids.

Resumen

El coronavirus del síndrome respiratorio de Oriente Medio (del inglés, MERS-CoV) es el agente etiológico de una enfermedad respiratoria que causa una alta mortalidad en los seres humanos, con 2.562 casos confirmados laboratorialmente y 881 muertes notificadas a la OMS hasta noviembre de 2020. Se cree que éste patógeno zoonótico emergente ha evolucionado a partir de un coronavirus de murciélago, pero el dromedario es la única fuente confirmada de infección zoonótica. A pesar de la reducción global de casos de MERS desde 2015, el virus sigue siendo enzoótico en dromedarios en la Península Arábiga y África.

En los seres humanos, los casos graves asociados a la infección por MERS-CoV son la consecuencia de un daño alveolar difuso desencadenado por una tormenta de citocinas proinflamatorias y una alteración de las respuestas de interferón (IFN). Por el contrario, los camélidos, el principal reservorio del virus, son portadores asintomáticos del MERS-CoV, lo que sugiere un papel crucial de la respuesta inmunitaria innata en el control de la infección en estos animales. Para obtener información sobre la inmunopatogénesis del MERS-CoV en camélidos, se diseñaron dos estudios.

El objetivo del estudio I de esta tesis doctoral fue demostrar esta hipótesis mediante la evaluación de la transcripción de genes involucrados en la respuesta inmune en el tracto respiratorio de alpacas infectadas con MERS-CoV Qatar15/2015 (cepa perteneciente al clado B). Los IFN tipo I y III se transcribieron a su máximo nivel sólo en la mucosa nasal de las alpacas y en concomitancia con el pico de infección (momento de mayor carga vírica en el tracto respiratorio), que ocurrió 2 días después de la inoculación (dpi). Esta transcripción se asoció a la inducción de genes estimulados por interferón (ISG) a lo largo de todo el tracto respiratorio. Simultáneamente a la infiltración focal leve de leucocitos en la mucosa nasal y submucosa, también se observó una regulación positiva de la citocina antiinflamatoria IL10 y una transcripción amortiguada de genes proinflamatorios bajo control de NF-κB. En el pulmón, la transcripción temprana (1 dpi) de quimiocinas (CCL2 y CCL3) se correlacionó con una acumulación leve y transitoria de leucocitos principalmente mononucleares. Una regulación estricta de los IFNs en los pulmones con expresión de ISG y una respuesta inflamatoria controladas podría contribuir a la eliminación del virus sin causar daño tisular. Por tanto, la mucosa nasal, la principal diana del MERS-CoV en los camélidos, es fundamental para

impulsar una respuesta inmune innata eficaz basada en la activación de ISG, así como en los efectos antiinflamatorios duales de los IFNs de tipo III y la IL10.

Mientras que las cepas de MERS-CoV de la región de Oriente Medio se subdividen en dos clados (A y B), todos los virus epidémicos contemporáneos pertenecen al clado B. Por lo tanto, las cepas de MERS-CoV del clado B parecen mostrar ventajas adaptativas sobre el clado A en humanos / huéspedes reservorios. En el estudio II de esta tesis doctoral se comparó una cepa de clado A epidémico temprano (EMC / 2012) con una cepa de clado B (Jordan-1/2015) en un modelo de alpaca que evaluó parámetros virológicos e inmunológicos. Además, la cepa Jordan-1/2015 tiene una deleción parcial de aminoácidos (aa) en el motivo de unión del ARN bicatenario (ds) de la proteína del marco de lectura abierto 4a (ORF4a). Los animales inoculados con la cepa Jordan-1/2015 tuvieron una mayor replicación de MERS-CoV en el tracto respiratorio y una mayor diseminación viral nasal, lo que indica una aparente mejor aptitud y capacidad de transmisión que su contraparte de la cepa del clado A. En la mucosa nasal, la cepa Jordan-1/2015 provocó una respuesta de IFNs temprana a 1 dpi, lo que confirma el papel de ORF4a como antagonista de IFNs *in vivo*. Sin embargo, ambas cepas provocaron la máxima transcripción de ISGs en el pico de la infección (a 2 dpi), correlacionándose con una disminución de las cargas virales tisulares (evidente a 3 dpi). El análisis de alineación del genoma reveló varias sustituciones de aa específicas del clado B que se producen en el gen de la replicasa y la proteína S, lo que podría explicar una mejor adaptación de las cepas del clado B en los huéspedes camélidos.

En general, los resultados expuestos en la presente tesis doctoral destacan las complejas interacciones entre el MERS-CoV y los factores del huésped mediante los cuales los camélidos controlan la infección en un corto período de tiempo. Además, las cepas de MERS-CoV aún están evolucionando, adquiriendo una mayor capacidad replicativa como se muestra en las alpacas en esta tesis. Esto se refleja en el campo por un predominio de las cepas del clado B de MERS-CoV sobre las cepas del clado A de la epidemia temprana, tanto en humanos como en camélidos.

Resum

El coronavirus de la síndrome respiratòria de l'Orient Mitjà (en anglès, MERS-CoV) és l'agent etiològic d'una malaltia respiratòria que causa una elevada mortalitat a les persones, amb 2.562 casos confirmats laboratorialmente i 881 morts notificades a l'OMS fins Novembre de 2020. Es pensa que aquest patogen zoonòtic emergent ha evolucionat a partir d'un coronavirus de rat penat, però el dromedari és l'única font confirmada d'infecció zoonòtic. Malgrat la reducció global de casos de MERS des de 2015, el virus segueix essent enzoòtic en dromedaris de la Península Aràbiga i Àfrica.

A les persones, els casos greus associats a la infecció per MERS-CoV són la conseqüència d'un dany alveolar difús desencadenat per una tempesta de citocines pro-inflamatòries i una alteració de les respostes d'interferó (IFN). Pel contrari, els camèlids, el principal reservori del virus, són portadors asimptomàtics del MERS-CoV, fet que suggereix un paper fonamental de la resposta immunitària innata en el control de la infecció en aquests animals. De cara a obtenir informació sobre l'immunopatogènia del MERS-CoV en camèlids, es van dissenyar dos estudis.

L'objectiu de l'estudi I d'aquesta tesi doctoral fou demostrar aquesta hipòtesi mitjançant l'avaluació de la transcripció de gens involucrats en la resposta immunitària en el tracte respiratori d'alpaques infectades amb MERS-CoV Qatar15/2015 (soca pertanyent al clade B). Els IFN tipus I i III es van transcriure al seu màxim nivell només a la mucosa nasal de les alpaques i en concomitància amb el pic de la infecció (moment de màxima càrrega vírica al tracte respiratori), fet que es va donar 2 dies després de la infecció (dpi). Aquesta transcripció es va associar a la inducció de gens estimulats per interferó (ISG) al llarg de tot el tracte respiratori. Simultàniament a la infiltració focal lleu de leucòcits a la mucosa i submucosa nasal, també es va observar una regulació positiva de la citocina antiinflamatòria IL10 i una transcripció esmorteïda de gens proinflamatoris sota el control de NF-κB. En el pulmó, la transcripció primerenca (1 dpi) de quimiocines (CCL2 i CCL3) es va correlacionar amb una acumulació lleu i transitòria de leucòcits principalment mononuclears. Una regulació estricta dels IFNs en pulmons amb expressió de ISGs i una resposta inflamatòria controlades podrien contribuir a l'eliminació del virus sense causar dany tissular. Per tant, la mucosa nasal, la principal diana del MERS-CoV en camèlids, és fonamental per impulsar una resposta

immunitària innata eficient basada en l'activació d'ISGs, així com dels efectes antiinflamatoris duals dels IFNs de tipus III i l'IL10.

Mentre que les soques de MERS-CoV de la regió d'Orient Mitjà es subdivideixen en dues clades (A i B), tots els virus epidèmics contemporanis pertanyen al clade B. Per tant, les soques d'aquest clade B sembla que tenen avantatges adaptatives sobre el clade A en persones i hostes reservoris. A l'estudi II d'aquesta tesi doctoral es va comparar una soca de clade A de les epidèmies inicials (EMC / 2012) amb una soca de la clade B (Jordan-1/2015) en un model d'alpaca que avaluà paràmetres virològics i immunològics. A més, la soca Jordan-1/2015 té una deleció parcial d'aminoàcids (aa) en el *motif* d'unió de l'ARN bicatenari (ds) de la proteïna del marc de lectura oberta 4a (ORF4a). Els animals inoculats amb la soca Jordan-1/2015 van tenir una major replicació del MERS-CoV al tracte respiratori i una major disseminació viral nasal, fet que indicaria una millor aptitud i capacitat de transmissió que la seva contrapart de la soca del clade A. A la mucosa nasal, la soca Jordan-1/2015 va provocar una resposta primerenca d'IFNs a 1 dpi, cosa que confirmaria el paper de l'ORF4a com antagonista d'IFNs en condicions in vivo. No obstant, les dues soques van provocar la màxima transcripció d'ISGs durant el pic de la infecció (2 dpi), correlacionant-se amb una disminució de les càrregues víriques tissulars (evident a 3 dpi). L'anàlisi d'alineació del genoma va mostrar diverses substitucions d'aa específiques del clade B que es produeixen a la replicasa i la proteïna S, fet que podria explicar una millor adaptació de les soques del clade B en els camèlids.

En general, els resultats exposats en aquesta tesi doctoral destaquen les interaccions complexes entre el MERS-CoV i els factors de l'hoste mitjançant els quals els camèlids controlen la infecció en un curt període de temps. A més, les soques de MERS-CoV encara estan evolucionant, adquirint així una major capacitat replicativa com es mostra en les alpaques d'aquesta tesi. Aquest fet es reflexa a nivell de camp per un predomini de les soques del clade B de MERS-CoV sobre les soques del clade A dels moments inicials de l'epidèmia, tant en humans com en camèlids.

PART I

General introduction, hypothesis and objectives

Chapter 1

General introduction

1.1 History of MERS-CoV

A previously unknown human coronavirus emerged in the Kingdom of Saudi Arabia (KSA) in June 2012 (Zaki et al., 2012a). The novel virus was named Middle East respiratory syndrome coronavirus (MERS-CoV) due to its geographic origin. Dromedary camels (*Camelus dromedarius*) are the main source for zoonotic transmission to humans, and MERS-CoV retrospective studies have shown its circulation in camels for at least several decades (Azhar et al., 2014; Corman et al., 2014a; Reusken et al., 2013b; Stalin Raj et al., 2014). Proof for a bat reservoir of MERS-CoV has also been reported, indicating a possible bat origin of this virus (Corman et al., 2014b; Ithete et al., 2013; Memish et al., 2013; Wang et al., 2014). According to World Health Organization (WHO), 2,562 laboratory-confirmed cases and at least 881 fatalities have been reported to the as per November 2020 (WHO, 2020). The KSA is the most affected country with 2,121 laboratory-confirmed patients. Although most cases were diagnosed in the countries from Middle East, travel-associated cases have been documented in other regions (Bermingham et al., 2012; Cotten et al., 2013; Hsieh, 2015; Tsiodras et al., 2014). So far, all patients reported in North America, Europe and Asia had a previous history of travel to the Middle East region. However, in 2015 a major outbreak occurred in South Korea with 186 cases and 38 associated deaths, highlighting the cause for worldwide public health concern (Kim et al., 2017). Currently, MERS-CoV has continued to cause sporadic outbreaks mainly in the KSA, suggesting that continuous preparedness is needed for MERS prevention and control globally.

1.2. Etiology

1.2.1 Nomenclature and taxonomy

In its first description, this previously unknown virus was named human coronavirus Erasmus Medical Center (HCoV-EMC) since it was first identified in the mentioned hospital, in the Netherlands (Zaki et al., 2012a). Soon afterwards, virus isolates were given various names such as human beta-coronavirus 2c England-Qatar, human betacoronavirus 2c Jordan-N3, betacoronavirus England 1, and novel coronavirus (de Groot et al., 2013). Ten months after its discovery, the Coronavirus Study Group of the

International Committee on Taxonomy of Viruses proposed the name of Middle East respiratory syndrome coronavirus (MERS-CoV, as acronym) for the novel agent (de Groot et al., 2013).

MERS-CoV belongs to the order *Nidovirales*, family *Coronaviridae*, subfamily *Coronavirinae*, subgroup 2c of genus *Betacoronavirus*. Being the sixth coronavirus able to cause human infections, MERS-CoV is phylogenetically related to (90% nucleotide sequence homology) several bat coronaviruses including HKU4 and HKU5 (Bermingham et al., 2012) and more distant from the Severe acute respiratory syndrome-coronavirus (SARS-CoV) and the newly discovered SARS-CoV-2 (de Groot et al., 2013; Petrosillo et al., 2020; Wu et al., 2020). As characterized by evolutional differences as well as MERS-CoV sequences isolated from different geographical regions, phylogenetic studies subdivided the virus into three main clades, provisionally named clades A, B and C (Alharbi et al., 2015; Chu et al., 2018; Kiambi et al., 2018). Clade A contains extinct strains , such as the very first human isolate EMC/2012 (Lau et al., 2016); clade B, the only clade circulating in the Arabian Peninsula, encompasses hundreds of the human and dromedary isolates including the Qatar15/2015 and the Jordan-1/2015 strains that have been used in the present thesis (Lamers et al., 2016; Widagdo et al., 2019; Yusof et al., 2017); and clade C only covers dromedary strains isolated from North African continent (Chu et al., 2018).

1.2.2 Molecular organization

MERS-CoV is an enveloped, positive-sense, single-stranded RNA virus with a large RNA genome of 30,119 nucleotides (nts), which includes at least 10 predicted open reading frames (ORFs), as previously reported (van Boheemen et al., 2012; Cotten et al., 2013). The 5’ proximal three-fourths of the single-stranded MERS-CoV RNA comprises the large replicase open reading frames ORF1a and ORF1b, which code for two large polyproteins, polyprotein 1a (pp1a) and polyprotein 1ab (pp1ab). These polyproteins are cleaved by two viral proteases : the papain like protease, PLpro, and the 3C-like protease, 3CLpro (Bailey-Elkin et al., 2014; Fehr and Perlman, 2015; Mielech et al., 2014a), a process that is needed for the release and maturation of non-structural proteins (nsps) involving in the replication and transcription of the viral genome. Proteolytic processing of pp1a and pp1ab is essential for viral maturation

(Yang et al., 2014). The downstream region of ORF1b contains a variable number of smaller genes, such as structural and accessory proteins. The structural proteins include the spike (S), envelope (E), membrane (M), and nucleocapsid (N) proteins, and their organization within the virus and the viral genome is shown in Figure 1-1. Among all these proteins, the S protein is critical for receptor binding and virus-cell membrane fusion, thereby initiating the infection process. Upon MERS-CoV entry to the host cells, the S protein is cleaved into a receptor-binding subunit S1, and a membrane-fusion subunit S2 (Gao et al., 2013a; Li, 2015; Lu et al., 2013; Wang et al., 2013). The receptor binding domain (RBD) of the S1-protein mediates viral entrance through binding to dipeptidyl peptidase-4 (DPP4, also known as CD26), a serine protease that is identified as the functional receptor of MERS-CoV (Raj et al., 2013). The MERS-CoV RBD may bind DPP4 from various animal species, such as dromedary camels, bats, pigs, ferrets and llamas. The binding affinity depends on key residues of DPP4 that determine host species restriction and susceptibility to MERS-CoV (van Doremalen et al., 2014; Vergara-Alert et al., 2017a; Widagdo et al., 2016a, 2017). The RBD (aa residues 358–588) of the MERS-CoV S1 protein is composed of a core subdomain and a receptor-binding motif (RBM) (Mou et al., 2013). The core subdomain comprises a five-stranded antiparallel β sheet (b1, b3, b4, b5 and b10) in the center and several connecting helices (Lu et al., 2013). The RBM is composed of a four-stranded antiparallel β-sheet being linked to the core (Lu et al., 2013). Analogous to the S2 subunit of other coronaviruses, the MERS-CoV S2 mediates membrane fusion by undergoing structural reorganizations (Gao et al., 2013a; Lu et al., 2014). In this process, two heptads repeat regions termed HR1 and HR2 in S2 subunit form amphipathic helices of a coiled-coil structure. As a result, an hydrophobic fusion peptide is inserted into the cell membrane and the viral and cell membranes are brought into proximity for fusion (Du et al., 2017). Additionally, some MERS-CoV accessory proteins facilitate the virus to circumvent the immune responses. For instance, MERS-CoV ORF3, ORF4a, ORF4b, ORF5 and ORF8b coded proteins inhibit interferon (IFN) induction. (Lee et al., 2019; Menachery et al., 2017; Yang et al., 2013).

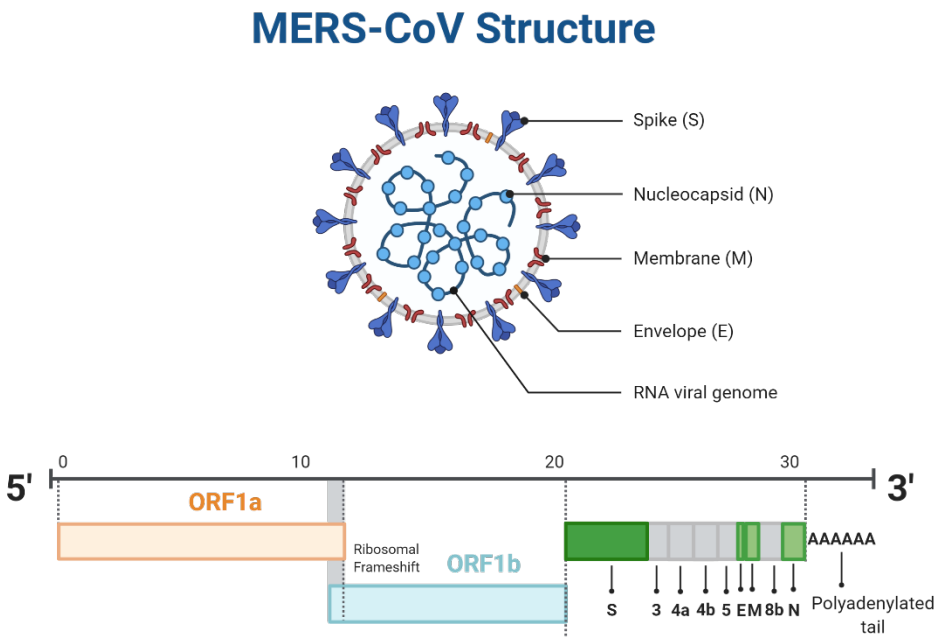

Figure 1-1. MERS-CoV structure and genomic organization. The Middle East respiratory syndrome coronavirus (MERS-CoV) is enveloped virus that contains a single-stranded, positive-sense RNA genome. The virion particle is approximately 120 to 160 nanometers in diameter and contains a genome of 30 kb in length. The genome is arranged in the order of 5' to 3' with the replicase, the spike (S), ORF3, 4a, 4b, 5, the envelope (E), the matrix (M), ORF8b and the nucleocapsid (N). A polyadenylated tail is positioned at the end of the genome.

1.2.3 Replication cycle

CoVs replication is dependent on the host RNA processing machinery. To complete the replication cycle, the virus needs to bind to the host cell and get imported into the cytoplasm. Then the genomic RNA is released for replication and synthesis of the different proteins before assembling and then egress of the newly formed viral particles (Perlman and Netland, 2009). As mentioned above, MERS-CoV enters the host cells by binding of the S1 domain of the S protein to the DPP4. Subsequently, the S2 domain fuses with the cellular membrane, following the release and uncoating of viral genomic RNA into the cytoplasm. The translation begins at ORF1a and then continues at ORF1b after a frameshift, by which MERS-CoV pp1a and pp1ab are synthesized. Subsequently, the proteases Mpro/3CLpro and PLpro cleave pp1a and pp1ab, resulting in 16 mature non-structural proteins (nsp1–nsp16). The nsps of CoVs are essential to build up the replication-transcription complex used for genomic replication and gene transcription (Snijder et al., 2006). The complexes assemble at the perinuclear cell regions and

rearrange the nsps, which are derived from the rough endoplasmic reticulum (RER), into double-membrane vesicles (DMVs). The N proteins encapsidate the newly synthesized genomic viral RNAs. The structural proteins S, M and E are then embedded into the RER membrane and are immediately carried to the endoplasmic reticulum–Golgi intermediate compartment (ERGIC), in which the assembled virion is formed. The assembly of CoV particles is completed through budding viral particles out as a smooth-wall vesicle to the plasma membrane to egress via exocytosis (Figure 1-2).

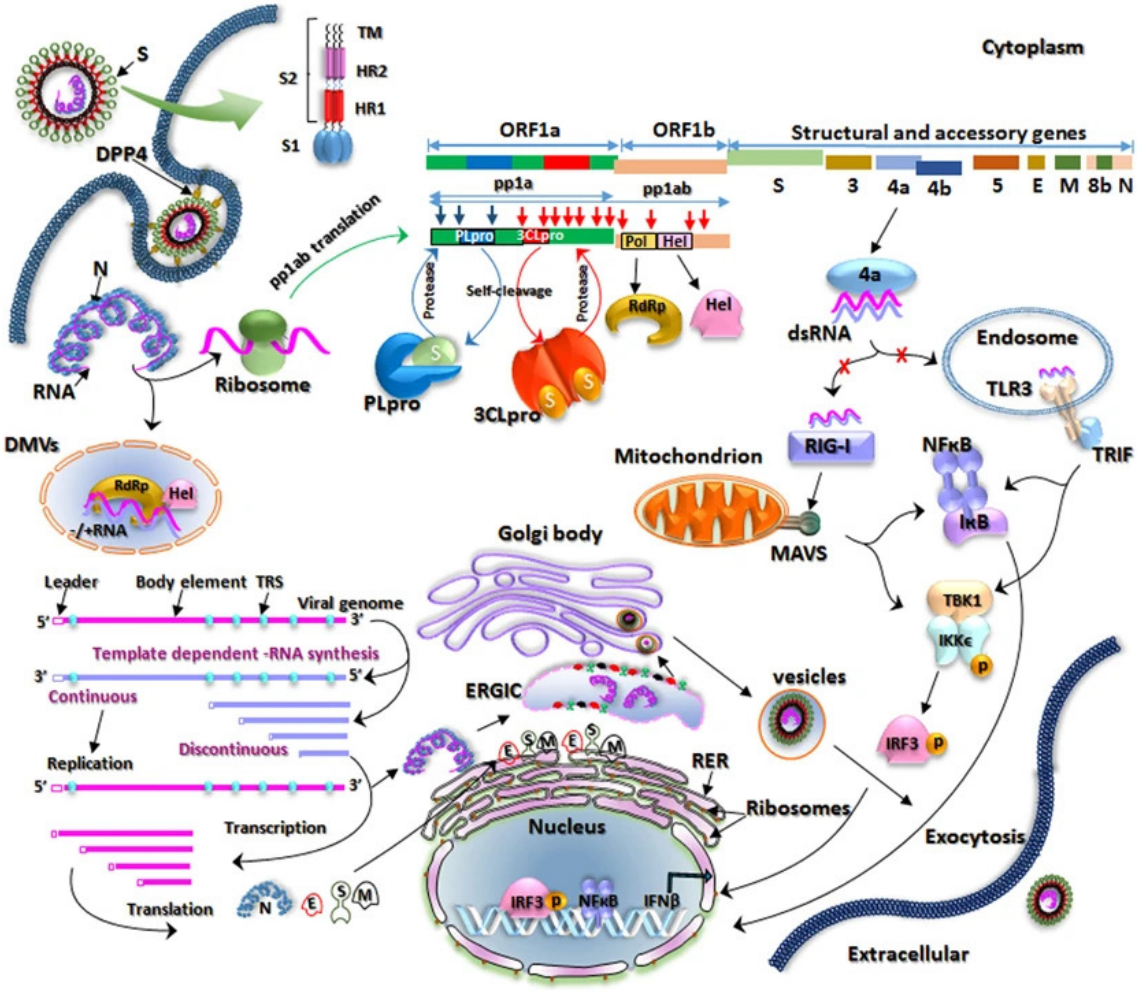

Figure 1-2. Schematic of the replication cycle of MERS-CoV. MERS-CoV binds to DPP4 on the host cell through its RBD in the S1 subunit of the S glycoprotein, resulting in virus-cell fusion followed by the release of genomic RNA into the cytoplasm. Subsequently, ORF1a and b are translated into pp1a and pp1ab, respectively, which are then cleaved by the PLpro and 3CLpro into 16 mature nsps. Viral replication and transcription occur in DMVs. The newly produced genomic RNAs are encapsidated by the N proteins in the cytoplasm and then transported to the ERGIC for further assembly. The structural proteins S, M and E are inserted into the membrane of the RER and then translocated to the ERGIC to interact with the RNA-encapsidated N proteins. The budded vesicles are then transported to the cell surface for release following maturation in the Golgi bodies. Double-stranded RNA is partially generated during viral replication. Adapted from Durai et al, 2015 (Durai et al., 2015).

1.3 Epidemiology and transmission

To date, 27 countries have reported MERS cases, with most of them described in the KSA. Moreover, all MERS cases reported in other continents can be linked to patients who had previously visited the Middle East region. Several MERS-CoV outbreaks have been related to healthcare settings, with the largest one detected in the KSA, especially in 2014 and 2015, when hospital-acquired cases occurred (Alenazi et al., 2017; Hastings et al., 2016). Additionally, secondary and tertiary cases were reported in community clusters and hospital outbreaks in the KSA and South Korea. Tertiary, quaternary, and quinary generations accounted for 24%, 13%, and 3% of all hospital-based transmissions in a large outbreak in the KSA (Alenazi et al., 2017). This was largely due to infection control deficiencies, including limited isolation of suspected MERS-CoV patients and patient crowdedness and inconsistent or inadequate use of protective precautions (Hastings et al., 2016), as shown in Figure 1-3. These large and complex outbreaks were halted by increased awareness and reporting, by robust contact tracing, active surveillance, quarantine and isolation.

Bats were initially suspected to be original hosts for MERS-CoV due to existing coronaviruses known to reside among them (Memish et al., 2013; Shi, 2013; Smith and Wang, 2013). Analysis of DPP4 sequences, distribution of the DPP4 receptor in various bat species, and *in vitro* infection studies with different bat cell lines as well as *in vivo* data revealed that bats are potentially susceptible to MERS-CoV (Caì et al., 2014; Cui et al., 2013; Munster et al., 2016; Widagdo et al., 2017). However, MERS-CoV direct transmission from bat to human is so far speculative, since this hypothesis has yet to be supported by any conclusive evidence. It is considered that bats are more likely to be the primary host of the ancestor of MERS-CoV (Corman et al., 2014b).

Dromedary camels are the major source for zoonotic MERS transmission to humans as serological surveys in these animals from the Arabian Peninsula and African countries (Tunisia, the KSA, Qatar, Egypt, Jordan, Oman, Nigeria, Kenya, and Ethiopia) showed a high prevalence of neutralizing antibodies against MERS-CoV (Chu et al., 2015; Corman et al., 2014a; Farag et al., 2015; Haagmans et al., 2014; Raj et al., 2014a; Reusken et al., 2013a, 2014, 2013b). In fact, this virus has been circulating widely in this species for a relative long period of time, as MERS-CoV neutralizing antibodies have been found in eastern Africa as early as 1983 (Müller et al., 2014). Further evidences came with the detection of identical sequences in viruses obtained from nasal

swabs (NS) of dromedary camels and infected patients (Azhar et al., 2014; Haagmans et al., 2014; Hemida et al., 2014). In addition, several MERS-CoV lineages, including those that have caused human infections, have been isolated from dromedaries in the KSA (Alharbi et al., 2015). The sequence of a virus isolate obtained from dromedary camels, on different occasions over a month, was not altered, indicating the high genomic stability and thus suggesting that this specie is probably the natural and not necessarily the intermediate host for MERS-CoV (Hemida et al., 2014).

However, the exact route by which MERS- CoV humans remains unclear. Studies have shown that the large proportional of primary cases lack contact with animals (Gossner et al., 2016). Indeed, there is a potential risk of transmission from milk and meat products derived from these animals. Frequent ingestion of raw, unsterilized camel milk is commonly seen among the desert Bedouin as well as in the KSA, and viral RNA was found in raw milk collected in a marketplace in Qatar (Mackay and Arden, 2015a; Reusken et al., 2014). Although viral RNA was detected in lymph nodes of experimentally infected animals and slaughtered camels, infected animals did not exhibit any evidence for the presence of the live virus in the meat (Adney et al., 2014; Bart L. Haagmans et al., 2016; Farag et al., 2015). Nevertheless, a potential respiratory secretion or fecal contamination of milk or meat during slaughter cannot be ruled out. Camel urine is also consumed in the Middle East for supposed health benefits (Gossner et al., 2016). Apart from consumption, close contact between human and dromedary camels occurs in a variety of ways. Several festivals, races, sales, and parades with the presence of dromedaries imply a close contact of the animals with humans. During the Hajj pilgrimage, dromedary camels represent an animal of ritual significance (Mackay and Arden, 2015a). Therefore, the aforementioned activities may result in close human-camel contacts that could represent potential risks to human exposure to MERS-CoV (Figure 1-3). Several screening studies have shown that juvenile camels (<2 years) with primary infections rather play a more important role in MERS-CoV epidemiology than aged animals, which tend to be seropositive but with no evidence of ongoing viral infection (Farag et al., 2015; Hemida et al., 2013, 2014).

MERS-CoV transmission between humans occurs mainly via close contact and is probably via large droplets. While transmission of MERS-CoV among family members accounts for 13–21% of MERS cases, 62–79% cases of infection have been reported in hospitals (Chowell et al., 2015), as indicated in Figure 1-3. The outcome of the very

first documented MERS-CoV human-to-human transmission was a person with severe pulmonary disease acquired in a healthcare setting in Jordan (Mackay and Arden, 2015b). It seems that transmission of MERS-CoV is mostly characterized as sporadic, inefficient, and requires close and prolonged contact, and most human cases of MERS-CoV do not efficiently transmit to more than another human so far (Drosten et al., 2014, 2015) (reproduction ration ≤1). Transmission of MERS-CoV among people can occur during both symptomatic and incubation phases (Al-Abdallat et al., 2014; Al-Tawfiq and Auwaerter, 2019; Alfaraj et al., 2018; Omrani et al., 2013). The virus can persist in the environment for up to 24 hours, which is also an unneglectable risk for human exposure (van Doremalen et al., 2013).

In terms of the transmission dynamics and time-dependent reproduction number, some patients affected by MERS were likely infected in the context of super spreading events in South Korea (Kim et al., 2016b). In order to control healthcare setting-associated transmission between humans, the WHO established effective prevention and control guidelines for dealing with human to human MERS-CoV spread. These include improved infection control awareness and implementation measures for patients with severe disease outcome, as well as reinforcing the education to healthcare workers (WHO, 2015). Since people with comorbidities, such as diabetes, renal failure or a compromised immune system, are at a higher risk of developing acute symptoms of MERS, they should keep distance with camels from the region in which the virus is known to be pandemic.

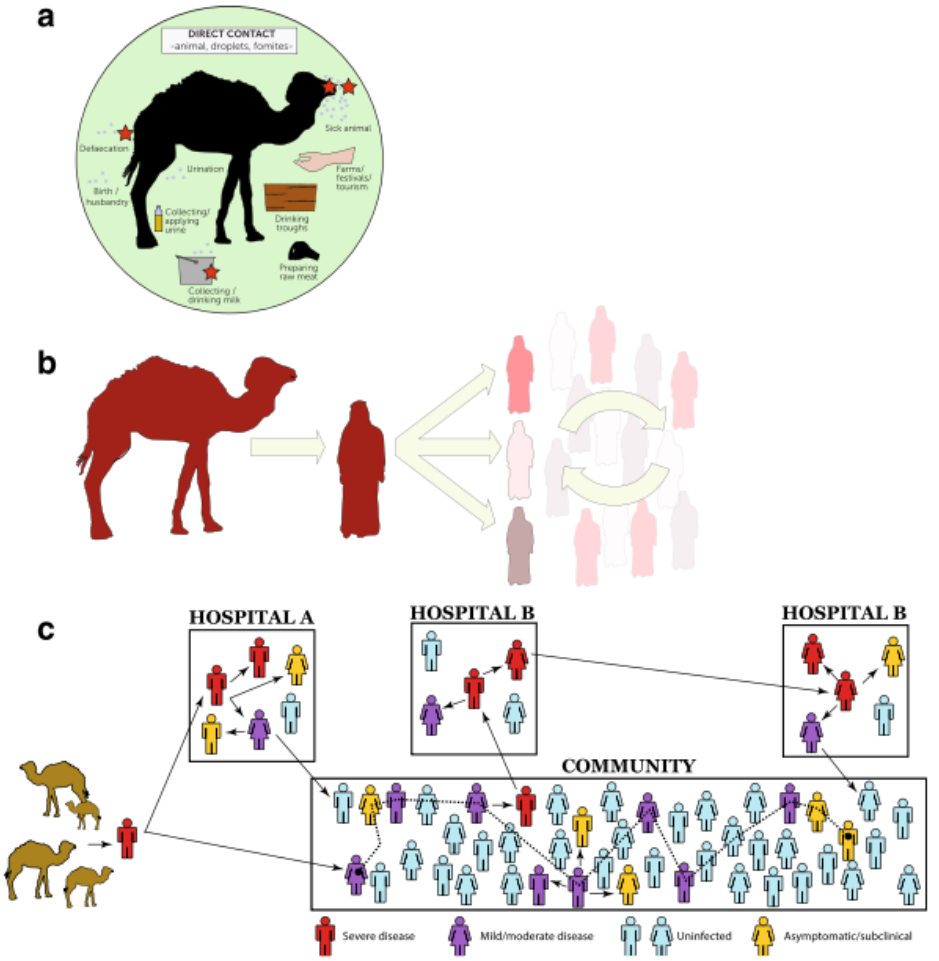

Figure 1-3. A speculative model of how MERS are transmitted between humans and dromedary camels. a. Potential risk factors of MERS-CoV spillover at the camel-human interface. The model depicts risks that may originate from an aerosol transmission mode (wet droplets) or a direct contact component (within the green circle). b. A speculative model of how humans acquire and spread MERS-CoV following close contact with camels. Although the direct transmission from dromedary camels to humans appears to be infrequent, person to person spread of MERS-CoV is regularly facilitated by the lack of effective control measures. c. A speculative model in which potential subclinical/asymptomatic (an infection has no symptoms or noticeable signs of illness) infection might be implicated during person to person transmission. Adapted from Mackay and Arden, 2015 (Mackay and Arden, 2015b).

1.4 Pathology

1.4.1 Pathology of MERS-CoV in humans

Knowledge on MERS-CoV induced pathological changes comes from few autopsy and biopsy cases, and from experimental studies with different animal models of disease.

Pathological features of MERS include exudative diffuse alveolar damage with hyaline membranes, pulmonary edema, congestion of alveolar walls, type two pneumocyte hyperplasia, multinucleate syncytial cells and interstitial pneumonia (mainly lymphocytic) or severe acute hemorrhagic pneumonia (Alsaad et al., 2018; Ng et al., 2016). Infiltration of few neutrophils, lymphocytes and plasma cells can be found in mucosa and submucosa of trachea and bronchus. Bronchial submucosal glands might be focally necrotic. The kidney may show thickened Bowman capsules, tubular epithelial cell degeneration, increased globally sclerotic glomeruli (five to ten percent of total glomeruli), nuclear hyperchromasia, loss of brush surface of the proximal tubular epithelial cells, atherosclerosis, hyaline arteriolosclerosis and focal interstitial inflammation. No interstitial fibrosis, tubular atrophy, endarteritis- like lesion or vasculitis have been reported (Alsaad et al., 2018; Ng et al., 2016). Evidence of diminished lymphoid follicles and a polymorphic population of reactive lymphocytes have been described in several lymph nodes (Ng et al., 2016). Liver may display mild chronic lymphocytic portal inflammatory cell infiltrates as well as perivenular necrosis and inflammation as well as loss of hepatocytes (Alsaad et al., 2018; Ng et al., 2016). Multiple immunoblasts and normal cells with left-shifted granulopoiesis have been described in spleen and bone marrow, respectively (Ng et al., 2016). Skeletal muscles may be atrophic with myofibre changes including lymphohistiocytic inflammatory infiltrate (Alsaad et al., 2018), although this is not a direct lesion attributed to MERS-CoV infection. Electron microscopy studies have shown the presence of viral particles in lung epithelial cells, alveolar macrophages, macrophages infiltrating the skeletal muscles, and renal proximal tubular epithelial cells (Alsaad et al., 2018).

1.4.1 Pathology of MERS-CoV in infected animals

MERS-CoV infection results in variable pathological outcomes depending on the animal species tested.

Rhesus macaque: Gross examination of the lungs of MERS-CoV inoculated animals revealed that lungs were firm, edematous, with discolored foci. Microscopically, animals developed moderate interstitial pneumonia characterized by thickened alveolar wall with edema, fibrin and some inflammatory cells, hyaline membranes formation, type II pneumocyte hyperplasia, perivascular inflammatory infiltrates, hemorrhages,

and degeneration and necrosis of pneumocytes and bronchial epithelial cells (Falzarano et al., 2013; Munster et al., 2013; De Wit et al., 2013; Yao et al., 2014).

Common marmoset: Grossly lungs from experimentally inoculated animals may be dark red and edematous. Microscopically, animals developed bronchointerstitial pneumonia accompanied by a mixed population of multinucleated cells, and type two pneumocyte hyperplasia accompanied with bronchiolar lesions. Respiratory epithelial cells in bronchi were eroded and attenuated. Airways were largely infiltrated by inflammatory cells mixed with varying amounts of fibrin, edema, and hemorrhage (Baseler et al., 2016; Yu et al., 2017).

Camelids: Dromedary camels inoculated with MERS-CoV have shown mild to moderate rhinitis characterized by multifocal necrosis of epithelial cells and infiltration of few leukocytes in nasal mucosa and lamina propria. Multifocal mild tracheitis and bronchitis with infiltration of inflammatory cells in the lamina propria, as well as epithelial necrosis and exocytosis of lymphocytes and neutrophils, have been described. In addition, follicular hyperplasia may be observed in lymphoid tissues (Adney et al., 2014; Bart L. Haagmans et al., 2016). Bactrian camels and new world camelids, alpacas and llamas, exhibited a very similar pathological outcome than that of dromedaries. Despite infiltration of some leukocytes, no severe histopathological lesions were observed in the lungs of any camelid species tested, upon MERS-CoV infection.

Rabbit: On days 3 and 4 post-MERS-CoV inoculation, mild rhinitis with heterophils in the epithelia and underlying lamina propria and mild to moderate necrosis and epithelial hyperplasia and hypertrophy were noted in the nasal turbinate of MERS-CoV infected rabbits. Lung lesions were characterized by the mild thickened alveolar septa, with mild hypertrophy of type two pneumocytes. Additionally, some alveoli were often accumulated by moderate numbers of alveolar macrophages (Haagmans et al., 2015).

1.5 Modulation of innate host response by MERS-CoV infection

When functioning properly, the host immune system identifies invading MERS-CoV, leading to viral clearance without promoting immunopathology. This is evidenced by the fact that camelids or humans with mild symptoms eventually recover after MERS-CoV infection (Adney et al., 2014, 2016a; Zhao et al., 2017). However, an aberrant

immune response causes acute inflammation, tissue damage or even lethal outcome to the severely infected patients and common marmosets (Alosaimi et al., 2020; Falzarano et al., 2014; Ng et al., 2016). Mechanistic aspects of how the host recognize MERS-CoV and eventually establish either protective or pathological countermeasures are complex and involve diverse immune signaling pathways.

Similar to other RNA virus infections, the host immune response against MERS-CoV can be canonically divided into two significant branches, innate and adaptive immunity. The innate immune response is initiated upon the rapid recognition of the viral antigen by various types of immune cells, such as monocytes or macrophages, dendritic cells (DCs) and natural killer cells (NKs), as well as non-immune cells including epithelial ones (Nicholson, 2016). All these cells exert their function through complex effector mechanisms, including pathogen sensing via pattern recognition receptors (PRR) signaling pathways, type I and III IFNs, inflammatory cytokines and chemokines, and the complement cascade (Takeuchi and Akira, 2009). The two arms of the adaptive immune system are the humoral and cell mediated immunity. The adaptive immune response is comparatively slow upon the first encounter with the virus but highly specific.

Since the pathogenesis of MERS-CoV and the innate immunity are the two main focuses of this PhD Thesis, these will be reviewed in the corresponding sections.

1.5.1 Viral detection and activation of the innate immunity

The primary targets for MERS-CoV are epithelial cells lining the respiratory tract (Adney et al., 2014; Kindler et al., 2013; Ng et al., 2016; Zhou et al., 2015) in which the innate immune response is initiated. Cell PRRs comprising toll like receptors (TLRs) and retinoic acid-inducible gene like receptors (RLRs) recognize invading pathogens and thus initiate a signaling cascade that eventually induce cytokines, such as inflammatory cytokines/chemokines and IFNs. The signaling of a specific route depends on the type of pathogens, type of the infected cell and the stage of infection in that same cell.

1.5.1.1 Sensing of RNA viruses via pattern recognition receptors

RIG like receptors

RLRs are constitutively located in the cytosol of almost all cell types and are always prepared for capturing non-self double stranded RNA (dsRNA). Two main types of RLRs bind to viral RNA, RIG1 (retinoic acid-inducible gene 1) and MDA5 (melanoma differentiation-associated protein 5), thereby initiating the downstream signaling pathway (Figure 1-4). The inactive form of RIG1/MDA5 has a RNA helicase domain with an ATP-binding motif and two N-terminal caspase recruitment domains, CARD (Rawling and Pyle, 2014; Yoneyama et al., 2004). Upon recognition of viral dsRNA through ATP-driven translocase activity of CARDs and helicases, RIG1/MDA5 undergoes conformational changes to an open and activated state and form a translocon complex with a chaperone molecule, 14-3-3ε (Liu et al., 2012). This chaperone protein mainly stabilizes the tripartite motif-containing protein 25 (TRIM25)-mediated ubiquitination in the CARD domains of RIG1/MDA5, thereby facilitating its oligomerization and translocation from the cytosol to the mitochondria (Liu et al., 2012). Of note, RIG1 can be further stimulated by the protein activator of the IFN-induced protein kinase (PACT) (Kok et al., 2011). On the mitochondrial surface, tandem CARD domains of RIG1/MDA5 form homotypic interactions with the CARD of the adapter, the mitochondrial antiviral-signaling protein (MAVS, also referred to as IPS-1, VISA, or CARDIF).

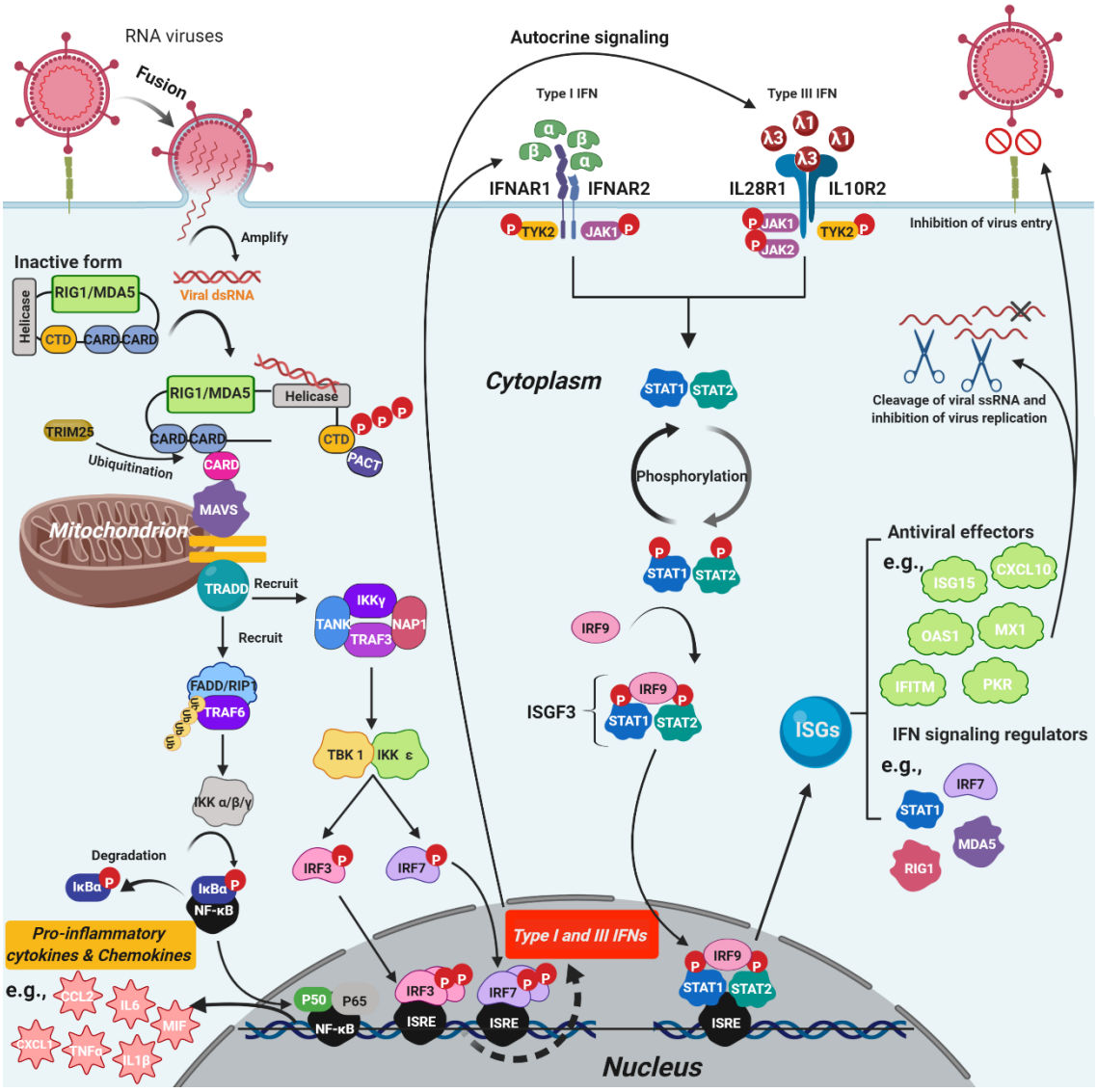

Figure 1-4. Induction of innate immune genes by RLRs. In response to RNA viruses, IFNs and proinflammatory genes were induced by RLRs signaling pathways in the infected cells. Type I and III IFNs bind to respective receptors, activate the JAK-STAT pathway and then induce various ISGs. Abbreviations: RIG1, Retinoic Acid-Inducible Gene I; MDA5, Melanoma Differentiation-Associated Protein 5; CTD, C-terminal domain; CARD, Caspase recruitment domain-containing protein; PACT, Protein ACTivator of the interferon-induced protein kinase; TRIM25, Tripartite motif-containing protein 25; MAVS, Mitochondrial antiviral-signaling protein; TRADD, TNFRSF1A Associated Via Death Domain; FADD, Fas-associated protein with death domain; RIP1, Receptor-interacting serine/threonine-protein kinase 1, TRAF, TNF Receptor Associated Factor; IKK, Inhibitor of nuclear factor kappa-B kinase subunit; IκBA, Nuclear factor of kappa light polypeptide gene enhancer in B-cells inhibitor, alpha; NF-κB, Nuclear factor NF-kappa-B; P50, Nuclear factor NF-kappa-B p50 subunit; P65, Nuclear factor NF-kappa-B p65 subunit; TANK, TRAF family member-associated NF-kappa-B activator; NAP1, 5-azacytidine-induced protein 2; TBK1, TANK-binding kinase 1; IRF, Interferon Regulatory Factor; ISRE, the Interferon-Stimulated Response Element; JAK, Janus kinase; TYK2, Non-receptor tyrosine-protein

(Continued)

kinase; STAT, the signal transducer and activator of transcription; ISGF3, Interferon Stimulated Gene Factor 3; CCL2, The chemokine (C-C motif) ligand 2; CXCL1, The chemokine (C-C motif) ligand 1; TNFα, Tumor necrosis factor α; MIF, Macrophage Migration Inhibitory Factor; ISG15, Interferon-stimulated gene 15; OAS1, 2'-5'-oligoadenylate synthetase 1; IFITM, Interferon-induced transmembrane protein; CXCL10, C-X-C motif chemokine 10; MX1, Interferon-induced GTP-binding protein Mx1; PKR, Protein kinase RNA-activated also known as protein kinase R.

Toll like receptors

On the other hand, endosomal TLRs, mainly TLR3 and TLR7, are also responsible for uptaking the viral RNA. Unlike RLRs localizing in the cytosol of most cell types, some TLRs (e.g. TLR7) are restricted to specific cell types. Dimerization of TLR3 monomers occurs upon viral dsRNA binding, followed by signal transmission through interaction between the toll/interleukin-1 receptor (TIR) homology domains and a TIR-domain-containing adapter-inducing interferon-β (TRIF) in the cytosol (Liu et al., 2008). This interaction is responsible for the recruitments of TRAF, TBK1 and IKKε, transmitting signals downstream to phosphorylate IRF3. Thus, phosphorylated IRF3 dimerizes and translocates into the nucleus, thereby activating NF-κB (Nuclear factor NF-kappa-B) and inducing pro-inflammatory cytokines. TRAF3 also recruits the IKK and TBK1 along with NEMO for IRF3/IRF7 phosphorylation, dimer-formation and translocation into the nucleus, in which induction of type I/III IFNs occurs in a manner similar to what is described in the RIG1/MDA5 pathway (Akira et al., 2006; Kawai and Akira, 2010). Besides, TLR7 captures viral ssRNA. Dimerization of TLR7 leads to the interactions of TIR domains and the adaptor molecule Myeloid differentiation primary response 88 (MyD88), thereby recruiting the Myddosome complex encompassing MyD88, phosphorylated Interleukin-1 receptor-associated kinase1 (IRAK1), IRAK4, and TRAF6 (De Nardo, 2015). Afterwards, TRAF6 is ubiquitinated and activates mitogen-activated protein kinase 7 (TAK1) complex. As a result, pro-inflammatory cytokines are induced via NF-κB signaling pathway (Napetschnig and Wu, 2013), the same process that one of the downstream events of TLR3 has been described above. Ubiquitinated TRAF6 also recruits and activates a TRAF3-IRAK-IKKα complex, which in turn phosphorylates IRF7, leading to its translocation into the nucleus to induce IFN production (Kawasaki and Kawai, 2014) as shown in Figure 1-5.

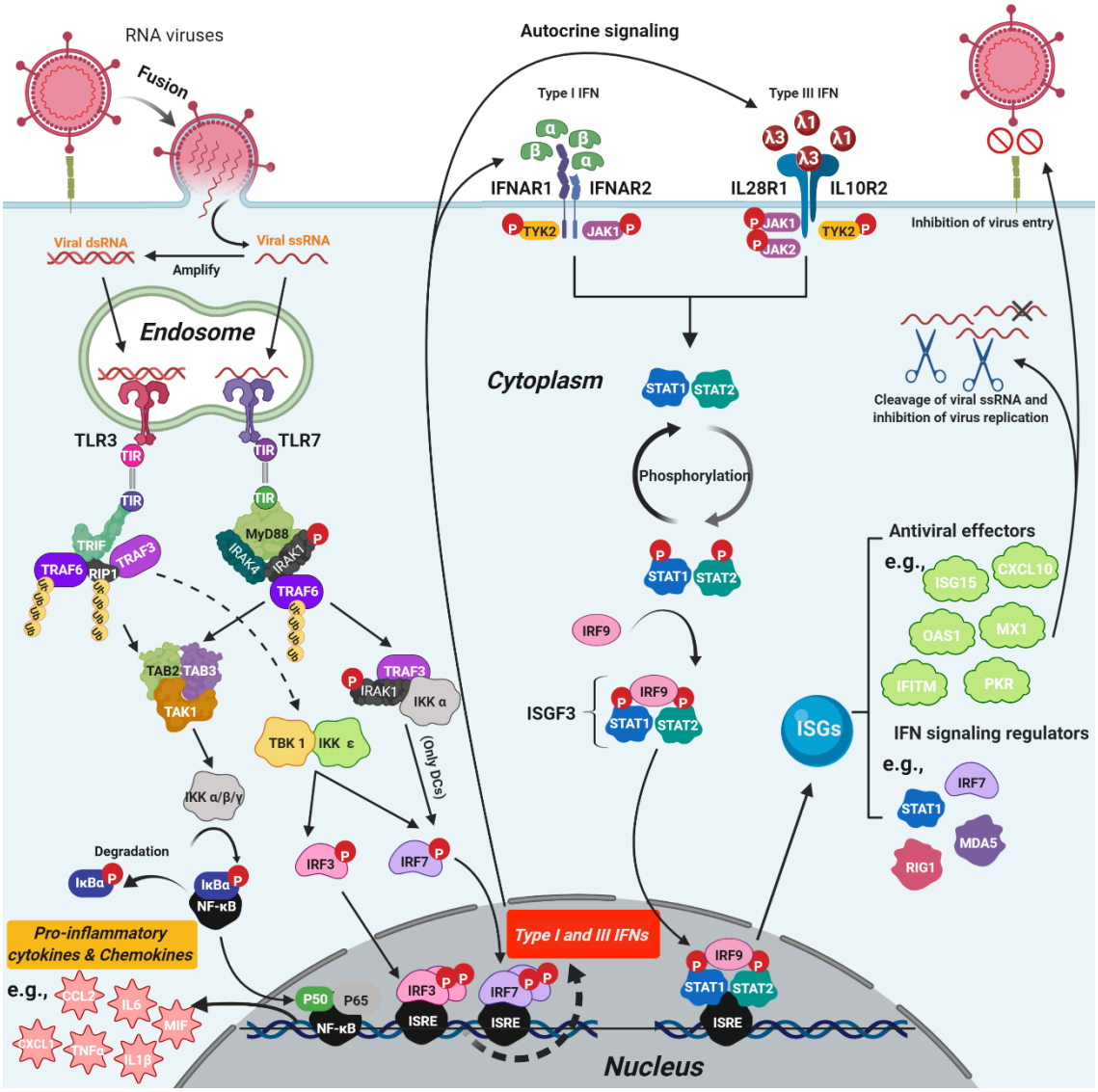

Figure 1-5. Induction of innate immune genes by TLRs. In response to RNA viruses, IFNs and proinflammatory genes were induced by TLRs signaling pathways in the infected cells. Once type I and III IFNs bind to their own receptors, the JAK-STAT pathway is activated, thereby inducing various ISGs.

1.5.1.2 Production of Interferon stimulated genes in response to RNA viruses

Following the recognition of RNA viruses via PRRs, the associated adapter proteins transmit downstream signals to nuclear factor (NF-κB) and IFN regulatory factors (IRF3, IRF5 and IRF7), further inducing pro-inflammatory cytokines (IL6, IL8, IL15, TNFα, CCL3, CCL2 CXCL1, NLRP3 and pro-IL1β) and IFNs (predominantly type I and III IFNs), respectively (Figure 1-4 and 5). Subsequently, IFNs are released from the cells and bind to specific IFN receptors in the cell membrane, leading to induction of the JAK-STAT intracellular signal transduction (Figure 1-4 and 5). Type I IFNs

signal through the IFN receptor (IFNAR) complex that is composed of an α-chain (IFNR1) and a β-chain (IFNR2). Afterwards, phosphorylation of tyrosine kinase 2 (TYK2) and Janus kinase 1 (JAK1) occurs. Similarly, type III IFNs bind to a heterodimeric receptor complex comprising IL28R1 and IL10R2 chains, followed by the phosphorylation of TYK2, JAK1 and JAK2 (Mendoza et al., 2017a). Type I and III IFNs, through distinct receptors, bind to the same JAK1 and TYK2 and activate a similar JAK/STAT pathway to induce interferon stimulated genes (ISGs) (Mendoza et al., 2017b). Phosphorylation of the JAK proteins further activates and phosphorylates the signal transducer and activator of transcription (STAT)1 and STAT2 to form a heterodimer (Dumoutier et al., 2003; Stark et al., 1998). As a result, STAT1-STAT2 dimers bind to IRF9, forming an ISGF3 complex that translocates to the nucleus and signals through the Interferon-Stimulated Response Element (ISRE) on the promoters of ISGs, initiating their transcription (Kotenko et al., 2003; Sheppard et al., 2003). While type I and III IFNs induce the expression of a comparable set of ISGs (Hoffmann et al., 2015), type I IFN signaling also activates pro-inflammatory cytokines and chemokines, which in turn recruit leukocytes to the site of infection.

1.5.2 IFN induction by MERS-CoV

The ability of the host cells to counteract RNA viruses, at the early infection stages, is dependent largely on the induction of IFNs and proinflammatory cytokines, and their relative contributions are the critical determinants for the disease outcome (L. Ferreira et al., 2019). Based on the structural features, receptor usage and biological activities, so far three distinct types of IFNs have been discovered: type I, II and III IFNs (Kotenko et al., 2003; Sheppard et al., 2003; Zanoni et al., 2017). Mainly type I and III IFNs participate in the innate host response. Type I IFNs suppress viral replication by inducing up to hundred types of ISGs and are also critical for orchestrating adaptive immunity. In response to the viral infection, type I IFNs are abundantly produced and become easily detectable in the blood (L. Ferreira et al., 2019). Type III IFNs, however, become particularly important in response to the early infection against respiratory viruses such as MERS-CoV, SARS-CoV or influenza viruses, as they are predominantly expressed by airway epithelial cells and specific myeloid cells (Kotenko et al., 2019). Although type III IFNs show expression profiles, signaling pathways and

gene expression programs resembling those of type I IFNs, they are known to induce milder inflammatory responses (Lazear et al., 2019). Both type I and III IFNs induce a wide range of ISGs which are effective for viral resistance (Hoffmann et al., 2015; Kotenko, 2011). In this section, IFN responses from MERS-CoV infected patients, human cell lines and animal models are reviewed.

1.5.2.1 IFNs in clinical specimens

Limited data available from the patient who succumbed to MERS-CoV infection showed no expression of IFNα in their broncho-alveolar lavage cells as well as in serum on the first week post infection. By contrast, the patient with mild symptoms could promote innate antiviral response, with a paucity of IFNα expression and thus control viral replication, suggesting a key role of the type I IFN in modulating the host immune response (Faure et al., 2014).

1.5.2.2 IFNs in MERS-CoV infected human cell lines

Due to the insufficient clinical data and limited autopsy samples, the investigation of IFN-mediated innate immune responses has mainly been focused on human cell lines. Monocyte-derived dendritic cells (Mo-DCs) fail to express IFNβ in response to MERS-CoV (Chu et al., 2014b); IFNs are not produced by human macrophages and immortalized epithelial cells (Comar et al., 2019; Zielecki et al., 2013) after infection with MERS-CoV. The absence of IFN response suggests that this highly pathogenic CoV has evolved mechanisms to block the production of IFNs and thus suppress innate antiviral responses (Kindler and Thiel, 2016). A wide range of viral factors modulates the host IFN responses and their underlying mechanisms have been broadly investigated. For instance, MERS-CoV ORF4a blocks MDA5 activation by dsRNA binding or sequestration (Niemeyer et al., 2013) and efficiently antagonizes PACT-induced activation of RIG1 and MDA5 (Siu et al., 2014); ORF4b, another MERS-CoV accessory protein, perturbs phosphorylation of IRF3 and subsequent activation of IFNβ in both the cytoplasm and nucleus (Yang et al., 2015). Efficient MERS-CoV replication can be achieved, leading to cell damage via direct cytopathic effect (CPE) or immunopathology via exacerbated pro-inflammatory cytokine responses. Accordingly, recombinant viruses lacking ORF4a and ORF4b elicited a strong type I and III

induction in various cell types (Comar et al., 2019). Some MERS-CoV African strains displaying genome deletions, particularly in the ORF4b, can induce higher levels of IFNβ, IFNλ1 and ISGs after 48 hours of infection as compared to that of the prototypic strain EMC/2012 (Chu et al., 2018). Plasmacytoid DCs (pDCs) are the only type of cells promoting the large production of type I and III IFNs in response to the MERS-CoV EMC/2012 (Scheuplein et al., 2015). Nonetheless, whether such a high secretion of IFNs by pDCs also occurred *in vivo* condition and responsible for viral clearance remains to be demonstrated in further studies.

Intriguingly, MERS-CoV infection in Calu3 cells delayed type I and III IFN production (Menachery et al., 2014). Such an aberrant IFN response can be lethal, since *in vivo* study confirmed that delayed induction of IFNβ by MERS-CoV failed to effectively inhibit virus replication, thereby enhancing immunopathology (Channappanavar et al., 2019a).

1.5.2.3 IFNs in MERS-CoV susceptible animals

Although numerous animal species are susceptible to MERS-CoV under experimental condition, limited data are available for immunopathogenesis purposes. It has been shown that IFNβ was not induced in lungs of common marmosets upon MERS-CoV infection (Falzarano et al., 2014). In IFNAR−/−, hDPP4–transduced mice, viral clearance was delayed and MERS-CoV mediated histopathological alteration, such as peribronchial, perivascular, and interstitial infiltrates and increased leukocytes, appeared earlier relative to wild type mice (Zhao et al., 2014), indicating the protective role of type I IFNs. Similarly, increased viral loads and mortality were also noted when blocking IFNAR1 in mice (Channappanavar et al., 2019a).

Remarkably, it has been shown that early type I IFN administration (before virus titers peak) protected mice and rhesus macaques from MERS-CoV infections (Channappanavar et al., 2019a; Falzarano et al., 2013; Zhao et al., 2014) while delayed type I IFN treatment promotes infiltration of inflammatory monocytes and macrophages towards lung tissue of mice (Channappanavar et al., 2019a), leading to lethal disease. Accordingly, the timing of type I IFN response *in vivo* relative to viral replication is also a determinant of the disease outcome in MERS-CoV infection.

Together, type I and III IFNs are critical for counteracting MERS-CoV at the early

stage of the infection. However, dysregulated (impaired or delayed) type I IFN responses in host cells lead to increased accumulation of lung leukocytes and thus immunopathology (Channappanavar et al., 2019a).

1.5.3 MERS-CoV induced pathogenic pathways in target cells

Severe pulmonary injury caused by MERS-CoV infection in humans and other animal models indicates diverse potentially pathogenic pathways. Most prominent, however, is the aberrant immune response upon MERS-CoV infection, characterized by the overexpression of various proinflammatory cytokines and chemokines (Alosaimi et al., 2020). Aforementioned cytokines play an essential role in response to MERS-CoV as they orchestrate cellular functions, including pro/anti-inflammatory and antiviral responses. A proper inflammatory response is beneficial and disturbs viral infected cells while extensive pro-inflammatory responses increase the concentrations of cytokines in the systemic circulation. Therefore, persistent production of these cytokines may lead to the development of pathological consequences such as tissue damage or even severe acute respiratory distress syndrome (ARDS) in some cases (Bohmwald et al., 2019; Mogensen and Paludan, 2001).

In the lower respiratory tract of MERS-CoV infected patients, proinflammatory genes IL1α, IL1β, IL8, IL18, CXCR3, SOCS5 and CCR2 were highly expressed (Alosaimi et al., 2020). Also, in the serum samples from MERS-patients who developed severe diseases, the levels of IL6 and CXCL10 were significantly elevated (Kim et al., 2016a). *In vitro* results are in line with what is observed in humans. MERS-CoV infection resulted in delayed but high induction of IL1β, IL6 and IL6 in Calu-3 cells (Lau et al., 2013). Furthermore, and compared with SARS-CoV, MERS-CoV induced significantly higher levels of IFN-γ, CXCL10, IL12, and CCL5 expression in Mo-DCs (Chu et al., 2014b), and remarkably upregulated IL12, IFNγ, CXCL10, CCL2, CCL3, CCL5, and IL8 in monocyte-derived macrophages (Zhou et al., 2014). Another *in vitro* study also demonstrated that the overexpression of MERS-CoV N protein in A549 and 293FT cell lines resulted in high expression of TNF, IL6, IL8 and CXCL10 transcripts (Aboagye et al., 2018). Intriguingly, in response to MERS-CoV, common marmosets induced signs that resemble human MERS-CoV disease, with extensive lung lesions accompanied by the upregulation of pro-inflammatory cytokines (Falzarano et al.,

2014). Serum levels of IL1RA, IL2, IL13, IL15, IFNγ, and MCP1 were also significantly upregulated at 1 day post inoculation (dpi) in rhesus macaques with mild to marked interstitial pneumonia, and all levels returned to baseline by 6 dpi (De Wit et al., 2013). Most of these cytokines/chemokines are essential for chemotaxis and activation of neutrophils and monocytes (Fan et al., 2001; Tsushima et al., 2009; Ware and Matthay, 2000).

Thus, there are cumulative evidences that most of the pathology in humans and Non-human primates (NHPs) could be attributed to the exacerbated pro-inflammatory responses, with macrophages and DCs playing a central role in inflammatory cytokine regulation; meanwhile, inhibition of IFN synthesis favours virus replication in pneumocytes.

1.5.4 Evasion of the innate antiviral response

CoVs successfully utilize a number of strategies to block or evade host innate immune responses, including those triggered by activation of the type I IFN pathway, which appears crucial for the initial immune response (Katze et al., 2002; Randall and Goodbourn, 2008). In that respect, MERS-CoV is not an exception. MERS-CoV encodes at least nine proteins that suppress host IFN production through distinct pathways. These include accessory proteins ORF3, 4a, 4b, 5 and 8b, structural protein M and N and non-structural proteins PLpro and nsp1.

1.5.4.1 Open reading frame 4a

MERS-CoV ORF4a protein functions as an IFN-antagonist involving the dsRNA binding and leading to the inhibitory effect on MDA5/RIG1-dependent IFN activation. However, it does not significantly affect the biological activities of genes involved in the downstream cascades (Niemeyer et al., 2013; Siu et al., 2014). ORF4a protein also inhibits dsRNA-mediated protein kinase R (PKR) activation, probably by sequestering dsRNA, thereby preventing translation and formation of stress granules that play important roles in antiviral signaling pathways (Rabouw et al., 2016). Compared to other accessory proteins, ORF4a protein shows a potent role of antagonist, impeding IFN response through inhibition of the IFNβ promoter activity, NF-κB activation and

the downstream cascades (Yang et al., 2013). During MERS-CoV infection in human airway epithelium-derived A549 cells, a recombinant virus lacking ORF4a resulted in increased IFNL expression (Comar et al., 2019). However, the deletion of ORF4a did not activate PKR or OAS-RNase L pathways (Comar et al., 2019), indicating that MERS-CoV ORF4a protein is not the only viral factor involving in the innate immune evasion.

1.5.4.2 Open reading frame 4b

ORF4b protein potentially suppresses phosphorylation of IRF3 and activation of IFNβ through interfering with IKKε /TBK1 in the cytosol. Interestingly, ORF4b inhibits IRF3 and IRF7 signaling, while the deletion of the nuclear localization signal of ORF4b is unable to impede IFNβ production (Yang et al., 2015). It has been shown that the ORF4b protein inhibits the type I IFN and NF-kB signaling pathways, thereby facilitating immune evasion strategies (Matthews et al., 2014). ORF4b protein also suppresses the antiviral effects of IFN via the counteraction of ISRE promoter element signaling pathways (Yang et al., 2013). In addition, ORF4b protein antagonizes IFNL1 production; this function is dependent on both its catalytic activity and nuclear localization and independent of its interaction with the OAS-RNase L pathway (Comar et al., 2019).

1.5.4.3 Open reading frame 5

ORF5 protein of MERS-CoV is able to modulate NF-κB mediated inflammation. The depletion of ORF5 (dORF5) activates a robust pro-inflammatory cytokine cascade in response to MERS-CoV. However, the dORF5 mutant failed to induce changes in IFN signaling, suggesting a limited role for the accessory ORF5 (Menachery et al., 2017; Yang et al., 2013). More studies are required to decipher the exact mechanism of this ORF5 protein.

1.5.4.4 Open reading frame 3

Although ORF3 is conserved among CoVs, the function of its coded protein is largely unknown. With the removal of ORF3, 4a, 4b and 5, robust type I and III IFN responses

are induced (Menachery et al., 2017). However, the depletion of ORF3 alone may not influence MERS-CoV replication *in vitro*, as a growth-curve analysis showed the virus still grew efficiently in Vero cells (Tamin et al., 2019).

1.5.4.5 Open reading frame 8b

MERS-CoV ORF8b protein is another IFN-antagonist. ORF8b strongly inhibits MDA5 and RIG1 mediated IFNβ promoter activity, but the expression of downstream signaling molecules, including MAVS and TBK1, is largely unaltered (Lee et al., 2019).

1.5.4.6 M protein

M protein is a multiple membrane-spanning protein that plays a central role in the assembly and budding of CoVs. It localizes predominantly into the Golgi apparatus and overlaps with the ERGIC (Nal et al., 2005). Besides, the MERS-CoV M protein is also reported to suppress type I IFN expression by inhibiting the phosphorylation of IRF3 (Lui et al., 2016).

1.5.4.7 N protein

In epithelial cell lines, the structural protein N interacts with TRIM25 impeding ubiquitination of RIG1 and further expression of type I and III IFNs. Ectopic expression of TRIM25 attenuates the suppressive effect of the N protein. Besides, the C-terminal domain of the N protein effectively suppresses IFNβ promoter activity (Chang et al., 2020).

1.5.4.8 Papain like protease

PLpro of CoVs cleaves the polyprotein to generate various nsps by which the replication complex is formed (Clementz et al., 2010; Lindner et al., 2005, 2007). Besides, PLpro might contribute to the modulation of innate host responses to MERS-CoV infection. A previous study has shown that MERS-CoV PLpro antagonizes IFN and NF-κB expression via deISGylating and deubiquitinating activities. Subsequently, several endogenous pro-inflammatory cytokines, including CCL5 and CXCL10, are

also downregulated (Mielech et al., 2014a). However, the exact role of PLpro and its associated deISGylating and deubiquitinating activities in these processes needs to be further investigated.

1.5.4.9 Non-structural protein 1

Analogous to the nsp1 of SARS-CoV that subverts host cell pathways at the translational level, the nsp1 of MERS-CoV directly targets host-cell functions and immune responses to inhibits host mRNA translation as well as host mRNAs degradation (Lokugamage et al., 2015). Such activity is likely triggered by the induction of endonucleolytic RNA cleavage. Moreover, MERS-CoV nsp1 has a unique strategy to inhibit mRNA translation that is distinct from the SARS-CoV nsp1(Lokugamage et al., 2015). While MERS-CoV nsp1 is localized in both the nucleus and the cytoplasm of target cells and does not bind firmly to the 40S subunit, SARS-CoV nsp1 is distributed only in the cytoplasm and binds to the 40S ribosomal subunit to facilitate mRNA translation (Lokugamage et al., 2015).

As mentioned in this introduction, MERS-CoV does not rely solely on single virulence factors but employs various strategies to evade host responses. Otherwise, it would not be able to replicate, hijack the host cells and even adapt to new hosts in the presence of effective IFN responses. It is also worth noting that all these proteins of MERS-CoV act as innate immune antagonists (at least described by *in vitro* studies), which rely largely on the overexpression of viral and cellular proteins, and these interactions have rarely been tested *in vivo* models (De Wit et al., 2016). More mechanistic investigation on immune evasion of MERS-CoV is needed not only for the more detailed insight into the pathogenesis but also for improving the treatment against MERS.

1.6 Animal models

Several research groups worldwide have been focused on the development of new therapies and vaccines against MERS-CoV infection (Bart L. Haagmans et al., 2016; Channappanavar et al., 2019a; Rodon et al., 2019; de Wit et al., 2020). All compounds must be rigorously validated before they are implemented in humans and/or animals. A large part of testing involves *in vivo* trials that are usually demanded by regulatory

bodies. Therefore, searching for an appropriate animal model is mandatory to develop vaccines and antivirals against MERS-CoV. Currently, multiple animal species have been tested experimentally to ascertain their susceptibility to MERS-CoV infection.

In this section, the current situation on animal models for the MERS disease is reviewed.

1.6.1 Non-human primates

NHPs have been chosen for modeling MERS-CoV infection in humans. These include Old World Monkeys (i.e. rhesus macaque) and New World Monkeys (i.e. common marmoset).

Rhesus macaques showed transient, mild to moderate respiratory disease that appeared within 24 hours post-inoculation (hpi). Microscopically, lung lesions consisted of thickened alveolar septa by edema fluid and fibrin, and infiltration of few macrophages and neutrophils. Viral RNA was found in nasal and oropharyngeal swabs, bronchoalveolar lavage fluids, and upper and lower respiratory tracts (URT and LRT, respectively), while the lung was the only organ that harbored infectious virus (De Wit et al., 2013).

In contrast to rhesus macaques, common marmoset showed severe progressive pneumonia after the MERS-CoV challenge via several routes (ocular, oral, intratracheal, and intranasal). The animals had clinical signs of tachypnea, labored or shallow breathing, cyanosis, and oral hemorrhagic discharge that were noted at 1dpi, peaked at 4 to 6 dpi, and resolved around two weeks. Besides, a pulmonary interstitial pattern was detected radiographically as early as 1 dpi and was resolved by 13 dpi. MERS-CoV RNA was found in various tissues, including the respiratory, gastral, cardiovascular and lymphatic organs. The highest viral loads were detected in the lungs. In line with reported human infections, an increased level of alanine aminotransferase, aspartate transferase and creatinine were noted. Histological findings were characterized as multifocal to coalescing, moderate to marked acute bronchointerstitial pneumonia. The lesion was also characterized by type II pneumocyte hyperplasia on 6 dpi, indicating a chronic reparative stage of pneumonia. Induction of robust antiviral and inflammatory transcriptional responses was evidenced in lungs (Falzarano et al., 2014). Therefore, the marmoset model seems to recapitulate well severe MERS cases in humans, as both

exhibited similar disease progression in response to the virus.

The limitations of using NHP for MERS-CoV research include their cost and the need for complex husbandry requirements (level-3 biocontention facilities for animals, ABSL3).

1.6.2 Mice

Wild-type mice are resistant to MERS-CoV infection because a lack of interaction between DPP4 and the viral S1 protein (Cockrell et al., 2014). An alternative to infect mice with MERS-CoV is to express the human DPP4 (hDPP4) in murine tissues. Mice transduced with hDPP4 developed disease upon MERS-CoV infection (Zhao et al., 2014). As these mice showed pulmonary lesions but no clinical signs, they can be used as an animal model to mimic mild MERS-CoV disease (Zhao et al., 2014). Alternatively, hDPP4-transgenic mice were generated to modulate more acute disease in response to MERS-CoV infection (Agrawal et al., 2015). Unlike hDPP4-transduced mice that only express DPP4 in epithelial cells lining the airways and alveoli, hDPP4-transgenic mice globally expose hDPP4 in cells of a variety of organs. Upon intranasal inoculation with MERS-CoV, hDPP4-transgenic mice exhibited acute progressive respiratory disease that eventually resulted in a fatal outcome by 6 dpi. Gross and microscopic lesions have been observed in the lung, as represented by extensive pulmonary congestion and consolidation as well as bronchointerstitial pneumonia with perivasculitis. In line with the histological observations, high levels of infectious virus were detected in the lung at early dpi (Agrawal et al., 2015; Pascal et al., 2015). Interestingly, a study used CRISPR/Cas9 to modify the mouse DPP4 gene at two amino acids (aa) positions (288 and 330); thus, resembling the hDPP4 (Cockrell et al., 2017). After serial MERS-CoV passages in these mice, the virus replicated productively within the lungs, and evoked clinical signs indicative of ARDS (Cockrell et al., 2017). To conclude, wild-type mice do not support MERS-CoV replication whereas hDPP4-transduced, hDPP4 transgenic and CRISPR/Cas9-edited mice are susceptible to MERS-CoV, resulting in mild to severe, fatal disease.

1.6.3 Non-camelid domestic species

Inoculation of domestic pigs with MERS-CoV did not cause disease while a low level of virus replication, shedding, and seroconversion was described (Vergara-Alert et al., 2017b; De Wit et al., 2017). In addition, New Zealand white rabbits were used to model asymptomatic MERS-CoV infection. Like pigs, clinical signs were not noticed in rabbits (Haagmans et al., 2015). Although they shed infectious MERS-CoV from the URT, transmission virus between rabbits did not occur (Widagdo et al., 2019). Moreover, goats, sheep, and horses inoculated with MERS-CoV did not get infected (Adney et al., 2016b; Vergara-Alert et al., 2017a). Overall, pigs and rabbits can be used to model asymptomatic disease while goats, sheep, and horses seem to be of limited or no value for modeling MERS-CoV infections, indicating the resistance of these species to infection.

1.6.4 Other small animal models

Syrian hamsters (*Mesocricetus auratus*) inoculated with the HCoV-EMC/2012 isolate did not show clinical signs, weight loss, gross or microscopic lesions, nor viral RNA in tissues or nasal, oropharyngeal, urogenital and fecal swabs (de Wit et al., 2013). Since ferrets (*Mustela putorius furo*) can be infected by SARS-CoV, these animals were also tested for susceptibility to MERS-CoV. However, no infectious virus was detected from nasal and oropharyngeal swabs of inoculated ferrets but viral RNA was found up to 2 dpi (Raj et al., 2014b).

1.6.5 Camelids

1.6.5.1 Old world camelids

Dromedary camels are thought to be the major reservoir of MERS-CoV. Experimental inoculation of dromedaries with MERS-CoV led to mild nasal discharge, accompanied by rhinorrhea that persisted for two weeks and a mild increase in body temperature on 2 and 5–6 dpi. NS, URT, LRT and lymphoid tissues also contained viral RNA. However, infectious MERS-CoV was found only in the URT, trachea, large bronchi and tracheo-

bronchial lymph nodes. Although gross lesions were not detected, mild microscopic lesions were present in both the URT and LRT, but not in the alveoli. In association with the observed lesions, MERS-CoV antigen was detected in epithelial cells lining the URT, trachea and bronchus. Neutralizing antibodies were also detected as early as 14 dpi (Adney et al., 2014).

On the other hand, Bactrian camels are also susceptible to MERS-CoV infection (Adney et al., 2019). The DPP4 of Bactrian camels is 98.3% identical to that of the dromedary camels at the aa level, and identical for the 14 residues of the RBD able to bind the MERS-CoV S protein. In response to MERS-CoV inoculation, Bactrian camels developed a transient, primarily URT infection, accompanied by large quantities of MERS-CoV shedding (Adney et al., 2019).

However, it is rather impractical to work with such large animals due to their special requirement for housing conditions, costs and the need for large ABSL3.

1.6.5.2 New world camelids

New world camelids (alpacas and llamas) have been reported to be naturally and experimentally susceptible to MERS-CoV infection (Adney et al., 2016a; Crameri et al., 2016a; David et al., 2018; Reusken et al., 2016; Vergara-Alert et al., 2017a). Upon MERS-CoV intranasal inoculation, both species displayed a similar clinical-pathological outcome to that of dromedaries, but alpacas showed no clinical signs, while llamas exhibited mild mucus secretion. The virus was found in NS, the URT and trachea of both species. None of these animal species exhibited gross lesions, but mild to severe rhinitis characterized by epithelial necrosis with infiltration of leukocytes in the nasal mucosa (Adney et al., 2016a; Vergara-Alert et al., 2017a). Furthermore, experimentally inoculated alpacas and llamas can transmit infectious MERS-CoV to other non-inoculated animals via close contact (Adney et al., 2016a; Rodon et al., 2019), indicating that these new world camelids might be useful surrogates for camels in experimental studies.

These new world camelids behave more gently compared to dromedaries, and are of smaller body size, thereby lessening difficulties on handling under ABSL3 facilities. Additionally, these animals are more available at a commercial level than dromedary camels. Also important for research purposes, some specific reagents for immune

monitoring have been limitedly commercialized for new world camelids (Davis et al., 2000) but their efficiency was not tested for immunohistochemistry (IHC). Hence, new world camelids could represent suitable animal models as a surrogate for dromedaries under experimental conditions.

Chapter 2

Hypothesis and objectives

Hypothesis

Currently, it is acknowledged that the MERS immunopathology in humans is caused by an aberrant immune response of the host, characterized by excessive production of various inflammatory cytokines, leading to progressive atypical pneumonia with extrapulmonary manifestations (Alosaimi et al., 2020; Chan et al., 2013a, 2015a). In contrast, camelids, the natural reservoir of MERS-CoV, show minimal to no clinical signs and clear the virus around one week after the infection. How reservoir/intermediate hosts control MERS-CoV still remains a mystery. Unraveling these mechanisms will be useful for the improvement of antiviral treatments and vaccines against MERS-CoV and by extension to other highly pathogenic CoVs, such as a newly emerged severe acute respiratory syndrome coronavirus 2 (SARS-CoV-2). Since bats, one of the primary reservoir for many CoVs, are susceptible to MERS-CoV but do not succumb to the disease probably due to a dampened NLRP3 inflammasome (Ahn et al., 2019), the first hypothesis of the present PhD Thesis is that (i) camelids may also control acute inflammation through adjusted inflammatory responses, and that clearance of MERS-CoV is due mainly to a robust and timely host innate immune response.

In the Arabian Peninsula, all the contemporary epidemic MERS-CoVs belong to clade B strains that have replaced early epidemic clade A strains (Alharbi et al., 2015; El-Kafrawy et al., 2019; Naeem et al., 2020). However, characterization of phenotypic and pathogenic differences between these strains in animal models are scarce. A recent study by Wang et al has compared the pathogenicity and virulence of a clade B strain (ChinaGD01) with a clade A strain (EMC/2012) *in vitro* and *in vivo*. Mice infected with the ChinaGD01 strain showed more weight loss, higher viral titer and severe immunopathology in their lungs, and decreased T cells responses than did the EMC/2012 strain (Wang et al., 2020). Still, whether these differences can be reflected in MERS-CoV intermediate hosts requires a more in depth investigation. In 2015, a clade B mutant variant (Jordan-1/2015 strain), which exhibits a partial deletion in ORF4a gene, was isolated from a patient from Jordan (Lamers et al., 2016). ORF4a functions as a strong IFN antagonist as assessed by *in vitro* studies (Niemeyer et al., 2013; Siu et al., 2014). However, data is missing on the pathogenicity of the Jordan-1/2015 strain *in vivo*. Thus, the second hypothesis of this PhD Thesis is that (ii) clade B strain show a better replicative fitness and in particular the Jordan-1/2015 strain

would elicit a more robust IFN responses than the prototype strain EMC/2012 in a camelid host.

Objectives

1. To investigate the innate immune response of alpacas upon MERS-CoV experimental infection with a contemporary epidemic clade B MERS-CoV.
2. To compare the pathogenesis of the variant Jordan-1/2015 strain with the Qatar 15/2015 strain and the MERS-CoV prototype strain EMC/2012 in an alpaca model.

PART II

Studies

Chapter 3

Study I

Type I and III IFNs produced by the nasal epithelia and dimmed inflammation are key features of alpacas resolving MERS-CoV infection

(manuscript submitted)

Introduction

MERS is a disease caused by a zoonotic Coronavirus (MERS-CoV) that emerged in 2012 in the KSA (Zaki et al., 2012b) raising a total of 2,562 confirmed human cases in 27 countries, with 881 deaths until the November 2020 (WHO, 2020). In humans, MERS-CoV infection ranges from asymptomatic to severe or even fatal respiratory disease (Zumla et al., 2015). Dromedary camels are the main viral reservoir (Alharbi et al., 2015), and all camelids are susceptible to the virus, under both natural and experimental conditions (Adney et al., 2016a, 2019; Crameri et al., 2016a; David et al., 2018; Reusken et al., 2016; Vergara-Alert et al., 2017a). However, despite consequent tissue viral loads and high viral shedding at URT level, infection in camelids is asymptomatic, leading to a rapid clearance of the virus (Adney et al., 2014, 2016a; Vergara-Alert et al., 2017a) and the establishment of a solid acquired immunity. Indeed, field studies revealed a high proportion of serum neutralizing antibodies in dromedary camels (David et al., 2018; Reusken et al., 2013c). Innate immune responses are essential as they link adaptive immunity (Akira et al., 2001) and are key players in the pathology of diseases (Hartl et al., 2018). Nevertheless, the severity of MERS lesions in humans has been attributed to aberrant innate and adaptive immune responses based essentially on data obtained from macrophages isolated from healthy donors or infected patients, as well as dosage of cytokines/chemokines from bronchoalveolar lavages. The outcome of these studies reveals an overproduction of proinflammatory cytokines/chemokines due to the activation of C-type lectin receptors, RLRs and an impaired production of type I IFNs (Alosaimi et al., 2020; Kindler et al., 2013; Zhao et al., 2020; Zhou et al., 2014). High production and persistent high levels of these cytokines in macrophages are likely to exacerbate disease severity. Despite that macrophages can be infected, at least *in vitro*, MERS-CoV has a preferable tropism for respiratory epithelial cells (Kindler et al., 2013). To date, no data is available on innate immune responses affecting the human respiratory mucosa *in vivo* and most information was mainly obtained from *ex vivo* pseudostratified primary bronchial airway epithelial cells (Kindler et al., 2013; Zielecki et al., 2013), immortalized epithelial cells (Comar et al., 2019; Zielecki et al., 2013) or respiratory explants (Chan et al., 2013b, 2014; Chu et al., 2018). Although some contradictory results have been reported, MERS-CoV infections in these cells or tissues led to the conclusion that type I and III IFN are inhibited (Niemeyer et al., 2013; Yang et al., 2013) or, when delayed (Menachery et al., 2014), weakly expressed (Lau et al., 2013). Nonetheless, some

MERS-CoV African strains isolated from dromedary camels, as opposed to the Arabian human isolated EMC/2012 strain, can induce higher levels of IFNβ, IFNλ1, ISGs and proinflammatory cytokines mRNA in Calu-3 cells after 48 h of infection (Chu et al., 2018). Indeed, the prototypic strain EMC/2012 and MERS-CoV African strains belong to different clades (A and C respectively) displaying deletions particularly in the ORF4b (Chu et al., 2018). In that respect, several viral factors, including MERS-CoV accessory proteins 4a and 4b, have been shown in respiratory epithelial cell lines to antagonize the production of IFNs, to interfere with the NF-κB signaling pathway by avoiding production of proinflammatory cytokines (Matthews et al., 2014) and inhibiting the PKR-mediated stress response (Rabouw et al., 2016). In addition, in epithelial cell lines, the structural viral protein N interacts with TRIM25 impeding ubiquitination of RIG1 and further expression of type I IFNs and IFN-λ1 (Chang et al., 2020). Therefore, in contrast to the cytokine storm provoked by macrophages, epithelial innate immune responses seem to be profoundly paralyzed. This is of major consequence for the progression of the disease, since the respiratory mucosa is the primary barrier for MERS-CoV. Recent findings indicate that type III IFNs confer initial protection, restricting tissue damage at the mucosa level by limiting inflammatory responses and potentiating adaptive immunity. Furthermore, it is postulated that when the viral burden is high and the mucosal fitness is broken, type I IFNs take over, leading to enhanced immune responses provoking also uncontrolled pro-inflammatory responses (Lazear et al., 2019).

Owing that bats, the primary reservoir for coronaviruses, are tolerant to MERS-CoV (and other viruses) due to a dampened NRLP3 inflammasome (Ahn et al., 2019), it was of major interest to gain insights into innate immune responses induced by MERS-CoV in camelids. Therefore, by understanding how reservoir/intermediary hosts control MERS-CoV and by extension other coronaviruses, a wealth of information could be translated to other species experimenting severe disease for the improvement of prevention, treatments and vaccines.

In the present study, alpacas were experimentally infected and monitored at the transcriptional level for a set of innate immune response genes along URT and LRT during four consecutive days. Special attention was given to the nasal epithelium as it is the primary site of MERS-CoV replication. Regulation of IFNs, PRRs, IFN regulatory transcription factors (IRFs) and enzymes constituting the NRLP3 inflammasome or the NF-κB pathway was analyzed providing insights on signaling mechanisms important for

MERS-CoV replication and disease progression, elucidating key regulatory host factors to counteract MERS-CoV infection.

Material and methods

Cell culture and virus

A passage 2 of MERS-CoV Qatar15/2015 isolate (GenBank Accession MK280984) was propagated in Vero E6 cells and its infectious titer was calculated by determining the dilution that caused CPE in 50% of the inoculated Vero E6 cultures (50% tissue culture infectious dose endpoint [TCID50]), as previously described (Vergara-Alert et al., 2017a).

Ethics statement

All animal experiments were approved by the Ethical and Animal Welfare Committee of IRTA (CEEA-IRTA) and by the Ethical Commission of Animal Experimentation of the Autonomous Government of Catalonia (file Nº FUE-2018-00884575 – Project Nº10370). The work with the infectious MERS-CoV Qatar15/2015 strain was performed under BSL3) facilities of the Biocontainment Unit of IRTA-CReSA in Barcelona, Spain.

Animal study

Fifteen 6-8 month-old alpacas (*Vicugna pacos*) were purchased by private sale and housed at the ABSL3 animal facilities of the Biocontainment Unit of IRTA-CReSA, in Barcelona, Spain. Animals were randomly numbered (AP1-AP15) and acclimated for one week. Twelve alpacas (AP1-AP12) were intranasally inoculated with a 10^7 $TCID_{50}$ dose of MERS-CoV Qatar15/2015 isolate in 3 mL saline solution (1.5 mL in each nostril) by using a mucosal atomization device (LMA® MADgic®, Teleflex Inc; USA), as described previously (Rodon et al., 2019; Vergara-Alert et al., 2017a). Three alpacas (AP13-AP15) were kept as non-infected controls.

All animals were monitored at least once per day for clinical signs (nasal discharge, coughing or dyspnea), food consumption, and rectal temperature until euthanasia. NS samples were collected on the day of euthanasia for MERS-CoV RNA detection and

titration in Vero E6 cells as previously described (Vergara-Alert et al., 2017a). Three alpacas were euthanized per day with an overdose of pentobarbital followed by exsanguination on 0, 1, 2, 3 and 4 dpi. Complete necropsies were performed, and the following tissues were collected: nasal turbinate, trachea, large and small bronchus, and lung parenchyma (apical, medial and caudal lobes). All tissues were collected in (a) Dulbecco's Modified Eagle Medium supplemented with 100 U/ml penicillin and 100 µg/ml streptomycin for virus isolation and genomic RNA detection; in (b) 10% neutral-buffered formalin for histopathology and IHC; and in (c) methacarn (60% absolute methanol, 30% chloroform and 10% Glacial acetic acid) fixative for cytokine, MERS-CoV genomic and subgenomic mRNA detection in paraffin embedded tissues.

Genomic viral RNA detection by RT-qPCR

MERS-CoV viral RNA obtained from NS and tissue samples were prepared and analyzed according to a previously published RT-qPCR protocol (Vergara-Alert et al., 2017a). Genomic MERS-CoV RNA was quantified by the UpE qPCR (Corman et al., 2012). Samples with a cycle threshold of less than 40 were considered positive.

Virus isolation from NS

NS samples collected at various dpi were evaluated for the presence of infectious virus by titration in Vero E6 cells, as previously reported by scoring for the presence of CPE at 6 days after culturing (Vergara-Alert et al., 2017a). The amount of infectious virus in each sample was calculated by determining the TCID50.

Histopathology and IHC

A monoclonal mouse anti-MERS-CoV N protein antibody (Sino Biological Inc., Beijing, China) was used to detect the presence of MERS-CoV antigen, following a previously established protocol (Te et al., 2019). A grading system for IHC was established by a board-certified veterinary pathologist (-, no positive cells detected; +/-, less than 10 positive cells per tissue section; +, 10 to 50 positive cells per tissue section; ++, 50 to 150 positive cells per tissue section; +++, 150 to 300 positive cells per tissue section; and ++++, more than 300 positive cells per tissue section). Table 1 summarizes the

distribution and number of MERS-CoV infected cells found in the different tissue sections for each inoculated animal.

Methacarn-fixed paraffin-embedded tissue (MFPE) specimens

For the assessment of cytokine mRNA profiles and presence of genomic and subgenomic MERS-CoV, nasal turbinates, trachea and lung were fixed by immersion in methacarn for best preservation of RNA (Dotti et al., 2010) and paraffin embedded. Tissue specimens were cut into four serial sections of 6 to 7 µm each and subsequently mounted onto Leica RNase-free PEN slides (Leica, Bannockburn, IL, USA). Prior to deparaffinization, the slides were air-dried for 30 min, followed by staining with 1% Cresyl Violet acetate for MFPE-nasal specimens, and dehydrated through a series of graded ethanol steps prepared with RNase-free water before being air dried. The whole process was performed under RNase-free environment. MFPE-tracheal and lung samples were immediately processed for RNA isolation by scraping the whole section from the slides and referred thereafter to as 'scraped' tissues. MFPE-nasal specimens were processed for Laser capture microdissection (LCM) prior RNA extraction. Histopathology was also performed on tracheal and lung MFPE sections stained with hematoxylin and eosin.

Laser capture microdissection

For each animal, four consecutive sections from the same MFPE-block containing nasal specimens were cut and processed as described in the supplementary material and method section. One of the sections was subjected to IHC to localize infected/non infected cells in the tissues and served as a reference (template) for the three subsequent sections which were subjected to LCM. Infected and non-infected nasal epithelium (mucosa) areas, as assessed by IHC in the template section, as well as their respective underlying submucosa areas were delineated and micro-dissected using the Leica LMD6500 (Leica AS LMD; Wetzlar, Germany) system (6.3× magnification, Laser Microdissection 6500 software version 6.7.0.3754). More detailed information is provided in Figure 3-1 for visualization of the microdissection process.

Dissected specific areas from each three MFPE sections were measured (Supplementary table 3-1) and introduced into RNase-free 0.5 ml Eppendorf tubes with buffer PKD from

the miRNeasy FFPE Kit (Qiagen, Valencia, CA, USA). Direct microdissection of IHC stained MFPE sections were attempted but failed to provide RNA with enough quality and yields for further microfluidic quantitative PCR assays.

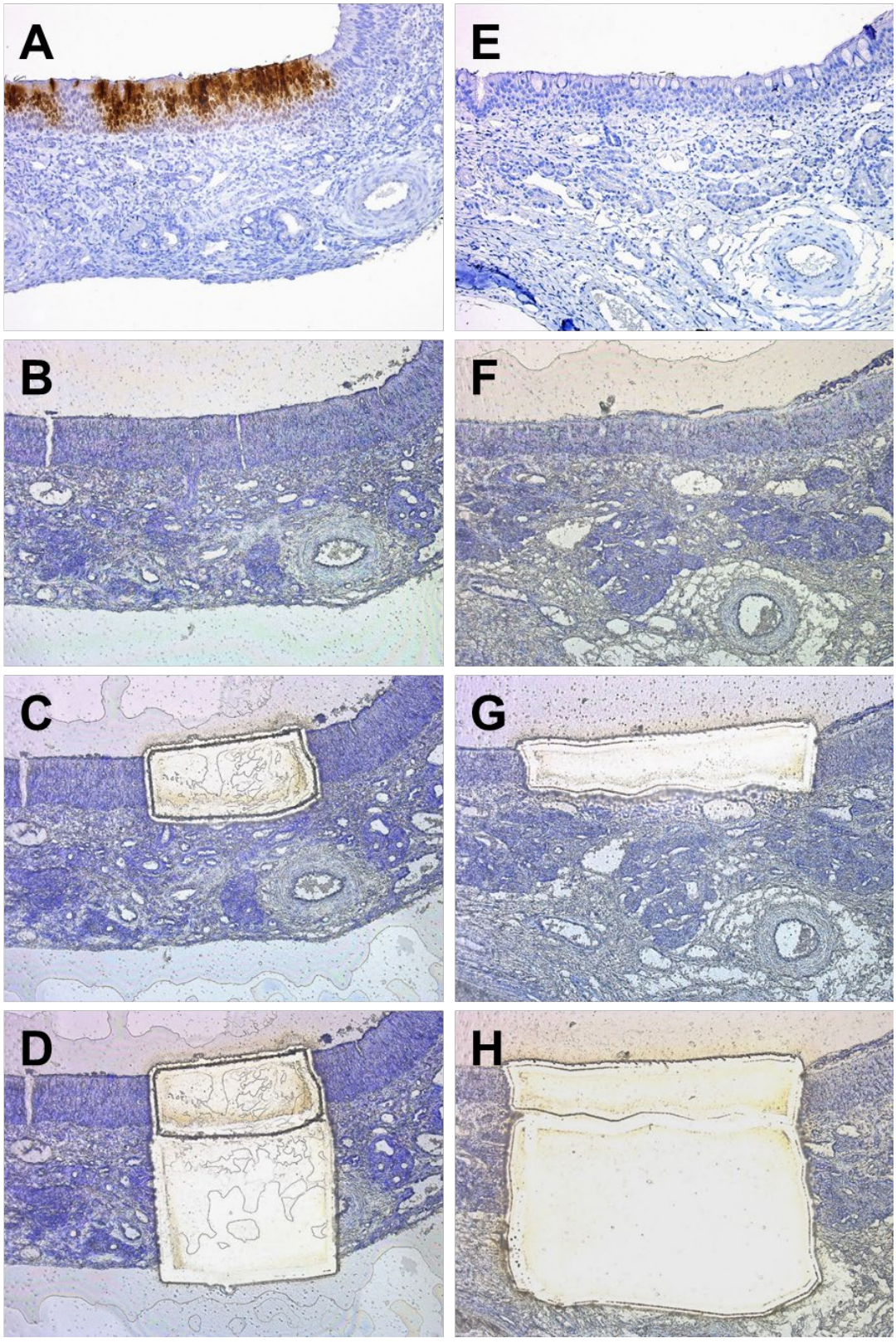

(Legend in the next page)

Figure 3-1. LCM of the nasal turbinate mucosa and underlying submucosa of MERS-CoV infected alpacas. For each animal, four consecutive 6-7 µm sections from the same MFPE block were performed and mounted onto Leica RNase-free PEN slides. One of the sections was stained by IHC to detect the presence of the viral N protein and visualize heavily infected mucosa areas (A) from non-stained areas apparently devoided of virus (E). This IHC stained section served as a template to localize by overlapping on the other contiguous MFPE sections, stained only with cresyl violet, infected (B) and "non- infected" (F) areas prior LCM. Then LCM was applied to collect the respective selected areas in the mucosa (C and G) and the underlying submucosa (D and H).

Total RNA isolation and cDNA synthesis

Total RNA extraction from micro-dissected or scraped tissues was performed using the miRNeasy FFPE Kit, following the manufacturer's instruction. Isolated RNA was concentrated by precipitation in ethanol, purified using RNeasy MinElute spin columns (Qiagen, Hilden, Germany) and treated for 10 min with DNase I (ArcticZymes, Norway). Supplementary table 3-1 summarizes the amount of tissues collected by LCM and their respective yields of RNA. cDNA was generated from 110 ng of total RNA using the PrimeScript™ RT reagent Kit (Takara, Japan) with a combination of both oligo-dT and random hexamers following manufacturer's instructions. Additionally, total RNA extracts from MERS-CoV infected nasal epithelia of AP5, 6, 7, 8, 9 and 11 were pooled at the same proportion per animal and used to generate cDNA controls for validation of gene expression assays.

Selection of innate immune genes, primers design

Thirty-seven innate immune genes were selected to study the gene expression and transcriptional regulation of the main known canonical signaling pathways acting on antiviral innate immunity and inflammation (Figure 3-2). Supplementary table 3-2 provides a brief description of their function within their respective signaling pathway. Alpaca genes and mRNAs (Wu et al., 2014) were obtained from GenBank database (https://www.ncbi.nlm.nih.gov/genbank). Primers were designed through comparative genomics of sequences of alpaca (*Vicugna pacos*) and also other camelid species. Comparison of mRNA and genomic sequences of each studied gene were performed with the alignment tool ClustalW to determine exon boundaries, even in some instances exons were already annotated in camelid genomes. Primer pairs were designed with the Primer3 (http://bioinfo.ut.ee/primer3-0.4.0/), or Primer Express 2.0 (ThermoFisher Scientific,

Life Technologies, Waltham, USA) with the following specifications: (i) bind at different exons or span exon-exon boundaries to avoid amplification of residual contaminating genomic DNA, (ii) 17-23 nts in length, (iii) GC content between 45 and 55%, (iv) amplicon length of approximately 80-200 bp, (v) melting temperature (Tm) of primers between 57-63°C with less than 2°C difference within primer pairs, and (vi) avoiding primer hairpin, self-primer dimer or cross-primer dimer formation. Furthermore, the avoidance of primer secondary structure arrangement and the specificity of each primer sequence was assessed *in silico* through the Beacon Designer™ (http://www.premierbiosoft.com/qOligo/Oligo.jsp?PID=1), by selecting for primers with greater ΔG than - 3.5 kcal/mol when possible, and Blast (https://blast.ncbi.nlm.nih.gov/Blast.cgi), respectively. Potential transcription of predicted pseudogenes was discarded by carrying out promoter region analyses.

Stimulated PBMCs from healthy alpacas were used for primer validation. Phytohemagglutinin, a combination of phorbol 12-myristate 13-acetate and ionomycin calcium salt, or Poly(I:C)-LMW/LyoVec™ stimulated PBMCs were used to induce the expression of the genes of interest. Total RNA was isolated from PBMCs using the RNeasy Mini kit (Qiagen, Germany), which was reverse-transcribed into cDNA using Primescript First strand (Takara, Japan). Primer efficiency, specificity, optimal annealing temperature, and differences of expression between stimulated and non-stimulated PBMCs were assessed by combining conventional PCR, gradient PCR, 2-step qPCR, Fluidigm Biomark qPCR and melting temperature analyses. Minus RT controls were included to all PCR assays to check the presence of DNA contamination. The whole set of reagents was fully validated prior the study of the innate immune responses occurring in alpaca upon MERS-CoV infection.

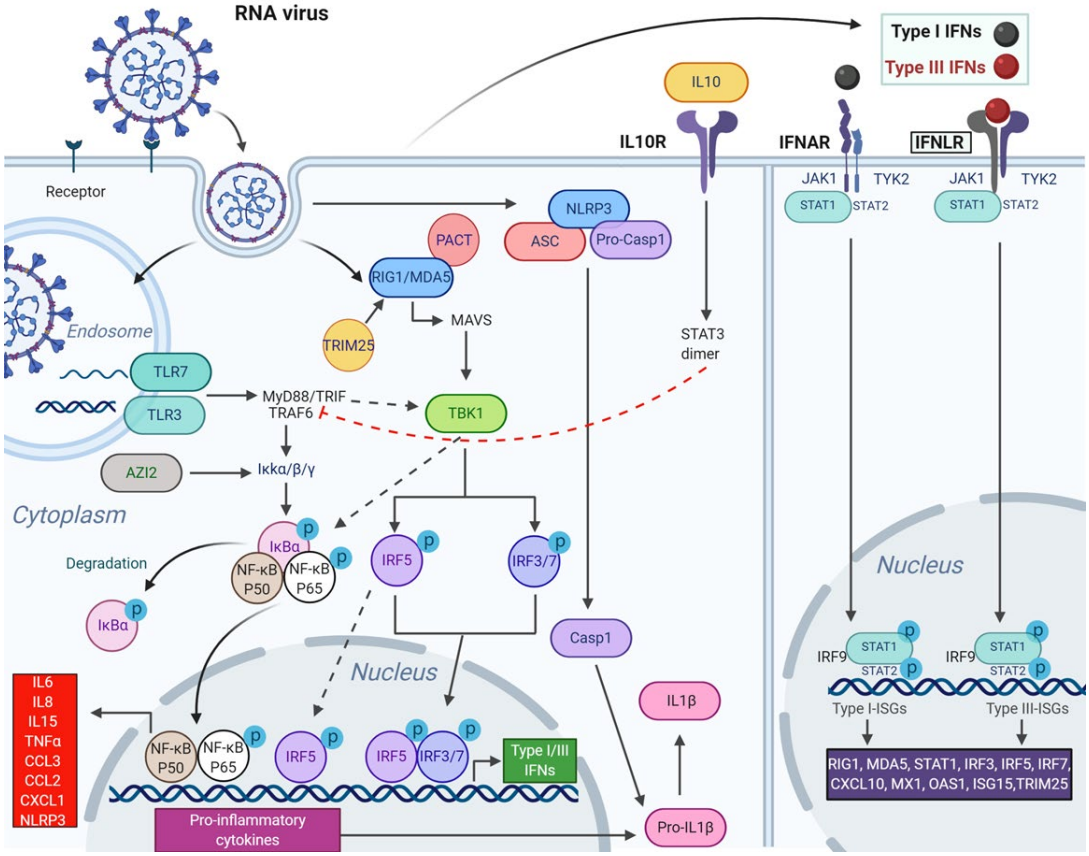

Figure 3-2. Pattern recognition receptors (PRRs), IFN signaling and pro-inflammatory cytokine pathways triggering antiviral innate immunity induced by RNA viruses. Upon sensing of RNA viruses, PRRs interact with their associated adapter proteins, thereby transmitting downstream signals to nuclear factor (NF-κB) and interferon regulatory factors (IRF3, IRF5 and IRF7) which further stimulate the production of pro-inflammatory cytokines (IL6, IL8, IL15, TNFα, CCL3, CCL2 CXCL1, NLRP3 and pro-IL1β) and IFNs (predominantly type I and III IFNs), respectively. Importantly, IRF5, is also a potent inductor of pro-inflammatory cytokines. The production of IFNs enhances the release of interferon stimulated genes (ISGs) which exert both, antiviral and host gene regulatory activities. IFNs can act in an autocrine and paracrine manner to induce the expression of ISGs via the JAK- STAT signaling pathway. While type I and III IFNs induce a similar set of ISGs (RIG1, MDA5, STAT1, IRF3, IRF5, IRF7, CXCL10, MX1, OAS1, ISG15, TRIM25), type I IFN signaling also activates pro-inflammatory cytokines and chemokines, which in turn recruit leukocytes to the site of infection. IL10 functions as an anti-inflammatory cytokine that activates STAT3 which is involved in the negative regulation of NF-κB. AZI2 and TBK1 (which also phosphorylate IRFs) participate positively in the NF-κB signaling pathway while IκBα inhibits translocation of NF-κB in the nucleus until degradation. Activation of the inflammasome, composed of NLRP3, PYCARD (ACS) and pro-CASP1 leads to the auto- cleavage of pro-CASP1 releasing CASP1 which further cleaves pro-IL1β into its mature form. The pro-apoptotic enzyme CASP10 and the adaptor CARD9 (acting downstream of C- type lectins signaling and upstream of the NF-κB pathway) are not represented in the diagram but were assayed for transcriptional regulation. Gene products, depicted with frames and colors were selected for microfluidic PCR assays, on basis of bibliographical data showing that they can be transcriptionally regulated following infection by RNA viruses. Furthermore, the selected genes sample most of the known signaling pathways triggered during a viral infectious process. P, phosphorylation.

Microfluidic quantitative PCR assay

The 96.96 Dynamic Array IFC was used to analyze the expression of 40 genes (37 target genes and 3 reference genes) and detect genomic and subgenomic viral regions using the UpE and M mRNA assays, respectively. This assay was performed in MFPE tissues from micro-dissected (nasal epithelia and submucosa) or scraped (trachea and lung) tissue sections of MERS-CoV infected (AP1-12) and non-infected (AP13-15) alpacas at different dpi (1 to 4 dpi). Briefly, cDNA samples, prepared as above, were preamplified for 16 cycles using a Preamp Master Mix (Fluidigm Corporation, South San Francisco, USA), treated with Exonuclease I (New England Biolabs, Ipswich, USA), diluted 1:20 with Nuclease free H_2O, loaded in duplicates into the corresponding array inlets and distributed across multiple reaction chambers. Quantification of the samples was performed on a Biomark HD system. The thermal cycle of the microfluidic qPCR was 60 s at 95°C, followed by 30 cycles of 5 s at 96°C and 60 s at 60°C. A dissociation step using EvaGreen detection was included for all reactions and was coupled with melting temperature analysis in order to confirm specific PCR amplifications of the designed primers. Additionally, total RNA extracts from MERS-CoV infected nasal epithelia of AP5, 6, 7, 8, 9 and 11 were pooled at the same proportion per animal and used to generate cDNA controls for validation of gene expression assays. The pooled cDNA controls were serially diluted 1:4 (1:4, 1:16, 1:64, 1:256, 1:1024) and assayed in triplicates to create relative standard curves and calculate primer efficiencies (Supplementary table 3-3). Non-template controls without nucleic acids were also included in the assays.

Relative quantification of innate immune response genes and statistical analyses

Data from the samples used for gene expression analyses by microfluidic qPCR was collected using the Fluidigm Real-Time PCR analysis software 4.1.3 (Fluidigm Corporation, South San Francisco, USA) and analyzed using the DAG expression software 1.0.5.6 (Ballester et al., 2013) to apply the relative standard curve method (see Applied Biosystems user bulletin #2). Briefly, the Cq threshold detection value was set at 0.020, the amplification quality threshold cut off value was established at 0.65 and amplification specificity was assessed by Tm analyses for each reaction. All reactions quantified before the assay endpoint showed specific amplification. Cq values obtained at the Fluidigm qPCR from the serially diluted cDNA controls were used to create standard curves for each gene, and to extrapolate the quantity values of the studied

samples. R-squared values were determined for each standard curve and the specific PCR efficiencies were calculated by applying the formula (10^(-1/slope value)-1)*100 (Supplementary table 3-3). The target amount is normalized by using the combination of three reference control genes (*GAPDH*, *HPRT1* and *UBC*). After, their suitability for normalization procedures was confirmed by control-gene stability analyses using the DAG expression software 1.0.5.6 (Ballester et al., 2013). The normalized quantity (NQ) values of individual samples from infected animals at different dpi were used for comparison against the NQ mean of three non-infected control animals (calibrator) per assay. Thus, the up- or down-regulated expression of each gene was expressed in fold changes (Fc) after dividing each individual NQ value with the calibrator. Unlike all other tested genes, IFNβ mRNA was undetectable in the nasal epithelia of non-infected control animals, therefore, comparisons for this gene in the nasal epithelia were performed in relation to the mean of IFNβ levels of three infected alpacas on 1 dpi. Supplementary table 3-4C, D, E and F recompiles all the results expressed in Fc relative to the control alpacas obtained with the Fluidigm microfluidic assay for all 37 genes tested. Supplementary table 3-4A shows the quantification, expressed in Cq values, of MERS-CoV UpE and M mRNA, obtained with the microfluidic qPCR assay. Supplementary table 3-4B indicates the expression levels (in Cq values) of all genes from non-infected alpacas euthanized at 0 dpi. The limit of detection for expressed genes was Cq=25.

Generation of graphs and heatmaps

All the line and bar graphs were created with Prism version 8 software (GraphPad Software Inc., La Jolla, CA). Data obtained from the relative quantification analyses was plotted as heatmaps, using the Pheatmap package in R program (https://cran.r-project.org/).

Statistical analysis

A logarithmic 10 transformations were applied on Fc values to approach a log normal distribution. Thus, the Student's *t*-test could be used to compare the means of the logarithmic Fc obtained at different dpi for each group of animals. Significant upregulation or downregulation of genes was considered if they met the criteria of a relative Fc of ≥2-fold or ≤2-fold respectively with $P < 0.05$. Having determined that RT-

qPCR data (Cq values) are normally distributed according to the Shapiro-Wilk normality test, the Tukey's multiple comparisons test was applied to compare Cq values of tissue samples at different dpi. Differences were considered significant at $P < 0.05$. Correlation coefficients were determined using the Spearman's correlation test.

Results

Clinical signs

The MERS-CoV Qatar15/2015 strain was selected for this study because Clade B strains are nowadays exclusively circulating in the Arabian Peninsula (Alharbi et al., 2015; El-Kafrawy et al., 2019). Following inoculation with this strain, only one alpaca (AP6) secreted a mild amount of nasal mucus on 2 dpi. None of the remaining animals showed clinical signs and basal body temperatures remained constant (below 39.5ºC) throughout the study.

Nasal viral shedding and MERS-CoV loads in respiratory tracts during infection in alpacas

On the day of euthanasia (0, 1, 2, 3, and 4 dpi), NS were collected. All MERS-CoV inoculated alpacas (AP1-AP12) shed viral RNA, but no major differences were detected between the different time points. Also, all inoculated animals excreted infectious MERS-CoV. Maximal viral loads in the nasal cavity were reached at 2 dpi. Of note, animal AP6 shed the highest loads of infectious virus (4.8 TCID50/ml). None of the alpacas, including negative controls (AP13-AP15), had viral RNA or infectious virus on 0 dpi (Figure 3-3A).

MERS-CoV RNA was detected in all homogenized respiratory tissues during infection. The higher viral loads were found on 2 dpi in nasal turbinates and bronchus with a significant increase compared to those detected on 1 dpi. Trachea and lung displayed the lowest viral RNA loads. In all cases, at 4 dpi, infectious virus was still excreted, and viral RNA was present in the respiratory tract (Figure 3-3B).

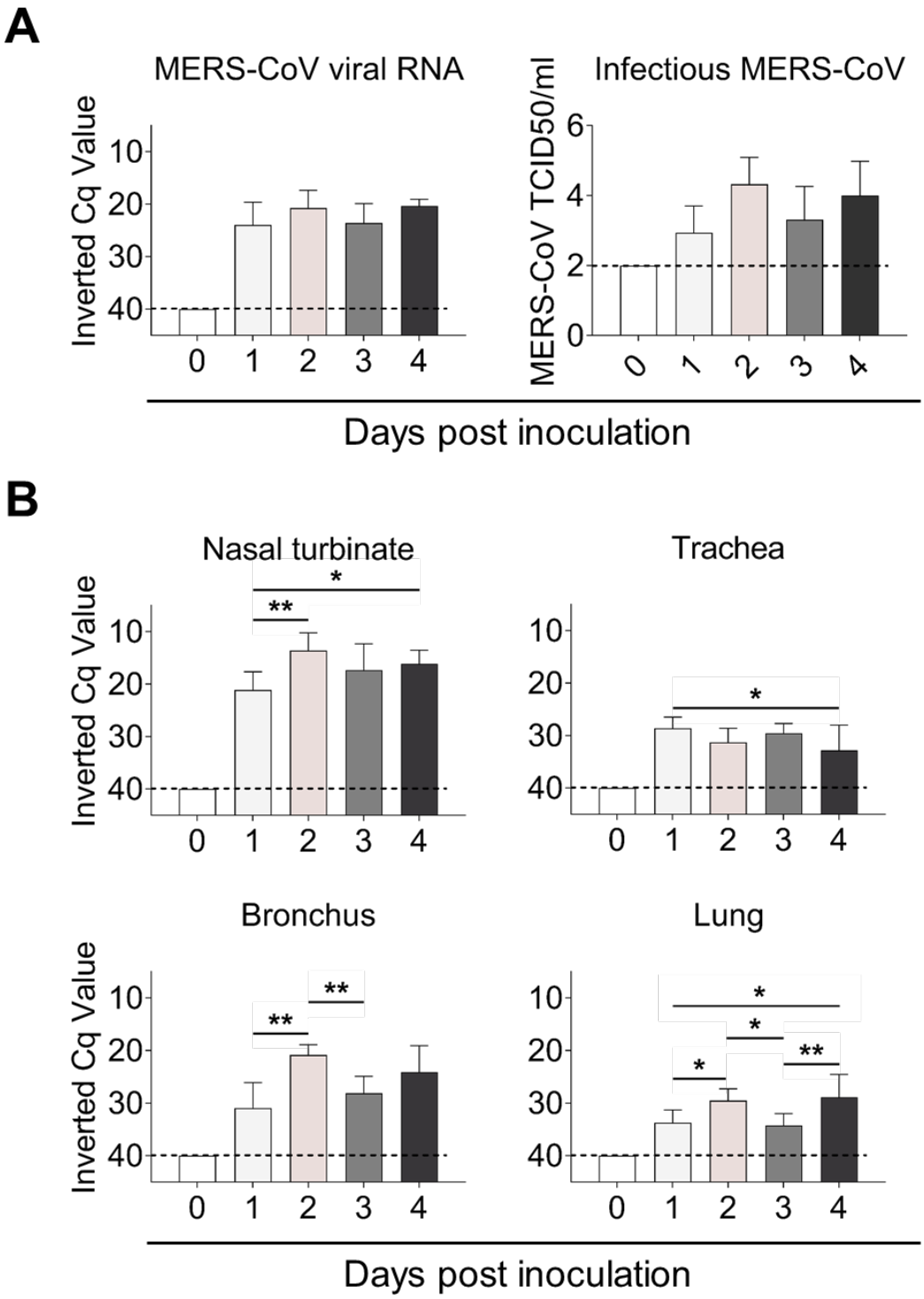

Figure 3-3. Viral loads in NS and respiratory tissues of MERS-CoV-infected alpacas. (**A**) Viral RNA (left) and infectious MERS-CoV (right) loads from NS samples collected at the day of euthanasia. (**B**) Viral RNA from respiratory tissues of alpacas collected at different dpi. Viral loads were determined by the UpE real-time RT-qPCR (A and B). Each bar represents the mean Cq value +SD of infected tissues from 3 animals euthanized on 0, 1, 2, 3 and 4 dpi, respectively (in total 15 animals). Statistical significance was determined by Tukey's multiple comparisons test. **P* < 0.05; ***P* < 0.01; ****P* < 0.001. Dashed lines depict the detection limit of the assays. Cq, quantification cycle; TCID50, 50% tissue culture infective dose.

MERS-CoV establishes early infections in URTs and LRTs of alpacas

On 2 and 3 dpi, histological lesions in MERS-CoV infected alpacas were limited to the respiratory tract, being of multifocal distribution and mild. Lesions in nasal turbinates were characterized by mild rhinitis, segmental hyperplasia of the nasal epithelium, lymphocytic exocytosis, loss of epithelial polarity and tight junction integrity. Additionally, small numbers of lymphocytes with fewer macrophages infiltrated the underlying submucosa. No microscopic lesions were observed in nasal turbinates on 0, 1 and 4 dpi in any of the animals, which displayed a multifocal localization of the MERS-CoV antigen detected by IHC. While only a few pseudostratified columnar epithelial cells in the nose contained MERS-CoV antigen on 1 dpi, the number of positive epithelial cells was remarkably high on 2 dpi; such number steadily decreased in the alpacas necropsied on the following days. On 4 dpi, the MERS-CoV antigen was scarcely detected with no evidence of microscopic lesions (Figure 3-4A).

Trachea and bronchus showed multifocal, mild tracheitis/bronchitis, with the presence of few lymphocytes in the epithelium and mild infiltration of the submucosa by lymphocytes and macrophages on 2 dpi. In line with these observations, MERS-CoV infected cells were rarely detected within the epithelium on 2 dpi by IHC, mostly in areas displaying these minimal lesions (Figure 3-4B). Remarkably, the trachea of AP6 harbored the highest viral load as detected by IHC. Few labeled cells were observed on 4 dpi (table 1) with no evidence of lesions. Additionally, lung lobes showed mild multifocal perivascular and peribronchiolar infiltration by lymphocytes and the presence of monocyte/macrophages within the alveoli, being more evident on 2 dpi. MERS-CoV antigen was occasionally observed in bronchiolar epithelial cells on 2 dpi (Figure 3-4B), and rarely on 4 dpi (table 1). Of note, pneumocytes were not labeled by MERS-CoV IHC (Figure 3-4B).

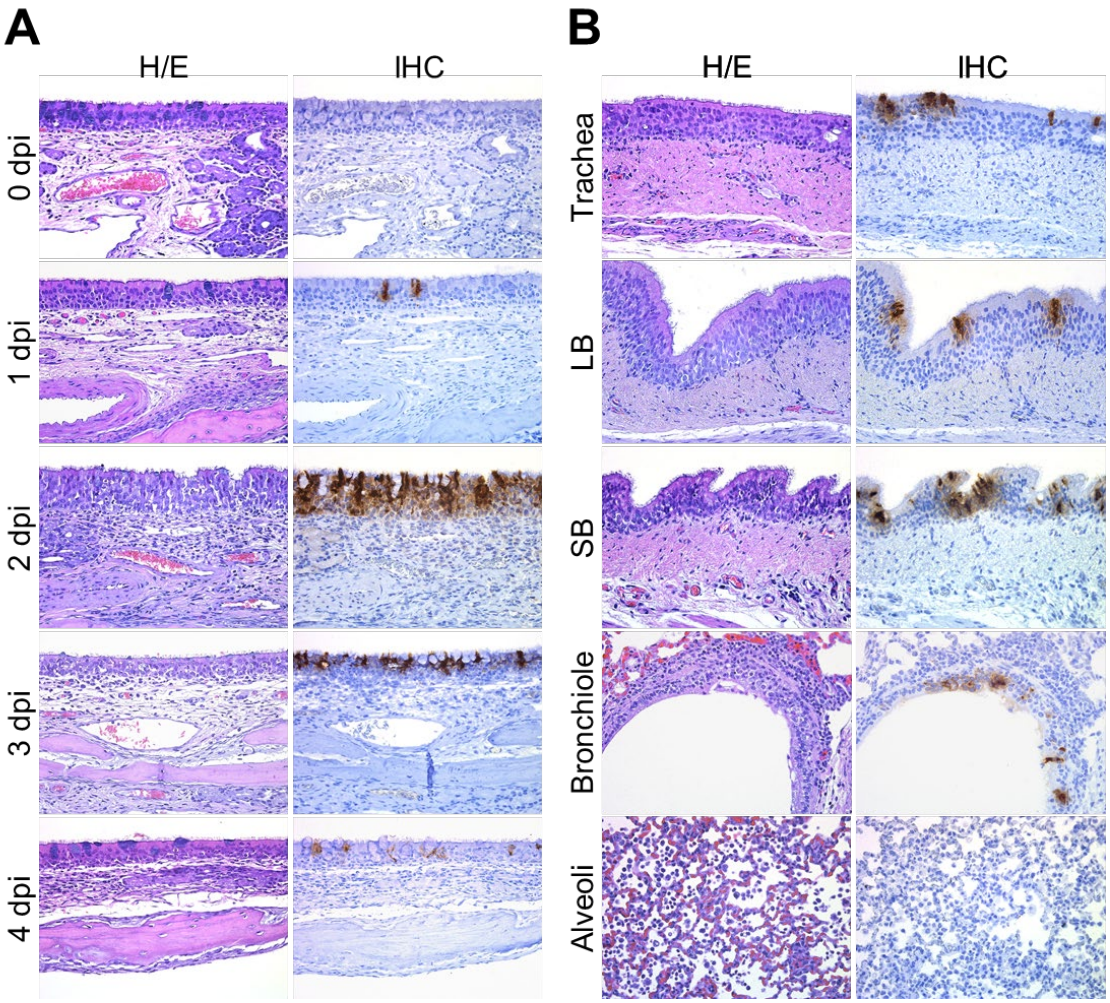

Figure 3-4. Histopathological changes and viral detection in respiratory tracts of alpacas inoculated with MERS-CoV**.** All respiratory tissues were fixed in 10% neutral-buffered formalin. (**A**) Nasal turbinate tissue sections of alpacas from the non-infected group (0 dpi), and from those necropsied on1 to 4 dpi. (**B**) Tissue sections of trachea, bronchus and lung (bronchiole and alveoli) from infected alpacas at 2 dpi. Original magnification: ×400 for all tissues. See table 1 for the detailed distribution of MERS-CoV antigen in respiratory tracts. Abbreviations: H/E, hematoxylin and eosin stain; IHC, immunohistochemistry; LB, large bronchus; SB, small bronchus.

Table 1. MERS-CoV N protein distribution in alpaca respiratory tracts by IHC.

	1 dpi			2 dpi			3 dpi			4 dpi		
Tissue	AP1	AP2	AP3	AP4	AP5	AP6	AP7	AP8	AP9	AP10	AP11	AP12
NT	+/−	+/−	+	++	+++	++++	++	+	+	+	+	+
TC	+	+	−	+/−	−	++	−	−	−	−	+	−
LB	−	−	−	++	+	++	−	−	−	−	+	−
SB	−	−	−	++	−	−	−	−	−	−	++	−
AL	−	−	−	−	+	+	−	−	−	−	−	+
ML	−	−	−	−	+	−	−	−	−	+	−	−
CL	−	−	−	−	−	−	−	−	−	−	−	−

Abbreviations: dpi, days post inoculation; AP, alpaca; day post inoculation; NT, nasal turbinate; TC, trachea, LB, large bronchus, SB, small bronchus; AL, apical lung; ML, medial lung; CL, caudal lung; -, no positive cells detected; +/-, less than 10 positive cells per tissue section; +, 10 to 50 positive cells per tissue section; ++, 50 to 150 positive cells per tissue section; +++, 150 to 300 positive cells per tissue section; and ++++, more than 300 positive cells per tissue section.

Viral loads in micro-dissected nasal tissues and whole tracheal and lung sections

Viral loads and viral transcription/replication were also assessed on MFPE tissue sections which were further used for cytokine quantification. Special attention was given to the nasal epithelium as it is the privileged tissue for viral replication. Thus, LCM was used to obtain, when possible and for each animal, nasal epithelial areas positive or negative for MERS-CoV, as assessed by IHC, in different but consecutive (parallel) MFPE tissue sections. Their respective underlying submucosa were also collected at 1 and 3 dpi (Figure 3-1).

Moreover, MFPE sections of tracheas and lungs were directly scrapped from the slide. Between 0.04 and 0.15 cm^2 were obtained for each LCM specimen and approximately 0.3-1 cm^2 per scrapped tissue were recovered. Between 0.27 to 2.41 µg of total RNA was obtained for each LCM and scrapped sample, respectively (Supplementary table 3-1). On 1 dpi only a few isolated nasal epithelial cells were IHC positive. These were micro-dissected, as described above, with the surrounding IHC negative cells to get enough RNA for the microfluidic PCR quantitative assay. To the contrary, due to the massive infection in nasal tissues at 2 dpi, only IHC negative nasal epithelial areas from AP4 could be collected. Viral loads in micro-dissected nasal tissues and MFPE tracheal

and lung scrapped samples were quantified with UpE primers using the microfluidic quantitative PCR assay. As illustrated in Figure 3-5, micro-dissected MERS-CoV infected epithelial areas, as assessed by their parallel IHC stained sections, showed higher viral loads than non-labelled epithelial areas, confirming the validity of the technique. In agreement with immunohistochemical observations, MERS-CoV RNA was of lower abundance in submucosal layers. As expected, and according to results obtained with tissue macerates, microfluidic quantification of MERS-CoV viral RNA revealed a much lower degree of virus replication in trachea and lung than in nasal tissues (Figure 3-5A). These results were confirmed with the M mRNA microfluidic PCR (Figure 3-5B and Supplementary table 3-4A) and, as expected, showed a greater extension of MERS-CoV infection in tissues, in particular in the nasal epithelia, than that revealed by IHC.

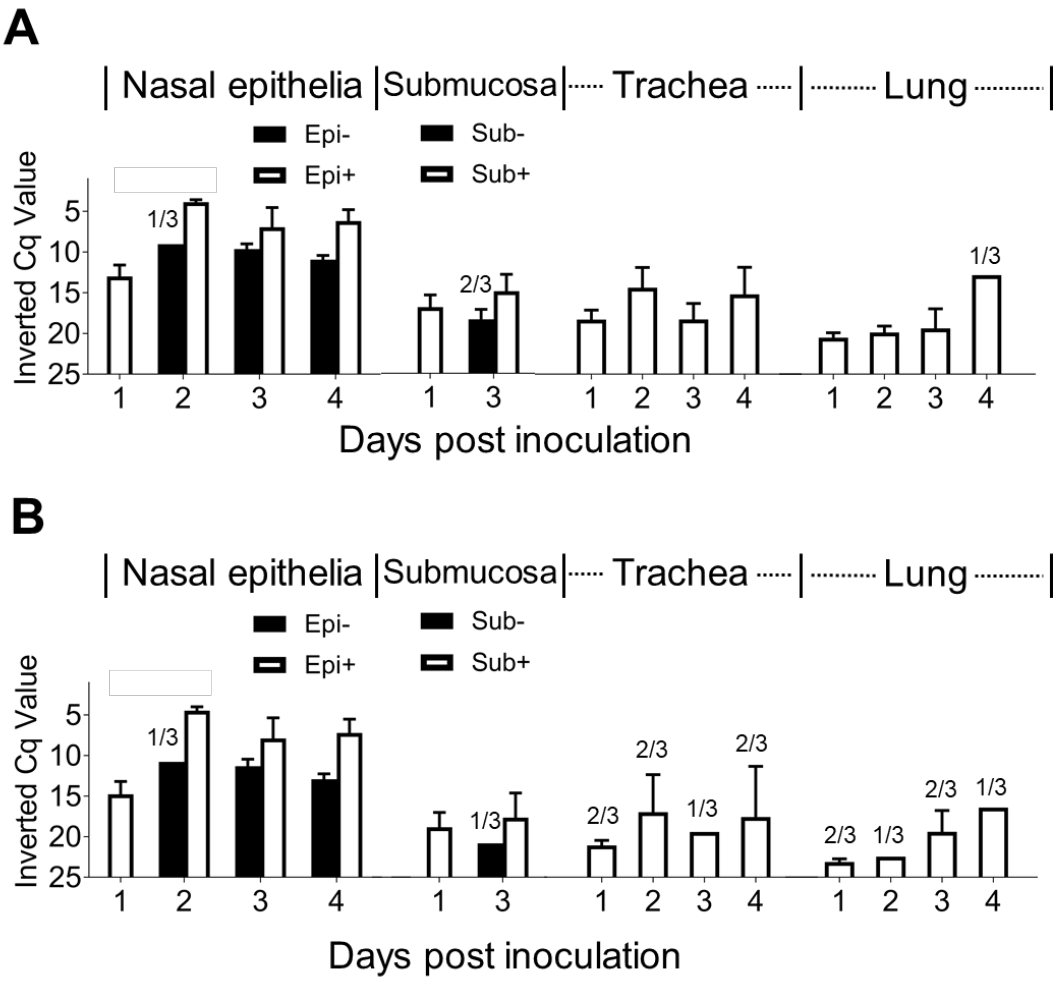

(Legend in the next page)

Figure 3-5. MERS-CoV UpE gene and M mRNA loads in MFPE samples. Micro-dissected (Nasal epithelia and underlying submucosa) and scrapped (Trachea and lung) MFPE tissue sections were prepared on the basis of an overlapping template section stained by IHC to localize the MERS-CoV N protein as described in Figure 3-1. RNA extracted from these samples collected in alpacas prior (0 dpi, n=3) MERS-CoV inoculation and after during 4 consecutive days (1 to 4 dpi, n=3 per day) were converted into cDNA and (A) the MERS-CoV UpE gene and (B) the M mRNA amplified with a PCR microfluidic assay (Fluidigm Biomark). Error bars indicate SDs when results were positive in more than one animal. At 1 dpi, only Epi+ were sampled by LCM, the majority of cells were IHC negative. At 2 dpi, only one animal displayed distinct Epi- areas within the nasal turbinates which could be micro- dissected. All other animals at 2 dpi had a massive infection of nasal turbinates with few IHC negative cells. Supplementary table 3-4A provides detailed information on Cq values obtained for each animal and indicates also the samples with no detectable viral RNA in the nasal submucosa trachea and lung. Abbreviations: Epi-, non-infected nasal epithelia, as assessed by IHC; Epi+, MERS-CoV infected nasal epithelia, as assessed by IHC; Sub-, submucosa underlying non-infected nasal epithelia, as assessed by IHC; Sub+, submucosa underlying MERS-CoV infected nasal epithelia, as assessed by IHC; MFPE, methacarn-fixed embedded-tissues; LCM, laser capture microdissection.

High induction of type I and III IFNs in the nasal mucosa occurs at the peak of infection in alpacas

In order to investigate the antiviral pathways induced upon MERS-CoV infection, relative mRNA expression levels for 37 innate immune response genes were assessed along the respiratory tract with the same cDNA samples as those used for viral UpE and M mRNA quantifications in a Fluidigm BioMark microfluidic assay. In all nasal mucosa of non-infected animals, IFNβ mRNA was undetectable and comparisons for this gene were performed against levels of expression found in animals infected on 1 dpi. For IFNλ3 very low basal levels, at the limit of detection (Cq=25), were found in 2 out of 3 animals on 0 dpi. All other gene transcripts were detected at basal levels in control non-infected animals and were used as calibrator values (Supplementary table 3-4B).

At the level of MERS-CoV infected nasal epithelia (positively stained by IHC), most of the transcription variations occurred and peaked at 2 dpi. Genes coding for IFNβ (mean of 200 Fc) and IFNλ3 (mean of 350 Fc), and to a lesser extent IFNα (mean of 6 Fc) and IFNλ1 (mean of 11 Fc) were significantly upregulated. Relative expression of type I IFNs (α and β) and type III IFNs (λ1 and λ3) decreased progressively on 3 and 4 dpi (Figure 3-6A and B).

The same patterns of gene transcription were observed for ISGs with antiviral activity (ISG15, MX1, CXCL10 and OAS1), IRF7, cytoplasmic viral RNA sensors (RIG1 and MDA5) and, although moderately upregulated, the endosome viral double and single stranded (ss) RNA sensors (TLR3 and TLR7 respectively) and the transcription factor

STAT1. The E3 ubiquitin ligase TRIM25, an important enzyme that plays a key role in RIG1 ubiquitination, was upregulated on 2 dpi (mean of 4.5 Fc) and decreased afterward (Figure 3-6A and B and Supplementary table 3-4C).

The pro-inflammatory antagonist IL10 was upregulated at 2 dpi (mean of 10 Fc) and returned to nearly steady state levels in the following days (Figure 3-6A and B). Only three genes involved in inflammation, TNFα, IL6 and IRF5 (mean of 2.5-3 Fc for each of them), were found slightly upregulated at 2 dpi, while the levels of expression of other critical pro-inflammatory factors, such as the cytokines IL8, IL1β, the adaptor PYCARD and the PRRs NLRP3, were marginally or not affected by the infection (Figure 3-6A and B and Supplementary table 3-4C). Although not statistically significant, CASP1, an essential component of the inflammasome (as PYCARD and NLRP3), experienced moderate mRNA increases (2 to 8 Fc following the animals) at 2 and 3 dpi (Figure 3-6A). Finally, the chemo-attractant chemokines CCL2 and CCL3 were non-significantly upregulated (mean of 5 Fc) as shown in Figure 3-6B.

Nasal epithelium negative by IHC for MERS-CoV exhibited a moderate but non-significant increase for type I and III IFNs mRNA on 2, 3 and 4 dpi. However, ISG15, MX1, RIG1, MDA5, TLR3, IRF7, IL10 and TRIM25 genes were upregulated at 3 dpi but to a lower degree than in positive IHC epithelial areas (Figure 3-6A and B). Invariably, all the above-mentioned genes had a significant decreased expression from 2 dpi onwards. Transcription of most of the inflammatory cytokines was not affected or slightly downregulated upon infection (Figure 3-6A and B, and Supplementary table 3-4C).

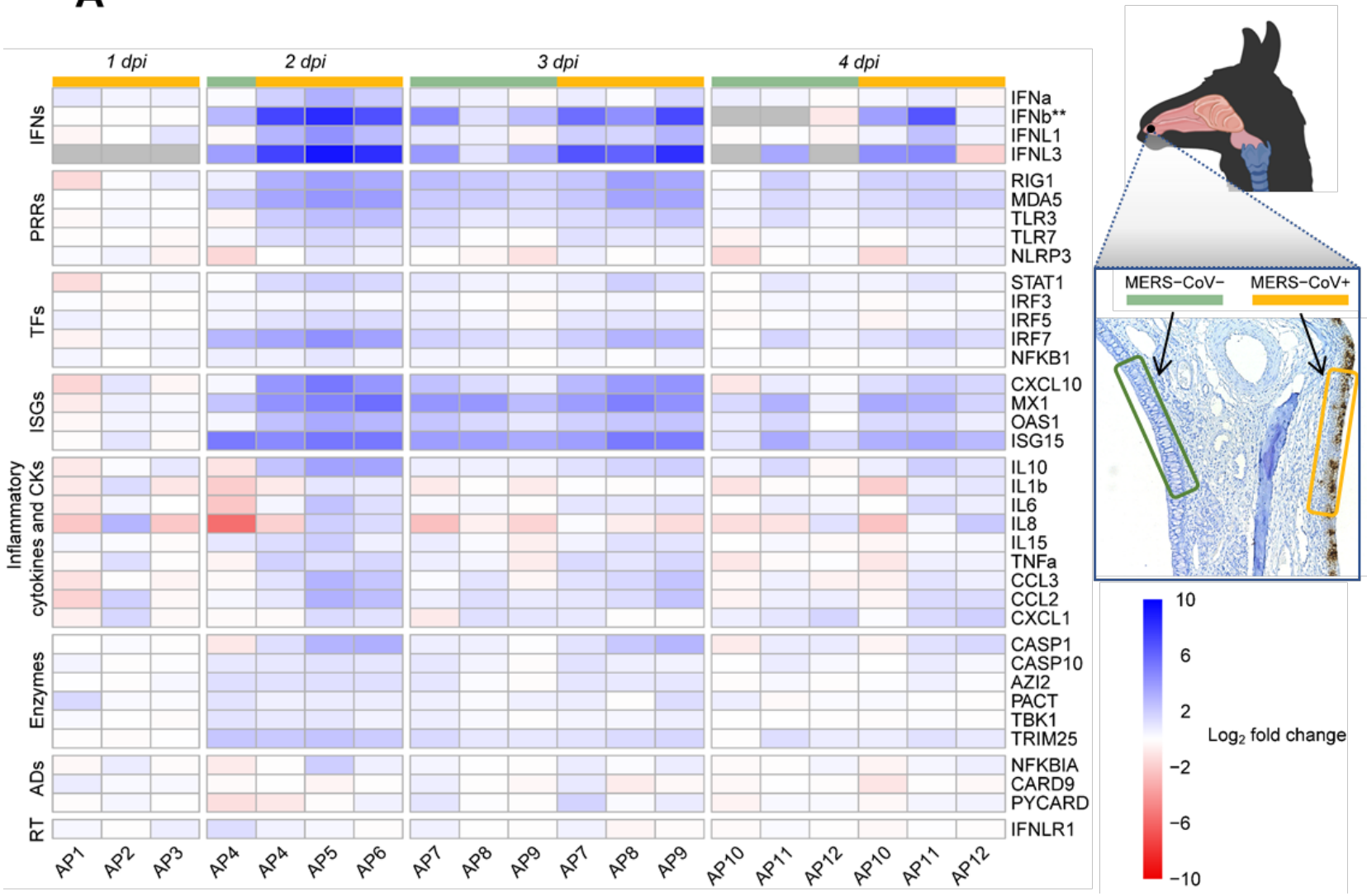
A
1 dpi
2 dpi
3 dpi
4 dpi
IFNs
PRRs
TFs
ISGs
Inflammatory cytokines and CKs
Enzymes
ADs
RT
IFNa
IFNb**
IFNL1
IFNL3
RIG1
MDA5
TLR3
TLR7
NLRP3
STAT1
IRF3
IRF5
IRF7
NFKB1
CXCL10
MX1
OAS1
ISG15
IL10
IL1b
IL6
IL8
IL15
TNFa
CCL3
CCL2
CXCL1
CASP1
CASP10
AZI2
PACT
TBK1
TRIM25
NFKBIA
CARD9
PYCARD
IFNLR1
AP1
AP2
AP3
AP4
AP4
AP5
AP6
AP7
AP8
AP9
AP7
AP8
AP9
AP10
AP11
AP12
AP10
AP11
AP12
MERS-CoV-
MERS-CoV+
10
6
2
−2
−6
−10
Log2 fold change

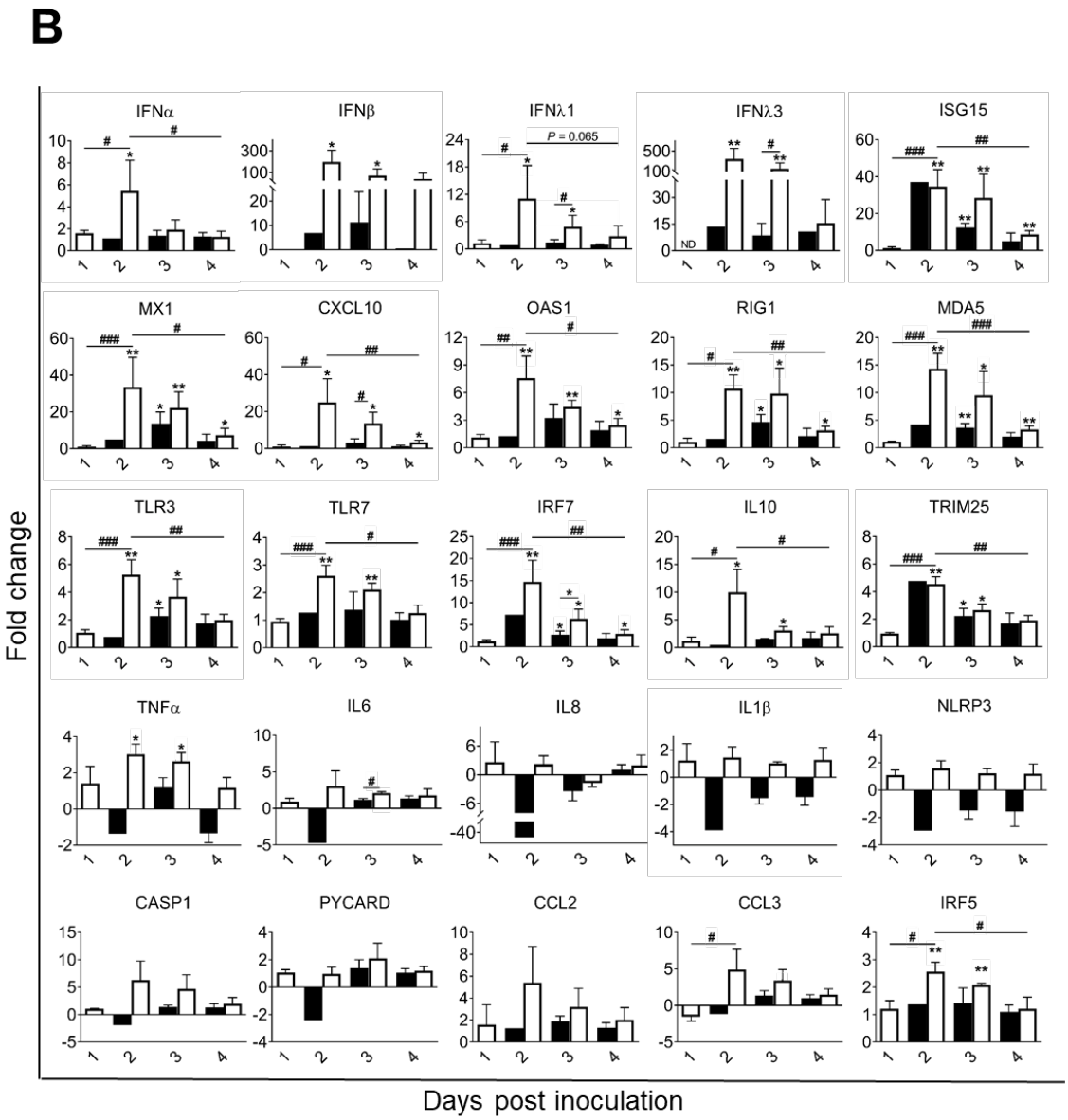

Figure 3-6. Kinetics of innate immune response genes induced at the nasal epithelia from MERS-CoV Qatar15/2015 infected alpacas. (**A**) The nasal epithelium of each alpaca (AP1 to AP15) was micro-dissected, as assessed by IHC (see the image of the nasal turbinate section in the upper right). Infected (orange)/non-infected (green) areas were isolated by LCM for RNA extraction and conversion to cDNA. The Fluidigm Biomark microfluidic assay was used to quantify transcripts of innate immune genes at different dpi. After normalization, Fc values between controls and infected animals were calculated. The resulting heatmap shows color variations corresponding to log2 Fc values; blue for increased and red for decreased gene expression values of infected animals compared to control animals, respectively. IFNβ was normalized with 1 dpi samples because it was not detected at 0 dpi. Grey rectangles indicate no detection of the corresponding gene. TFs, transcription factors; CKs, chemokines; ADs, adaptors; RT, receptor. MERS-CoV+ and MERS-CoV-, MERS-CoV positive and negative epithelium areas as assessed by IHC, respectively. (**B**) Average Fc of IFNs, ISGs, PRRs, transcription factors, inflammatory cytokines and chemokines, enzymes and adaptor genes in MERS-CoV+ nasal epithelia (white bars) and MERS-CoV- nasal epithelia (black bars) as assessed by IHC. Data are shown as means of ±SD. Statistical significance was determined by Student's *t*-test. **P* < 0.05; ***P* < 0.01; ****P* < 0.001 when compared with the average values of non-infected alpacas (n = 3); #*P* < 0.05; ##*P* < 0.01; ###*P* < 0.001 when comparisons between groups are performed at different dpi.

As shown in Figure 3-7, increased induction of type I IFNs in nasal epithelial micro-dissected samples was weakly correlated to increased viral MERS-CoV loads and transcription levels of IL10. In contrast, upregulation of type III IFNs had a stronger correlation with higher viral loads, as assessed by microfluidic PCR quantification of the viral M mRNA (r = 0.64, *P* = 0.004 for IFNλ1 and r = 0.64, *P* = 0.0163 for IFNλ3), the UpE gene (r = 0.65, *P* = 0.0033 for IFNλ1 and r = 0.64, *P* = 0.0163 for IFNλ3) and increased relative mRNA levels of IL10 (r = 0.9, *P* <0.0001 for IFNλ1 and r = 0.8, *P* = 0.0009 for IFNλ3). Our data indicate that antiviral mechanisms are set during the peak of infection in the nasal epithelia with a timely induction of type I and III IFNs, ISGs and IL10 without exacerbation of pro-inflammatory cytokines.

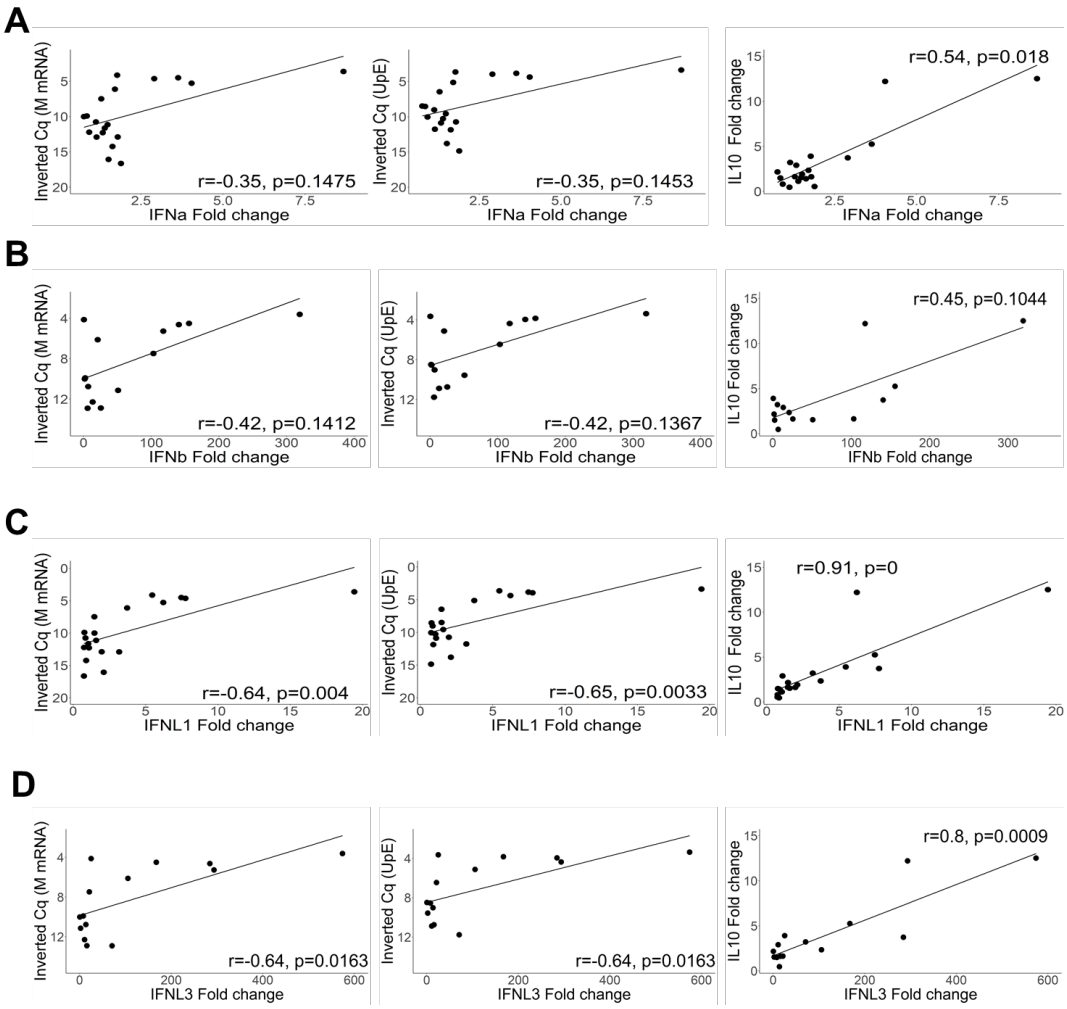

(Legend in the next page)

Figure 3-7. MERS-CoV loads and IL10 upregulation correlate with induction of type III IFNs but not type I IFNs in micro-dissected nasal epithelia. Portions of the nasal epithelia of each alpaca (AP1 to AP15) were micro-dissected from MFPE tissue sections on the basis of a section template stained by IHC allowing selection of areas positive or negative for the MERS-CoV N protein (Figure 3-1). After RNA extraction and conversion to cDNA the Fluidigm Biomark microfluidic assay was used to amplify, among others, transcripts IFNα, IFNβ, IFNλ1, IFNλ3 and IL10 and the viral UpE gene and M mRNA from all nasal epithelia (negative and positive by IHC) collected at different dpi (0 to 4 dpi). Values are expressed, after normalization with the HPRT1, GAPDH and UbC gene transcripts, as fold changes of the expression of cytokines in infected animals versus control animals (AP13-15 sacrificed at 0 dpi) and inverted Cq for the viral UpE gene and M mRNA (see Supplementary table 3-4A and Figure 3-5). IFNβ (IFNb) was normalized with 1 dpi samples because it was not expressed at 0 dpi. Inverted Cq values of MERS-CoV M mRNA and UpE, and relative expression levels of IL10 were plotted against relative expression levels of (A) IFNα, (B) IFNβ, (C) IFNλ1 and (D) IFNλ3 in micro-dissected nasal epithelia. Correlation coefficients were established using the Spearman's correlation test. dpi, days post inoculation.

ISGs and PRRs but not IFNs are upregulated in the nasal submucosa of infected alpacas: evidence for a potential IFN paracrine signaling

To further investigate the repercussion of MERS-CoV infection in the mucosa, innate immune responses occurring in the underlying submucosa were determined. Micro-dissected areas from the submucosa of control and infected animals (1 and 3 dpi) were analyzed for relative mRNA expression of innate immune genes. Except for IFNλ3 which was not detected in any inoculated or control animals, all other IFNs were expressed at basal levels in control non-infected alpacas. IFNβ was undetected at 1 dpi in two inoculated animals (AP2 and AP3) and below basal levels in alpaca AP1 while IFNα and IFNλ1 were marginally fluctuating. Most of the major transcriptional modifications occurred at 3 dpi. In submucosa underlying the most infected epithelia areas, IFNλ1 was expressed at basal levels while IFNα and IFNβ were not induced. On the contrary, ISGs, IRFs and PRRs, like ISG15 (mean of 77 Fc), OAS1 (mean of 6 Fc), MX1 (mean of 46 Fc), CXCL10 (mean of 14 Fc), RIG1 (mean of 12 Fc), MDA5 (mean of 16 Fc), IRF7 (mean of 9 Fc) and TLR7 (mean of 5 Fc) were highly to moderately upregulated. Expression of genes constituting the inflammasome was mostly not altered for NRLP3 or moderately increased for CASP1 (mean of 5 Fc) and PYCARD (mean of 3 Fc); but remarkably, IL1β was significantly downregulated (mean of 3 Fc; Figure 3-8A and B). Also, except for a non-significant increase of TNFα (mean of 5 Fc) and a slight upregulation of IRF5 (mean of 3 Fc; $P < 0.05$), no other pro-inflammatory factors were upregulated. Indeed, IL8 was downregulated (mean of -40 Fc). According to these findings, the anti-inflammatory cytokine IL10 (mean of 3.5 Fc) was moderately upregulated (Figure 3-8A, B and Supplementary table 3-4D). Furthermore, the

submucosa underlying epithelial cells with no MERS-CoV IHC labelling showed the same patterns of cytokine profiles as for that underlying heavily MERS-CoV infected mucosa but to a lesser degree of expression (Figure 3-8A and B). Overall, results obtained in the submucosa are indicative of a potential IFN paracrine signaling from the epithelium for the occurrence of ISGs induction in the absence of significant IFN mRNA synthesis. Moreover, despite mild focal infiltrations (Figure 3-4), genes involved in the inflammatory process were either suppressed, unaltered or mildly activated.

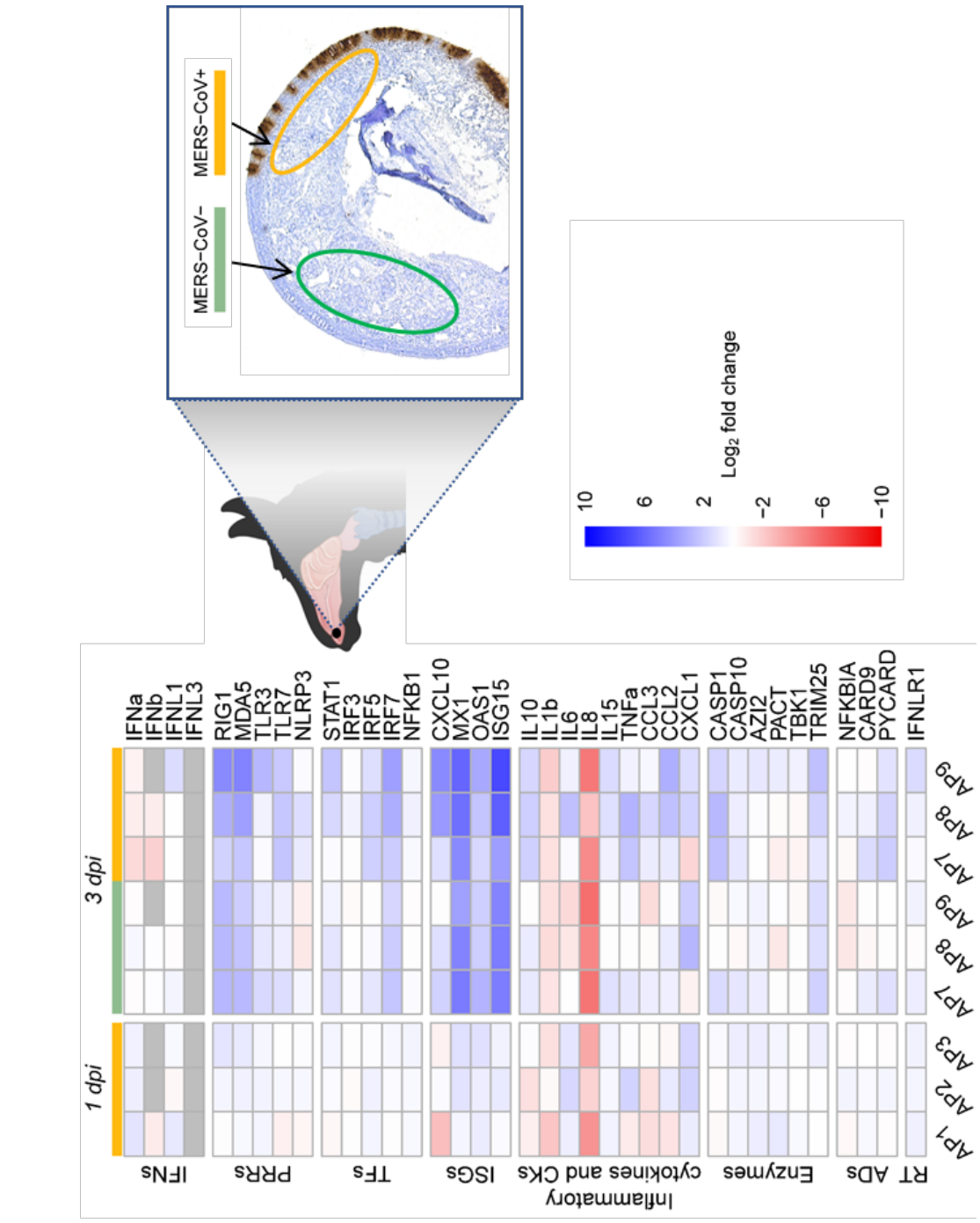
A
1 dpi
3 dpi
IFNa
IFNb
IFNL1
IFNL3
RIG1
MDA5
TLR3
TLR7
NLRP3
STAT1
IRF3
IRF5
IRF7
NFKB1
CXCL10
MX1
OAS1
ISG15
IL10
IL1b
IL6
IL8
IL15
TNFa
CCL3
CCL2
CXCL1
CASP1
CASP10
AZI2
PACT
TBK1
TRIM25
NFKBIA
CARD9
PYCARD
IFNLR1
IFNs
PRRs
TFs
ISGs
Inflammatory cytokines and CKs
Enzymes
ADs
RT
AP1
AP2
AP3
AP7
AP8
AP9
AP7
AP8
AP9
MERS-CoV+
MERS-CoV−
Log2 fold change
10
6
2
−2
−6
−10

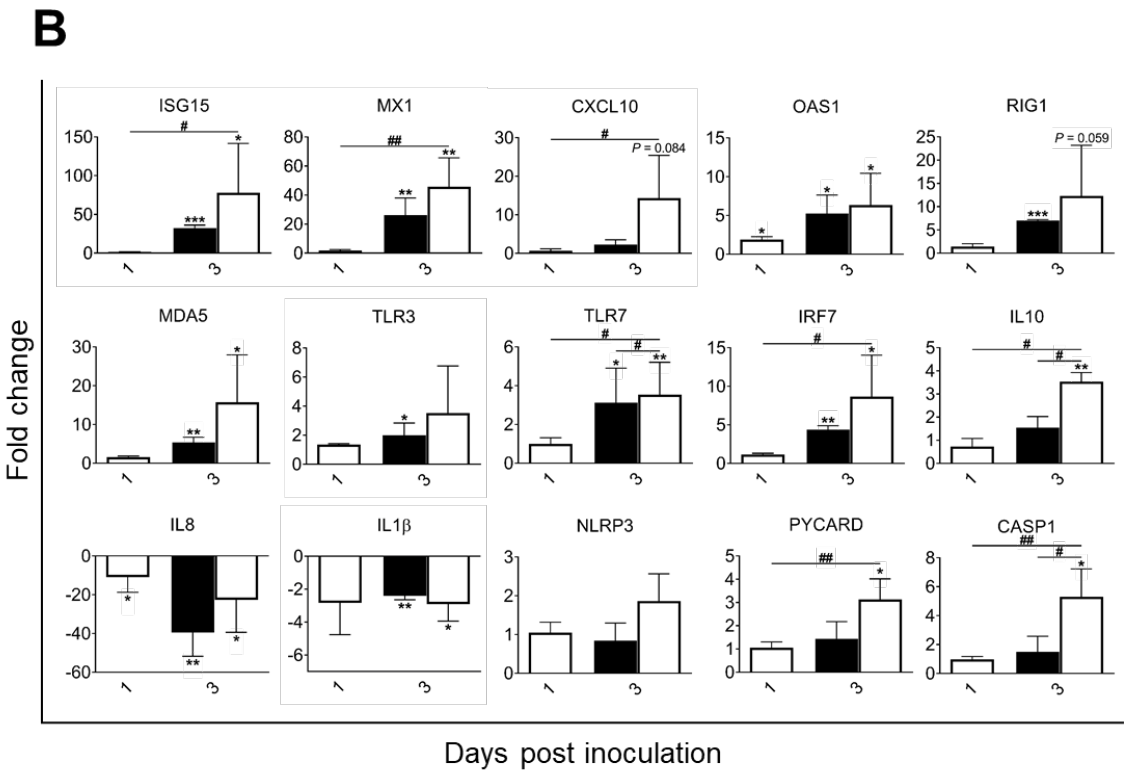

Figure 3-8. Kinetics of alpaca innate immune responses at the nasal submucosa in response to MERS-CoV Qatar15/2015. (**A**) The nasal submucosa of each alpaca (AP1, 2, 3, 7, 8, 9, 13, 14 and 15) was micro-dissected and areas underlying infected (orange)/non-infected (green) epithelium, as assessed by IHC (see the right panel), were selected and isolated for RNA extraction and conversion to cDNA. The Fluidigm Biomark microfluidic assay was used to quantify transcripts of innate immune genes at different dpi. After normalization, Fc values between controls and infected animals were calculated. The resulting heatmap shows color variations corresponding to log2 Fc values; blue for increased and red for decreased gene expression, respectively. The grey rectangles indicate no detection of the corresponding gene. TFs, transcription factors; CKs, chemokines; ADs, adaptors; RT, receptor. MERS-CoV+ and MERS-CoV-, MERS-CoV positive and negative epithelium areas as assessed by IHC, respectively. (**B**) Average Fc of ISGs, PRRs, IRF7, IL10, IL1β, IL8, NLRP3, CASP1and PYCARD genes in the submucosa underneath IHC MERS-CoV+ nasal epithelium (white bars) and IHC MERS-CoV- nasal epithelium (black bars). Data are shown as means of ±SD. Statistical significance was determined by Student's *t*-test. **P* < 0.05; ***P* < 0.01; ****P* < 0.001 when compared with the average values of non-infected alpacas (n = 3); #*P* < 0.05; ##*P* < 0.01; ###*P* < 0.001 when comparisons between groups are performed at different dpi.

ISGs are upregulated in the trachea of infected alpacas without increased endogenous IFNs mRNA

Innate immune response genes were further monitored along the URT. In trachea, IFNβ and IFNλ3 mRNA transcripts were not detected at any time post-inoculation including on 0 dpi. From 1 to 4 dpi, expression of IFNα and λ1 was slightly downregulated or unaltered, compared to basal levels found in non-infected controls (Figure 3-9A and Supplementary table 3-4E). Genes coding for ISGs (ISG15, MX1 and OAS1) and PRRs

(RIG1, MDA5 and TLR3) showed a significant mRNA upregulation mainly at 2 and 3 dpi. When compared with animals necropsied at 1 dpi, IRF7 was significantly upregulated (mean of 9 Fc) at 2 dpi (Figure 3-9A and B). The expression of IL10 was not significantly altered (Figure 3-9A and B). The induction of proinflammatory cytokine genes was inhibited or remained unchanged at all post-inoculation points (Figure 3-9A and B), except for AP6. This animal unlike other alpacas sacrificed at 2 dpi experienced an upregulation of proinflammatory cytokines and the inflammasome in the trachea. However, IL6 and PYCARD mRNA levels were almost unaltered (Figure 3-9A and B, and Supplementary table 3-4E). Excluding OAS1, AP6 was the animal with the highest expression levels of ISGs, RNA sensors, transcriptional factors and chemokines as shown in Figure 3-9A and B, and Supplementary table 3-4E. In that respect, AP6 could be considered as an out layer since, unlike other animals, it presented nasal discharges with the highest number of infected cells in nose and trachea and the highest viral loads in trachea (table 1 and Supplementary table 3-4A). Moreover, when compared to AP4 and AP5, which displayed nearly basal levels of CCL2 and CCL3 transcripts (Figure 3-9C and D), the tracheal submucosa of AP6 was moderately infiltrated by macrophages and lymphocytes (Figure 3-9E). This also provides indirect proof that the chemokines CCL2 and CCL3 were produced at the protein level and exerted chemoattraction.

A

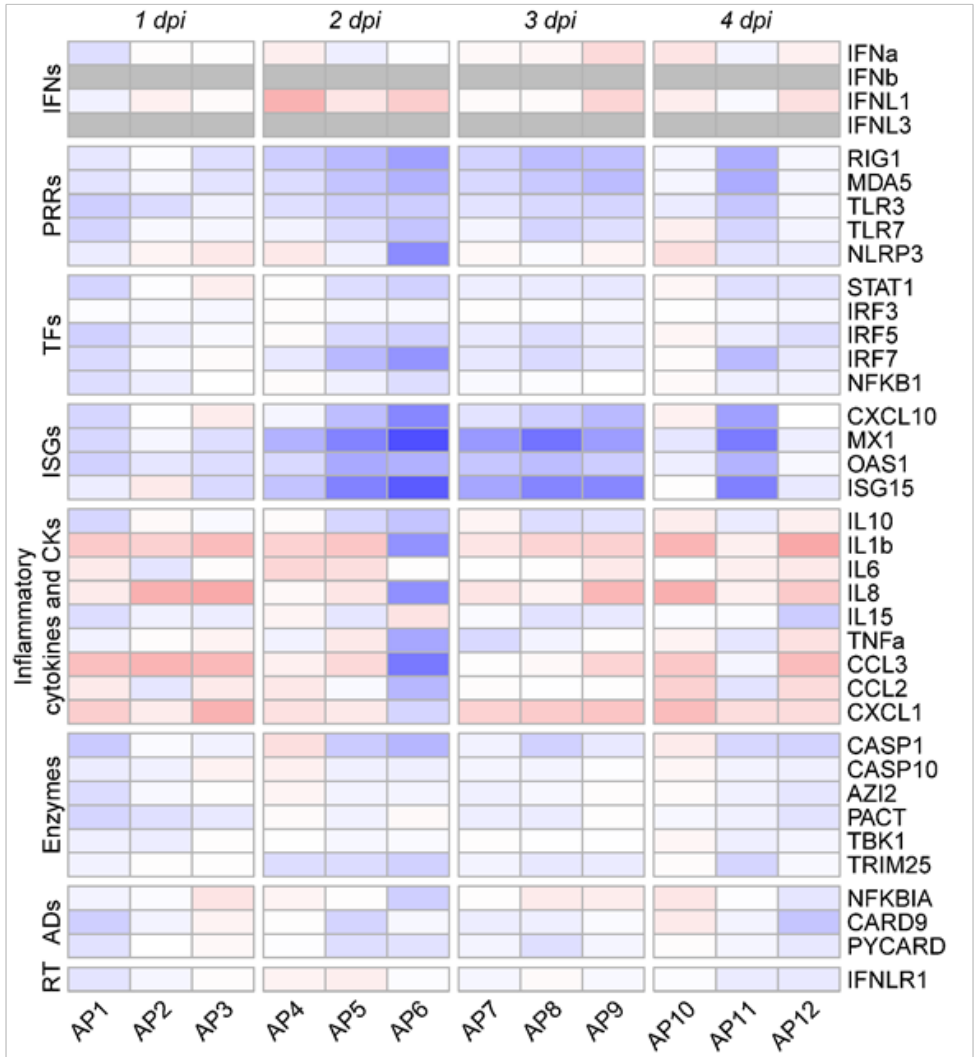
1 dpi
2 dpi
3 dpi
4 dpi
IFNs
PRRs
TFs
ISGs
Inflammatory cytokines and CKs
Enzymes
ADs
RT
IFNa
IFNb
IFNL1
IFNL3
RIG1
MDA5
TLR3
TLR7
NLRP3
STAT1
IRF3
IRF5
IRF7
NFKB1
CXCL10
MX1
OAS1
ISG15
IL10
IL1b
IL6
IL8
IL15
TNFa
CCL3
CCL2
CXCL1
CASP1
CASP10
AZI2
PACT
TBK1
TRIM25
NFKBIA
CARD9
PYCARD
IFNLR1
AP1
AP2
AP3
AP4
AP5
AP6
AP7
AP8
AP9
AP10
AP11
AP12

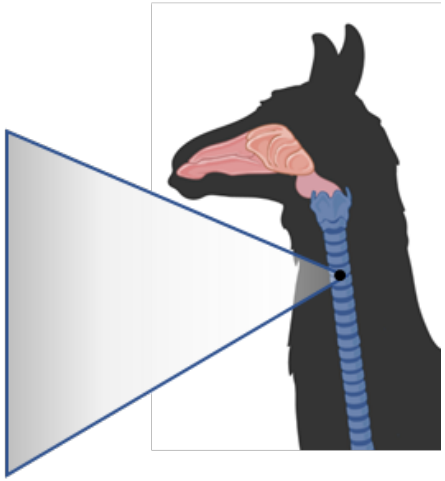

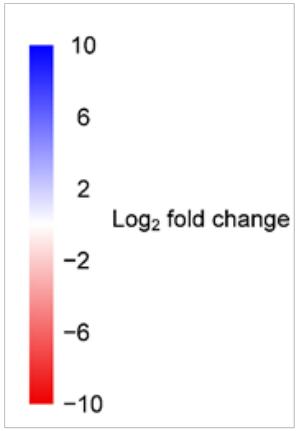
10
6
2
−2
−6
−10
Log2 fold change

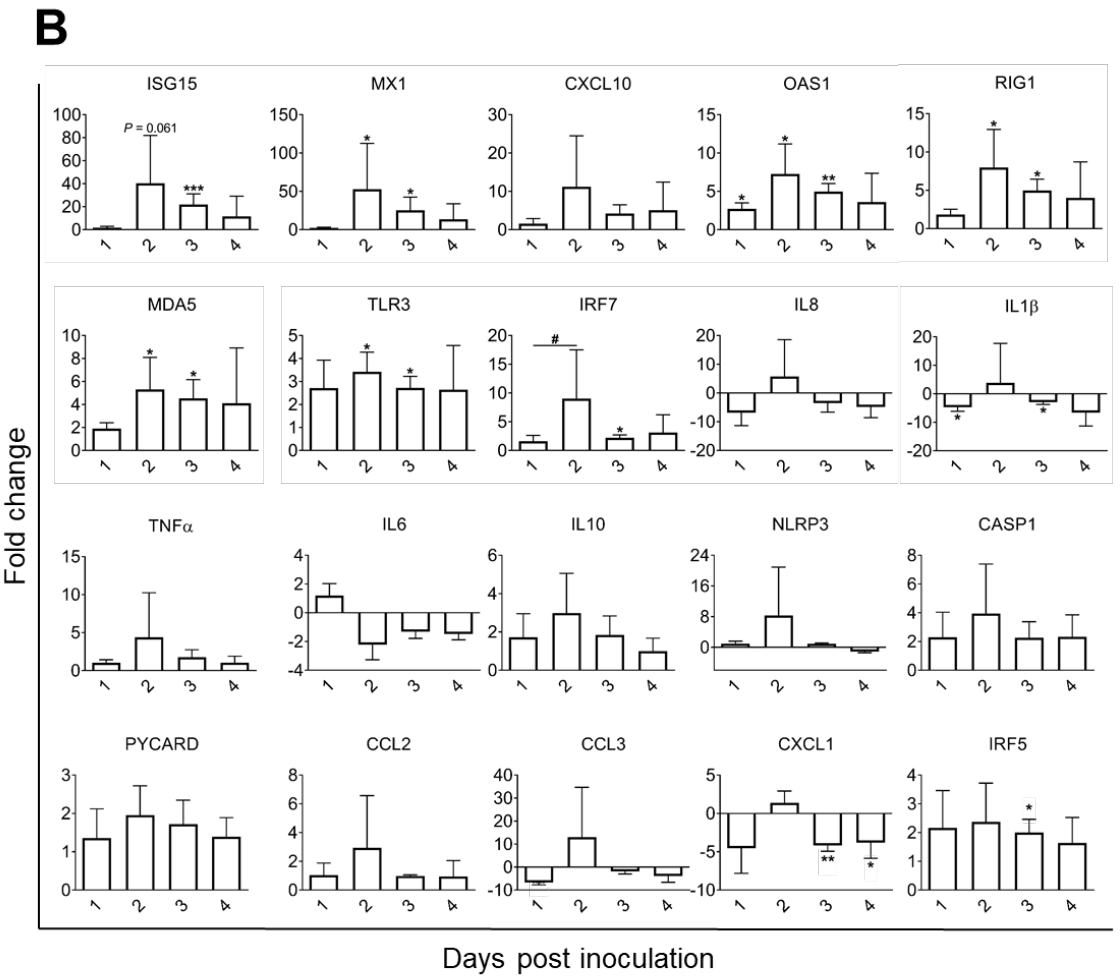

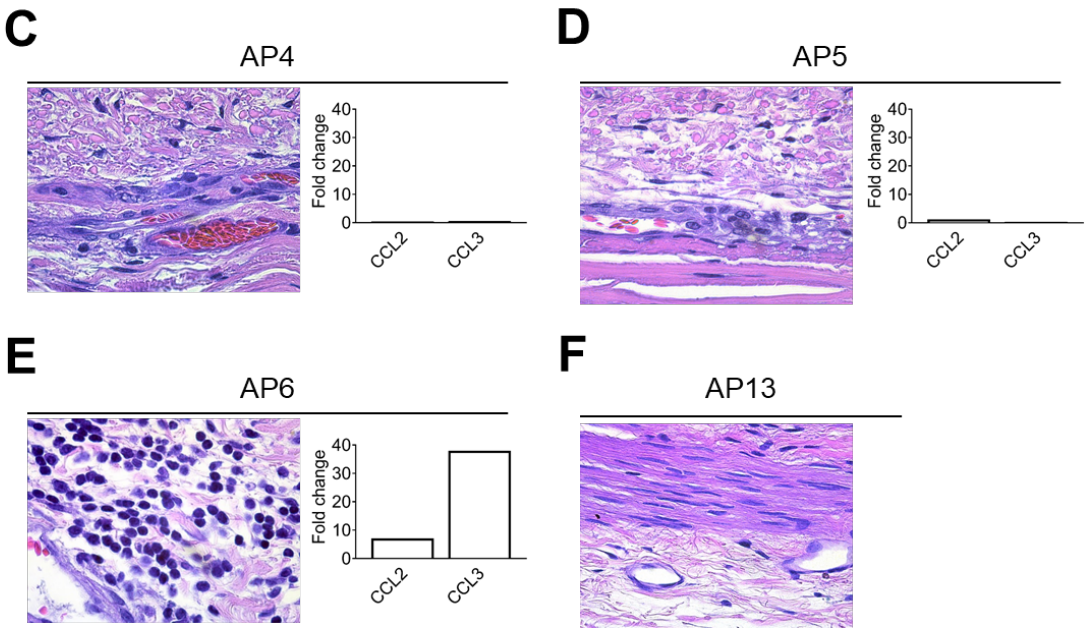

(Legend in the next page)

Figure 3-9. Kinetics of alpaca innate immune responses at the tracheal level in response to MERS-CoV Qatar15/2015. (**A**) Trachea samples were obtained by scraping MFPE sections from control (AP13-15) and infected alpacas (AP1-12), followed by RNA extraction and conversion to cDNA. A Fluidigm Biomark microfluidic assay was used to quantify transcripts of innate immune genes at different dpi. After normalization, Fc values between controls and infected animals were calculated. The resulting heatmap shows color variations corresponding to log2 Fc values; blue for increased and red for decreased gene expression, respectively. The grey rectangles indicate no detection of the corresponding gene. TFs, transcription factors; CKs, chemokines; ADs, adaptors; RT, receptor. (**B**) Average Fc of ISGs, PRRs, transcription factors, inflammatory cytokines and chemokines, enzymes and adaptor genes in trachea. Data are shown as means of ±SD. Statistical significance was determined by Student's *t*-test. **P* < 0.05; ***P* < 0.01; ****P* < 0.001 (n = 3) when compared with non-infected alpacas (n = 3). On 2 dpi, no inflammatory cells were observed in the tracheal submucosa of AP4 (C) and AP5 (D) (see H/E stained MFPE tracheal section at the left). The graph at the right depicts Fc of mRNA transcripts for CCL2 and CCL3 in relation to control animals. (E) Infiltration of monocytes and lymphocytes in the tracheal submucosa of AP6 (see H/E stained MFPE tracheal section at the left) was associated with increased mRNA transcripts of CCL2 and CCL3 (see the bar graph at the right). (F) No inflammatory cells were observed in the tracheal submucosa of the control animal.

Early induction of CCL2 and CCL3 correlates with infiltration of macrophages and lymphocyte like cells in the lungs of infected alpacas

Despite low infectivity of MERS-CoV in the LRT, infiltration of leukocytes was observed suggesting that cytokines and chemokines are at play. At the lung level, IFNα and IFNλ1 were expressed on 0 dpi in non-infected controls. In response to MERS-CoV, transcripts of IFNα and IFNλ1 fluctuated around basal levels (Figure 3-10A and Supplementary table 3-4F). IFNλ3 and IFNβ mRNAs were not detected in any of the animals including controls. Upregulation of ISGs (ISG15, MX1 and OAS1) and IRF7 started at 1 dpi, reached a peak at 2 dpi and weaned at 4 dpi. RIG1 and MDA5 were unevenly upregulated with a lower intensity than for other tissues (Figure 3-10B and Supplementary table 3-4F). Remarkably, NLRP3 was moderately but significantly upregulated at 1, 2 and 4 dpi concomitant with increased levels of TNFα and IL1β at 1 dpi (Figure 3-10A and B). However, transcription of CASP1 remained unaltered and the PYCARD gene was downregulated at 1, 2 and 4 dpi or unaltered at 3 dpi (Figure 3-10A and B, and Supplementary table 3-4F). IL15, a NKs activator cytokine, was significantly upregulated at 1 and 2 dpi while expression patterns of other proinflammatory cytokines varied between animals and days of infection (Figure 3-10A and B, and Supplementary table 3-4F).

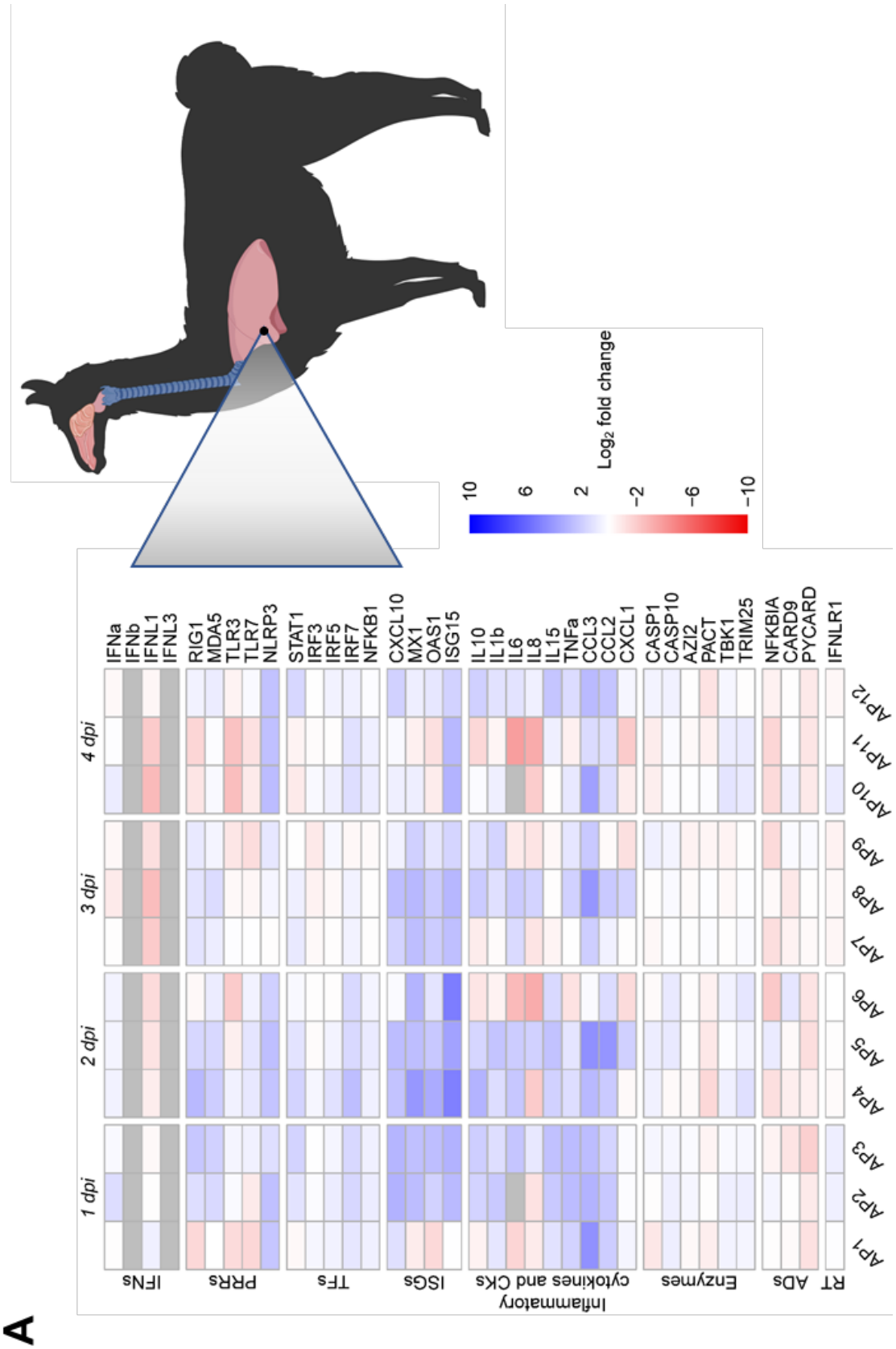
A
1 dpi
2 dpi
3 dpi
4 dpi
AP1
AP2
AP3
AP4
AP5
AP6
AP7
AP8
AP9
AP10
AP11
AP12
IFNs
IFNa
IFNb
IFNL1
IFNL3
PRRs
RIG1
MDA5
TLR3
TLR7
NLRP3
TFs
STAT1
IRF3
IRF5
IRF7
NFKB1
ISGs
CXCL10
MX1
OAS1
ISG15
Inflammatory cytokines and CKs
IL10
IL1b
IL6
IL8
IL15
TNFa
CCL3
CCL2
CXCL1
Enzymes
CASP1
CASP10
AZI2
PACT
TBK1
TRIM25
ADs
NFKBIA
CARD9
PYCARD
RT
IFNLR1
Log2 fold change
10
6
2
−2
−6
−10

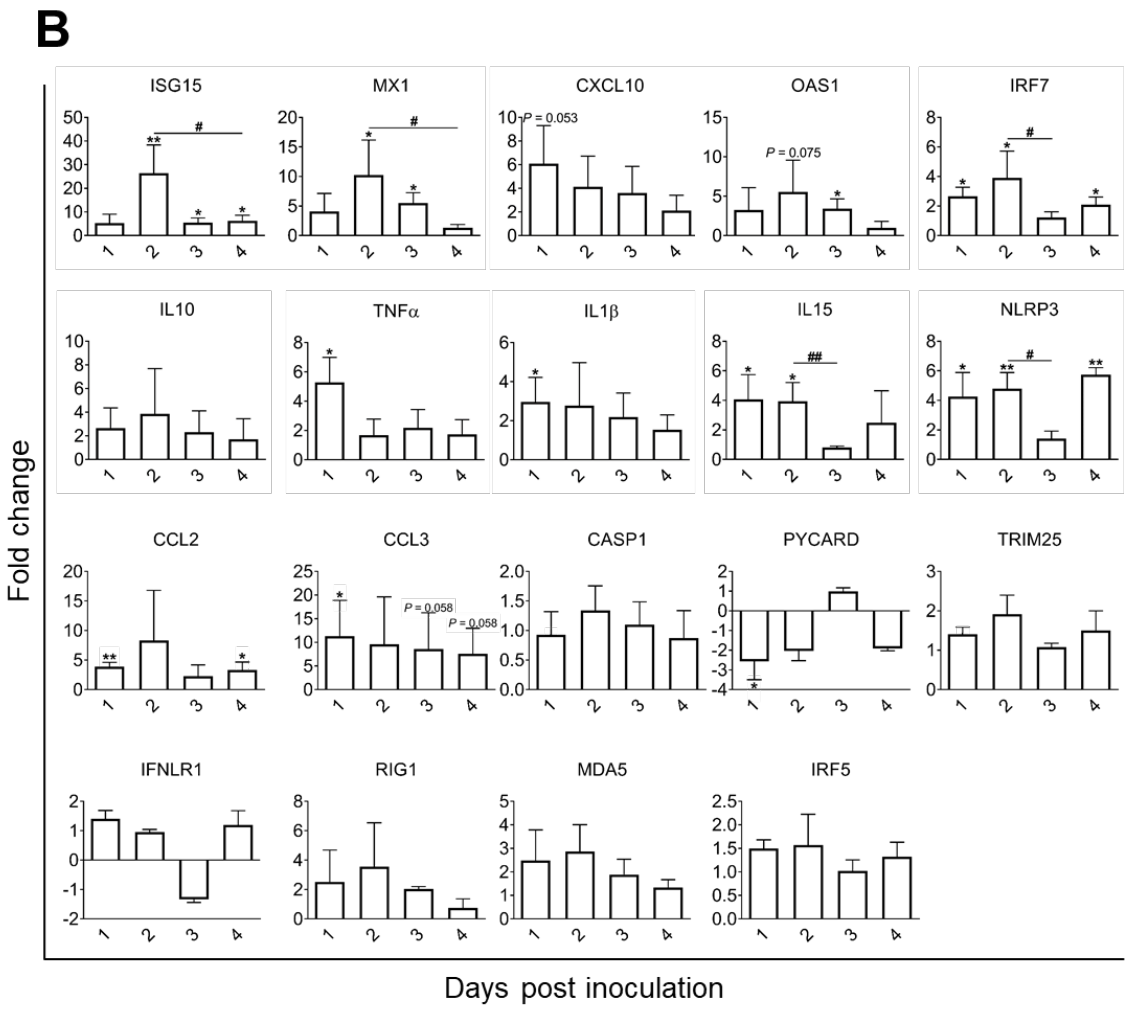

Figure 3-10. Kinetics of alpaca innate immune responses in the lungs following MERS-CoV Qatar15/2015 infection. (**A**) The lung sample of each infected alpaca (AP1 to AP15) was isolated for RNA extraction and conversion to cDNA. A Fluidigm Biomark microfluidic assay was used to quantify transcripts of innate immune genes at different dpi. After normalization, Fc values between controls and infected animals were calculated. The resulting heatmap shows color variations corresponding to log2 Fc values; blue for increased and red for decreased gene expression, respectively. The grey rectangles indicate no expression of the corresponding gene. TFs, transcription factors; CKs, chemokines; ADs, adaptors; RT, receptor. (**B**) Average Fc of ISGs, PRRs, transcription factors, inflammatory cytokines and chemokines, enzymes, adaptor and the IFN receptor genes in lung. Data are shown as means of ±SD. Statistical significance was determined by Student's *t*-test. **P* < 0.05; ***P* < 0.01; ****P* < 0.001 (n = 3) compared with non-infected alpacas (n = 3); #*P* < 0.05; ##*P* < 0.01; ###*P* < 0.001 (n = 3) when comparisons between groups are performed at different dpi.

In addition, CCL2 and CCL3 were moderately to highly upregulated at most of the time points (Figure 3-10A and B). All animals showed very mild infiltration of leukocytes in the alveoli in response to MERS-CoV (Figure 3-11B and 12B). Remarkably, AP6 showed accumulation of leukocytes without a notable induction of CCL2 and CCL3 mRNAs (Figure 3-12A and B). Moreover, this animal was the highest producer of

these chemoattractant chemokines in trachea. Nonetheless, the number of infiltrating leukocytes correlated with the induction of CCL2 (r = 0.62, *P* = 0.0236) and CCL3 (r = 0.59, *P* = 0.0323) as shown in Figure 3-12C and D. When considering AP6 as an out layer, correlations became stronger for both CCL2 (r = 0.72, *P* = 0.0077) and CCL3 (r = 0.87, *P* = 0.0002) as shown in Figure 3-11A. Overall, ISGs were induced in the absence of IFN gene expression suggesting an endocrine effect of IFNs produced in the nasal epithelia. In addition, despite transient accumulation of leukocytes correlating with induction of CCL2 and CCL3 in the lung, exacerbation of inflammatory responses did not occur.

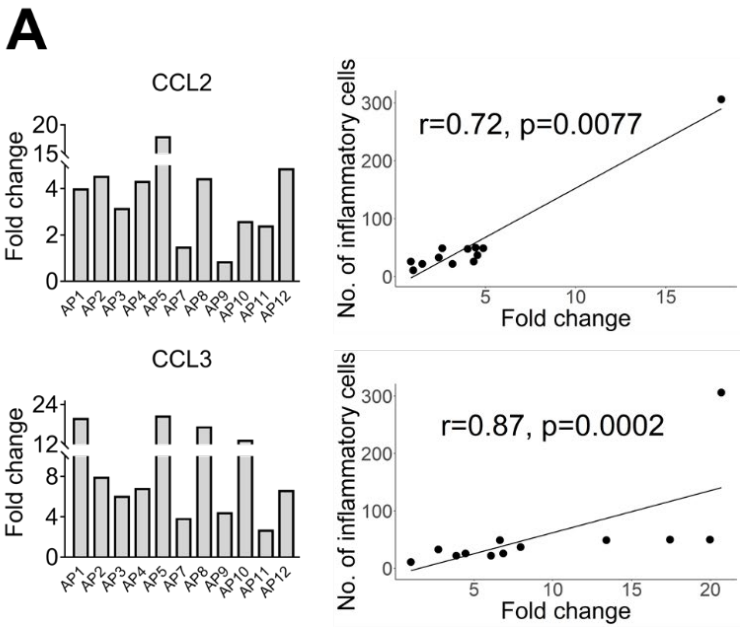

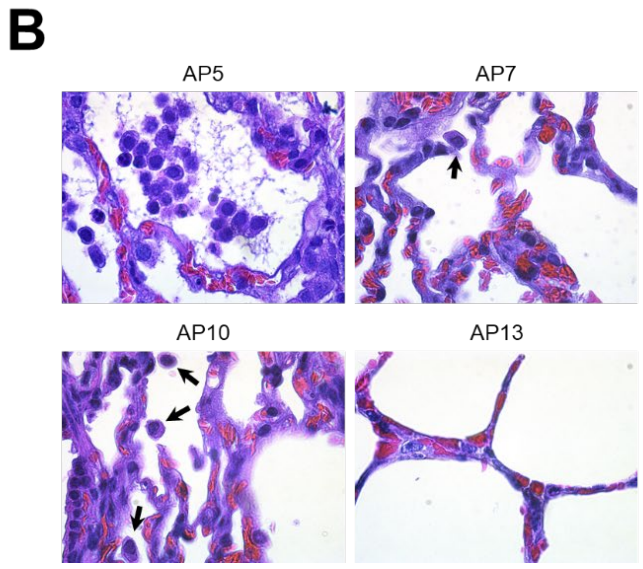

Figure 3-11. Infiltration of leukocytes in alveoli are correlated with upregulation of CCL2 and CCL3 mRNA. (**A**) Relative expression of CCL2 and CCL3 mRNA (Bar graphs at the left) was performed with a microfluidic PCR assay in the lung of alpacas (except AP6, see text). Leukocytes were counted in 3 microscopic fields (400X) per lung section in all animals (except AP6), including non-infected controls. Relative expression levels of CCL2 and CCL3 were plotted against the number of inflammatory cells (dot plot at the right). Correlation coefficients were established using the Spearman's correlation test (right panel). (**B**) The number of leukocytes in alveoli was the highest in AP5, lower in AP10 (arrows), occasional in AP7 (arrow) and hardly detectable in AP13. Original magnification: ×1000 for all samples.

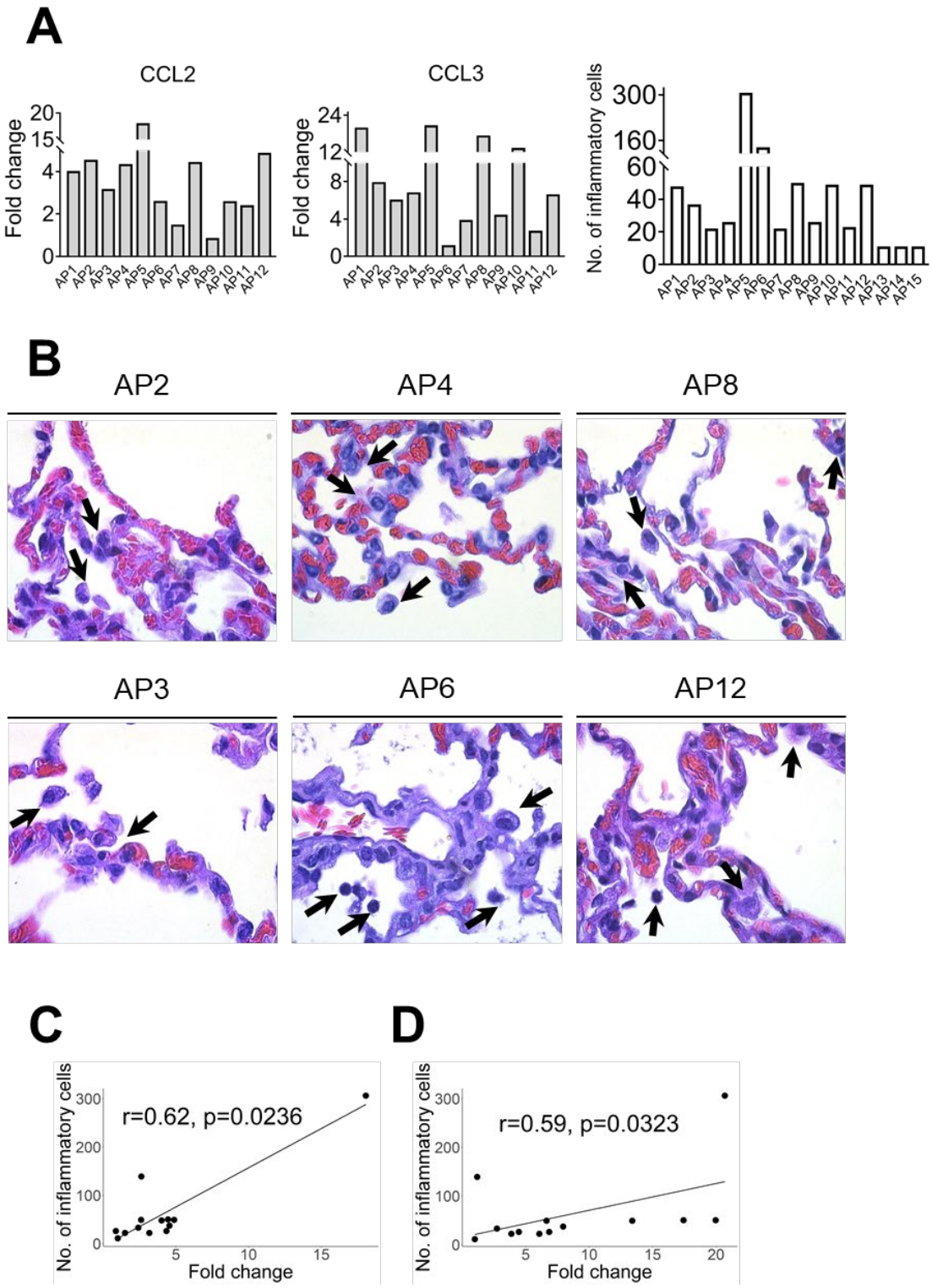

Figure 3-12. Correlation between the relative expression of chemokines (CCL2 and CCL3) and the number of inflammatory cells infiltrating lungs in alpacas. (A) Relative expression of CCL2 and CCL3 mRNA was performed with a Fluidigm Biomark microfluidic assay in the lung of alpacas (including AP6). Inflammatory cells were counted in 3 microscopic fields (400X) per MFPE lung section in all animals, including non-infected controls. (B) The number of inflammatory cells in alveoli was high in AP6, lower in AP4, 8 and 12 (arrows), occasional in AP2 and 3 (arrow). Original magnification: ×1000 for all samples. Relative expression levels of (C) CCL2 and (D) CCL3 were plotted against the number of inflammatory cells in lungs. Correlation coefficients were established using the Spearman's correlation. MFPE: methacarn-fixed paraffin-embedded.

Genes of the NF-κB pathway and IRF5 are transcriptionally unaltered in respiratory tissues during MERS-CoV infection

Transcription of the NF-κB p50 subunit (NFKB1) and some important regulators of the NF-κB pathway were checked along URTs and LRTs. These regulators included two enzymes, AZI2 and TBK1, downstream of the RLRs and TLR signaling pathways, essential for the phosphorylation of NF-κB, the NF-κB inhibitor NFKBIA and an adaptor CARD9 that mediates signals from C-type lectins to regulate the NF-κB pathway (Figure 3-2). All these genes were expressed at basal levels in the nasal mucosa, submucosa, trachea and lung of control non-infected alpacas. NFKB1, AZI2 and TBK1 were only marginally induced or remained unaltered in the nasal epithelia; however, NFKBIA and CARD9 were expressed at basal levels or even slightly downregulated in all the tissues. All the above mentioned genes were fluctuating around basal transcriptional levels across alpaca respiratory tracts (Figure 3-6A, 7A, 9A, 10A and Supplementary table 3-4 C, D, E and F) indicating that the NF-κB mediated signaling pathway was not exacerbated or downregulated in response to MERS-CoV. Moreover, IRF5, an inducer of TNFα and IL6 as well as an important factor for the polarization of M1 macrophages, was only slightly but significantly upregulated in the nasal epithelium (2 dpi) and submucosa (3 dpi). In all other tissues and, in particular lung, the majority of animals did not reach the threshold of 2 Fc for IRF5 (Figure 3-10B and Supplementary table 3-4F).

Discussion

To the authors' knowledge, the present study represents the first innate immune investigation performed *in vivo* in natural reservoir/intermediate hosts upon MERS-CoV infection. As camelids are the primary zoonotic reservoirs for human infection, it is essential to gain insight into the potential mechanisms of asymptomatic manifestation since they can unravel targets for prophylactic treatments in susceptible hosts. In the present study, all experimentally inoculated alpacas were successfully infected, as genomic viral UpE, subgenomic M mRNA and the N protein could be detected in most of the tissues examined by IHC, RT-qPCR or micro fluidic PCR assays from the URT and LRT at 1 to 4 dpi. This proved that the MERS-CoV Qatar15/2015 strain had spread and in some instance replicated throughout the whole respiratory tracts, although mainly at the URT where the virus receptor DPP4 is most abundant (Widagdo et al., 2016b). Acknowledging that respiratory mucosal epithelial cells are the main primary target for MERS-CoV and the paucity of data on the effect *in vivo* of the virus to the mucosal barrier on humans and other laboratory species (mainly human DPP4 transgenic or transduced mice and non-human primates) a special attention was given here to monitor innate immune responses occurring during the first 4 days of infection in the nasal epithelium of alpacas and the possible repercussions of these responses in the respiratory tract.

In mucosa, pathogens are sensed by PRRs leading to the production of type I and III IFNs via IRFs. In turn, IFNs can activate through the JAK-STAT pathway, in an autocrine, paracrine or endocrine manner, transcription of various antiviral and regulatory ISGs including also PRRs and IRFs. Fine tuning of these responses is paramount in determining the outcome of viral infectious diseases (Lazear et al., 2019). In MERS-CoV infected alpacas, during the first 24h, apart from IFNβ which started to be induced, type I and III IFNs were not altered in the nasal mucosa when compared to control animals. This short period seems to be crucial for the virus to establish a productive infection in alpacas for at least 5 to 6 days (Adney et al., 2016a) by delaying host protective mechanisms such as activation of PRR pathways (Chang et al., 2020; Channappanavar et al., 2019b; Zhao et al., 2020). Nonetheless, and only in the nasal epithelium, transcription of all type I and III IFNs peaked simultaneously at 2 dpi and weaned progressively. This wave of IFNs was concomitant with the induction of ISGs, PRRs and IRF7 not only at the nasal epithelial barrier and its underlying submucosa but also in trachea and lungs where IFN mRNAs were never detected or induced.

Therefore, the effect of the IFN response at the nasal mucosa may extend to distant respiratory tissues in a paracrine or endocrine manner. In that respect, in mice, IFNλ produced in the URT prevents dissemination of influenza virus to the lung (Klinkhammer et al., 2018).

The use of IHC and microfluidic PCR assays combined with LCM permitted to compare, in the same and different animals, areas of the nasal epithelium with high and low viral loads. Heavily infected mucosal areas were responsible for the highest induction of type III IFNs. Although markedly induced, type I IFNs did not significantly correlated with tissue viral loads. Consistent with this IFN production, the number of MERS-CoV infected cells detected by IHC was maximal on 2 dpi and decreased over time. However, all infected alpacas shed infectious viral particles in the nasal cavity from 1 dpi onwards according to previous studies (Adney et al., 2016a; Crameri et al., 2016a). This might be due to a high accumulation of virus in the nasal cavity which may take a few days to clear. Remarkably, results obtained herein contrast with those found in human epithelial cells and respiratory explants since the induction of type I and III IFNs was limited or inhibited in response to MERS-CoV (Chan et al., 2013b; Comar et al., 2019; Zielecki et al., 2013). The dampened IFN priming in humans is likely due to the role of IFN antagonism by MERS-CoV accessory proteins (Comar et al., 2019; Niemeyer et al., 2013; Rabouw et al., 2016; Shokri et al., 2019), through which virus replication is facilitated. It is important to note that the MERS-CoV strain (Qatar15/2015) used herein is from human origin and, unlike some dromedary isolated African strains, it does not display any deletions in the above-mentioned non-structural proteins (Chu et al., 2018). Therefore, alpacas are able to overcome IFN inhibitory mechanisms in a relative short time with the induction of antiviral or IFN positive regulatory ISGs. Nonetheless, the prominent manifestation of MERS in humans occurs in lungs with a massive inflammation provoked by infiltration of macrophages and lymphocytes (Alsaad et al., 2018). To the contrary, and although AP6 experienced discrete nasal discharges and displayed large numbers of infected nasal epithelial cells, alpacas only exhibited transient mild and focal infiltration of lymphocytes, macrophages and neutrophils in response to MERS-CoV. Such infiltrations were mainly observed on 2 dpi and gradually resolved afterwards. These findings suggested a rapid fine tuning of specific mechanisms to control inflammation mediated essentially by the mucosal barrier, leading to an efficient innate immune response. Indeed, type III

IFNs are known to induce milder inflammatory responses than IFNβ (Lazear et al., 2019) and IL10 is an anti-inflammatory cytokine (Ouyang et al., 2011). Furthermore, recent studies in mice indicate intricate mechanisms between IFNλ and IL10 via DCs conditioning protective mucosal immunity against influenza virus (Hemann et al., 2019). In this view, it is noteworthy to mention that pDC are seemingly the only cell-type that produce *in vitro* type I and III IFNs after MERS-CoV infection in humans (Scheuplein et al., 2015). By contrast, *in vivo*, pDCs which predominantly localize in the submucosa are not the main IFN producers (Ali et al., 2019; Mascarell et al., 2008). Due to the lack of specific cell markers for DCs in alpacas, detection of these cells in tissues and their contribution to innate immunity could not be performed. Nonetheless, a strong positive correlation between IFNλ1,3 and IL10 mRNA levels was observed in the nasal epithelium of alpacas and this could reflect a physiological cross-regulation between these structurally related cytokines upon MERS-CoV infection. By contrast, the weak correlation between IFNβ and IL10 mRNA induction suggests that only type III IFNs are directly or indirectly mediating anti-inflammatory action. Furthermore, IL10 was significantly up regulated, although at moderate levels, in the nasal submucosa underlying heavily infected epithelial cells. Moreover, IRF5 known to be a pro-inflammatory transcription factor and a key element in the M1 polarization of macrophages (Krausgruber et al., 2011; Weiss et al., 2013) was only slightly induced in the nasal mucosa and submucosa on 2 and 3 dpi. However, no IRF5 mRNA increased in the lung despite infiltration of mainly macrophages and lymphocytes as early as 1 dpi. Accordingly, CCL2, CCL3, CXCL10 and TNFα were induced in the lung in the absence of type I IFNs, as found for MERS-CoV infected human monocyte-derived macrophages (Zhou et al., 2014). With the observation that other pro-inflammatory cytokines are either weakly or not induced, it is suspected that inflammatory M1 macrophages are not abundant in the lung of infected alpacas. Also, IL15, an activator and attractor of NK cells and macrophages (Verbist and Klonowski, 2012), was only induced in lung as soon as 1 dpi, suggesting a role for clearance of the virus by these cells. Strikingly, NLRP3 mRNA was more abundant in the lung (with the exception of AP6 in trachea), maybe due to the presence of infiltrating macrophages where NLRP3 is mostly produced (Guarda et al., 2011; Shao et al., 2015). However, CASP1 and PYCARD, the two other components of inflammasome, were not induced. This scenario, combined with a discrete upregulation of IL1β and IL6 in some animals, will

not probably result in a cytokine storm in the lung. Accordingly, in other respiratory tissues, the major proinflammatory cytokines were occasionally mildly induced, suggesting also a functional but attenuated NF-κB signaling (Hayden and Ghosh, 2004). Moreover, during infection, genes involved in the regulation of the NF-κB cascade (AZI2, TBK1 and NFKBIA) and NFKB1were transcriptionally unaltered in all the respiratory tract of alpacas preventing acute inflammation in response to MERS-CoV.

In a mice model of MERS-CoV (Channappanavar et al., 2019b), IFNs production and MERS-CoV replication peaked simultaneously in lungs at 2 dpi resulting in a sublethal infection. While early induction or treatment with IFNβ were crucial for virus clearance and induction of protective immunity, late administration of IFNs led in lungs to enhanced infiltrations of monocytes, macrophages, neutrophils, expression of proinflammatory cytokines and increased mortality. Also, indirect proof was given that IFNs synthesis was under sensing of TLR7 but not MAVS in airway epithelial cells. However, this study did not report the effect of MERS-CoV infection in the URT (Channappanavar et al., 2019b). Benefits of early type I IFN treatment were also shown for non-human primates (Chan et al., 2015b) but IFN therapy on humans has failed so far certainly because it was applied essentially on critically ill patients (Arabi et al., 2020). Thus, some differences are noticed between a MERS-CoV sublethal infection in mice and that occurring in a natural host. Here, we highlighted the essential role of the nasal mucosa as a main producer of IFNs upon MERS-CoV infection driving in combination with IL10 a mild inflammatory response along the respiratory tract. The observation in alpacas of a dimmed NLRP3 inflammasome is consistent with that found in bat primary immune cells infected in vitro with MERS-CoV (Ahn et al., 2019), suggesting a primary role in the control of inflammation in reservoir/intermediary hosts despite high viral loads. Further, this study provides mechanistic insights on how innate immunity overcomes a MERS-CoV infection. A proposed model of cytokine and signaling pathways interactions resuming innate immune responses upon MERS-CoV infection in the respiratory tract of alpacas is depicted in Figure 3-13. Inherent to any study performed with large outbred animals under ABSL3 containment, the present study suffers some limitations. First, the number of animals used was kept to minimal to avoid prolonged exposure of personnel during sampling and necropsies hindering some statistical significances with variations between animals. Second, the LCM and microfluidic PCR allowed determination of gene expression at the tissue but not the

single cell level. This combined with the lack of antibodies defining cell types in alpaca and working in IHC impeded further characterization of DCs and leukocytes in tissues.

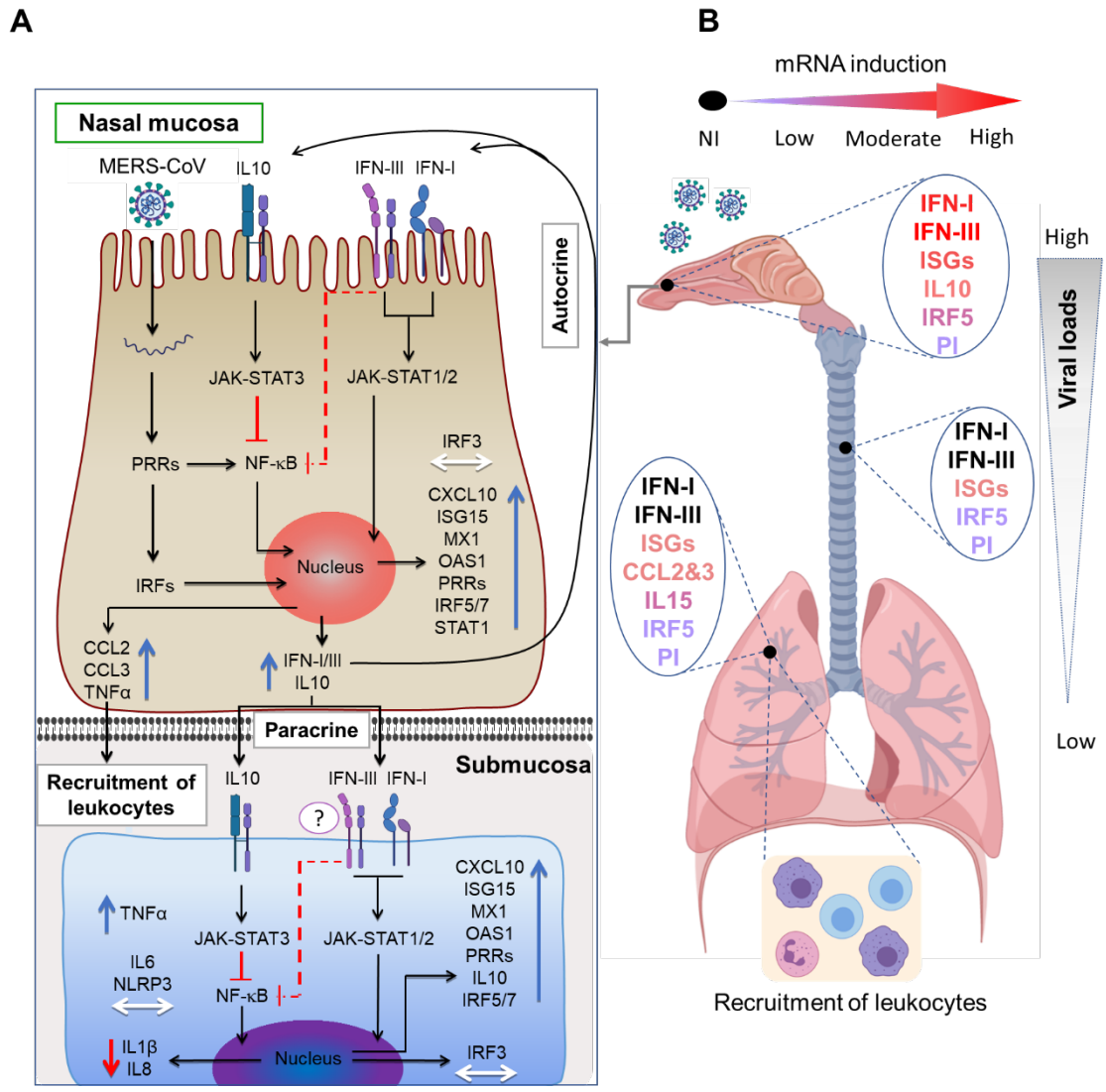

Figure 3-13. Proposed mechanistic model for MERS-CoV-induced protective innate immune responses in alpaca respiratory tracts. (**A**) Upon MERS-CoV infection of nasal epithelial cells, PRRs and IRFs are engaged to induce IFNs and ISGs exerting their effects in an autocrine or paracrine manner. Upregulation of IL10 combined with the action of type III IFNs will result in a dimmed synthesis of proinflammatory cytokines under NF-κB control. Induced chemokines lead to focal, mild infiltration of leukocytes. The paracrine effect of IFNs is evidenced in the nasal submucosa where ISGs are upregulated without endogenous induction of IFNs. IL10 and type III IFNs will act on the NF-κB pathway preventing production of IL8 and IL1β mRNAs depriving the NLRP3 inflammasome of its substrate. Slight increased levels of IRF5 mRNAs will indicate the presence of few M1 macrophages in the submucosa. Blue, red and white arrows indicate upregulation, downregulation and unaltered gene transcription respectively. (**B**) Concomitant to decreased viral loads, transcription of ISGs is lowered in trachea and lungs where IFNs are not induced. Infiltration of mainly mononuclear leukocytes occurs in the lungs as a result of chemokine synthesis in the absence of IRF5 induction but upregulation of IL15. Thus, reduced number of M1 macrophages and activation of NK cells will contribute to a controlled inflammation and clearance of the virus. PI, Pro-inflammatory cytokines; NI, not induced.

Supplementary tables 3-1, 3-2, 3-3, 3-4 and 3-5 are available online at:

https://drive.google.com/drive/folders/1RCPD9VoB9MYpHddiB8fkMb3vb6xgdkIr?usp=sharing

Chapter 4

Study II

Enhanced replication fitness of MERS-CoV clade B over clade A strains in camelids explain the dominance of clade B strains in the Arabian Peninsula

(manuscript submitted)

Introduction

MERS-CoV is a severe respiratory disease with a zoonotic origin representing a significant threat worldwide. The Arabian Peninsula continues to be the global epicenter of the disease (Memish et al., 2020; National Events et al.). While most cases have been documented in the KSA, a travel associated outbreak in South Korea in 2015 reminded that MERS-CoV is of global concern (Kim et al., 2017; Oh et al., 2018). Due to negative impacts on public health and the economy, MERS-CoV is listed as one of the WHO Research and Development Blueprint priority pathogens. So far, the dromedary camel is the only confirmed source of zoonotic infection, while new world camelids (alpacas and llamas) can also be infected by MERS-CoV under both natural and experimental conditions (Adney et al., 2016a; Crameri et al., 2016a; David et al., 2018; Reusken et al., 2016; Vergara-Alert et al., 2017a). Human acquisition is primarily due to close contact with infected camels (Azhar et al., 2014). Limited human-to-human transmission has been reported within families; contagion mostly occurring in health-care settings (Killerby et al., 2020).

MERS-CoV is phylogenetically divided into three major clades, temporarily named clades A, B and C (Alharbi et al., 2015; Chu et al., 2018; Kiambi et al., 2018). Sequence examination of various MERS-CoVs revealed that nowadays only clade B viruses are circulating in the Arabian Peninsula and have replaced clade A in humans and dromedary camels (Alharbi et al., 2015; El-Kafrawy et al., 2019; Naeem et al., 2020). Therefore, clade B viruses might possess an evolutional advantage against clade A isolates, exhibiting enhanced replicative fitness when infecting human/dromedary hosts. However, data characterizing phenotypic and pathogenic differences between these two clades of MERS-CoV are scarce. Recently, Wang et al. (Wang et al., 2020) showed that a clade B virus (ChinaGD01) led to more weight loss, severe lung lesions and higher lung viral titers in hDPP4 transduced mice than did the prototype virus EMC/2012 (clade A). However, in a previous study, apparent contradictory results were reported since clade A and B viruses exhibited comparable lung viral titers and lesions in hDPP4 transduced mice (Chu et al., 2018). Also, there was no significant difference in replication competence of these two clade viruses in human bronchial and lung explants (Chan

et al., 2014). Despite its role in antagonizing IFN defense mechanisms (Matthews et al., 2014; Yang et al., 2013, 2015), the accessory protein ORF4b is probably not implicated in virus replication *in vivo* (Chu et al., 2018). Rather, nsps, which also interfere with IFN production (Lokugamage et al., 2015; Mielech et al., 2014a) are thought to play a more important role in virus replication than accessory proteins. In that respect, clade B specific mutations were observed in ORF1ab (Wang et al., 2020). Also, the role of ORF4a as an IFN antagonist was not assessed *in vivo* but mainly determined under *in vitro* conditions (Comar et al., 2019; Niemeyer et al., 2013; Siu et al., 2014; Yang et al., 2013). A recombinant virus lacking ORF4a showed increased expression levels of type I and III IFNs and slightly decreased replication in human airway epithelium-derived A549 cells (Comar et al., 2019). Nevertheless, whether deletions/mutations of these viral factors lead to the increased zoonotic potential of clade B strains lacks direct proof in reservoir hosts.

Recently, we characterized the pathogenesis of a clade B MERS-CoV strain (Qatar15/2015) in an alpaca model (Chapter 3). Upon MERS-CoV infection, a few infected nasal epithelial cells could be detected by IHC as soon as 1 dpi. Nasal tissues were maximally infected at 2 dpi and infection extended to the bronchus where some infected epithelial cells were observed. On the following days, the virus was gradually cleared. Alpacas responded at the peak of MERS-CoV infection with an early and transient type I and III IFN responses detected only in the nasal mucosa concomitant with an induction of antiviral ISGs along the whole respiratory tract. Exacerbated inflammation was not observed in these animals, which displayed attenuated NF-κB and NLRP3 signaling cascades in conjunction with increased mRNA levels of the anti-inflammatory cytokines IL10 and type III IFNs. To assess differences in virulence, replication and pathogenesis that could explain field observations that MERS-CoV clade B strains have replaced clade A in camelids, we selected an early epidemic clade A isolate, EMC/2012 (van Boheemen et al., 2012), and a clade B strain, Jordan-1/2015 (Lamers et al., 2016), to experimentally infect alpacas. The Jordan-1/2015 strain harbors a 16 aa deletions in ORF4a suspected to affect the binding of dsRNA (Lamers et al., 2016). Therefore, this experimental set up also allowed to gain insights on the role of ORF4a in MERS-CoV pathogenesis. Alpacas

inoculated with Jordan-1/2015 exhibited higher MERS-CoV loads in the respiratory tract and larger viral shedding, demonstrating the increased replicative fitness of clade B strains in a camelid host. Thus, taken together, with results obtained with the Qatar15/2015 strain (Chapter 3), a rational explanation is suggested for the predominance of clade B strains in the Arabian Peninsula. In addition, mRNA expression of cytokines and chemokines along the respiratory tract was monitored for both strains during three consecutive days.

Material and methods

Ethics statement

All animal experiments were approved by CEEA-IRTA and by the Ethical Commission of Animal Experimentation of the Autonomous Government of Catalonia (file Nº FUE-2018-00884575 – Project Nº10370). The work with infectious MERS-CoV was performed in BSL3 of the Biocontainment Unit of IRTA-CReSA in Barcelona, Spain.

Cell culture and viruses

MERS-CoV EMC/2012 (GenBank Accession JX869059) and Jordan-1/2015 (GenBank Accession KU233364) isolates were propagated in Vero E6 cells and titrated, as previously described (Vergara-Alert et al., 2017a).

Aa alignment of MERS-CoV proteins from clade A and B strains.

The aa sequences from thirteen MERS-CoV strains encompassing six lineages (including the EMC/2012 and the Jordan-1/2015 strains) were aligned using the UniProt alignment tool (https://www.uniprot.org/align/). Details including accession number of the strains are provided in table 1.

Table 1. Information of the different MERS-CoV strains used for aa sequence alignment

Name of strain	Origin	Clade	Lineage	Accession Number
EMC/2012	Human	A	1	JX869059
Jordan-N3/2012	Human	A	1	KC776174
Camelus dromedarius/2015	Dromedary camel	A	2	KX108943
NRCE-HKU205/2013	Dromedary camel	A	2	KJ477102
KSA_CAMEL-376	Dromedary camel	B	1	KJ713299
Al-Hasa25/2013	Human	B	2	KJ156866
Riyadh_2_2012	Human	B	2	KF600652
England-KSA/1/2018	Human	B	3	MH822886
Jeddah/D90/2014	Dromedary camel	B	4	KT368844
Qatar15/2015	Human	B	5	MK280984
Jordan-1/2015	Human	B	5	KU233364
ChinaGD01	Human	B	5	KT006149
Riyadh_1_2012	Human	B	6	KF600612

Animal Study and experimental design

Twenty-one 6-8-month-old alpacas (*Vicugna pacos*) were purchased and randomly assigned a number (AP1-AP21). Three alpacas (AP19-AP21) were kept as non-infected controls and sacrificed upon arrival. The remaining animals were acclimated for one week at the ABSL3 facilities. Alpacas AP1-AP9 (group 1) and AP10-AP18 (group 2) were housed in two different pens and intranasally inoculated with a 10^7 $TCID_{50}$ dose of the MERS-CoV EMC/2012 and Jordan-1/2015 strains respectively, as described previously (Vergara-Alert et al., 2017a). Three animals from each group were sacrificed per day with an overdose of pentobarbital followed by exsanguination on 1, 2 and 3 dpi. This timing was based on a previous experiment performed in alpacas with the EMC/2012 and Qatar15/2015 (clade B) strains where maximal viral shedding was observed on 2 dpi (Adney et al. 2016; Chapter 3). Clinical signs were monitored and NS samples were collected on the day of euthanasia for MERS-CoV titration and RNA detection, as previously described (Vergara-Alert et al., 2017a). Complete necropsies were performed. Collected respiratory tissues included: nasal turbinates (frontal, medial and caudal),

trachea (frontal, medial and caudal), lung parenchyma (frontal, medial and caudal), large and small bronchus. Respiratory tissues were immersed in media for viral detection by RT-qPCR; or fixed in formalin or methacarn for IHC (Vergara-Alert et al., 2017a) and cytokine quantification respectively (Chapter 3).

Viral RNA detection by RT-qPCR

Samples from NS and tissue samples were processed as previously described (Vergara-Alert et al., 2017a). Genomic MERS-CoV RNA was quantified by the RT-qPCR detecting the UpE gene of MERS-CoV (Corman et al., 2012). Samples with a cycle threshold of less than 40 were considered positive.

Virus isolation from NS

NS samples collected at various dpi were evaluated for the presence of infectious virus by titration in Vero E6 cells, as previously reported (Vergara-Alert et al., 2017a). The amount of infectious virus in each sample was calculated by determining the $TCID_{50}$/mL.

Histopathology and IHC

A monoclonal mouse anti-MERS-CoV N protein antibody (Sino Biological Inc., Beijing, China) was used to detect the presence of MERS-CoV antigen, following a previously established protocol (Vergara-Alert et al., 2017a).

MFPE tissue specimens

For the assessment of cytokine mRNA profiles, nasal turbinates, trachea, and lung were fixed by immersion in methacarn and paraffin embedded. MFPE-tracheal and lung samples were processed for RNA isolation by scraping the whole section from the prepared slides and

referred to as 'scraped' tissues. MFPE-nasal specimens were processed for LCM prior RNA extraction. All these procedures were previously established (Chapter 3).

Laser capture microdissection

LCM was used to micro-dissect IHC-positive and negative nasal epithelia areas from the same tissue section, as previously described (Chapter 3). Briefly, four consecutive sections from the same MFPE-block containing nasal specimens were cut. One of the sections was subjected to IHC to localize infected/non infected cells in the tissues and served as a reference (template) for the three subsequent sections which were stained with cresyl violet and then, subjected to LCM.

Total RNA isolation and cDNA synthesis

Total RNA from micro-dissected or scraped tissues was extracted, and converted into cDNA synthesis, following standard protocols (Chapter 3).

Relative quantification of cytokines mRNA and viral genomic and subgenomic loads on MFPE tissues

A microfluidic RT-qPCR assay was used to quantify cytokine mRNA from the MFPE samples. Selection of innate immune genes and specific pair of primers to amplify their transcriptional products were described in a previous work (Chapter 3). In addition, primers specific for the genomic (UpE) and subgenomic (M mRNA) viral regions were added to the assay (Chapter 3). Data was analyzed with the software 4.1.3 (Fluidigm Corporation, South San Francisco, USA) and the DAG expression software 1.0.5. 6, as previously described (Chapter 3). The up- or down-regulated expression of each cytokine gene was expressed in Fc. Supplementary table 4-1 shows the quantification, expressed in Cq values, of MERS-CoV genomic (UpE) and subgenomic RNA (M mRNA), obtained with the microfluidic qPCR assay.

Statistical analysis

To use the Student's *t*-test, a logarithmic 10 transformations were applied on Fc values to approach a log normal distribution. Thus, the means of the logarithmic Fc obtained at different dpi for each group of animals could be compared. Significant upregulation or downregulation of genes was considered if they met the criteria of a relative Fc of ≥2-fold or ≤2-fold respectively with $P < 0.05$. The Shapiro-Wilk normality test was used to determine the normal distribution of RT-qPCR data (Cq values), prior applying the Tukey's multiple comparisons test to compare Cq values of tissue samples at different dpi. Differences were considered significant at $P < 0.05$. Correlation coefficients were determined using the Spearman's correlation test.

Results

Clinical signs

To compare the pathology induced by strains EMC/2012 (clade A) and Jordan-1/2015 (clade B), two groups of alpacas were intranasally inoculated with each strain. Three animals from each group were sacrificed per day and during three consecutive days. None of the animals showed clinical signs and basal body temperatures remained normal (below 39.5ºC) throughout the study, in response to both MERS-CoV strains.

Nasal viral shedding and MERS-CoV loads in respiratory tracts

NS were obtained from all animals on the day of euthanasia (0, 1, 2 and 3 dpi). All MERS-CoV inoculated alpacas shed viral RNA but no major differences were seen between the two isolates at all dpi. Although statistics could not be performed due to limited number of animals, Cq values were numerically lower for alpacas inoculated with Jordan-1/2015 than those with EMC/2012 on 2 and 3 dpi. NS were subsequently tested for the presence of infectious virus in Vero E6 cells. At 2 and 3 dpi, alpacas infected with the Jordan-1/2015 strain had higher viral

titers than did animals infected with EMC/2012. At these days, only one out of three animals of group 1 showed infectious virus (Figure 4-1A).

MERS-CoV viral RNA was detected in all tested tissues upon infection with the two strains. The highest loads were found in the nasal turbinates of the Jordan-1/2015 group at 2 and 3 dpi, displaying a significant lower Cq value in comparison to the EMC/2012 infected group (Figure 4-1B). Viral loads were lower in trachea, bronchus, and lung for both strains, but animals from group 2, inoculated with the Jordan-1/2015 strain, exhibited significantly higher rates of infection for the duration of the experiment (Figure 4-1B). Thus, the Jordan-1/2015 strain replicates better than EMC/2012 at least in nasal tissues from alpacas.

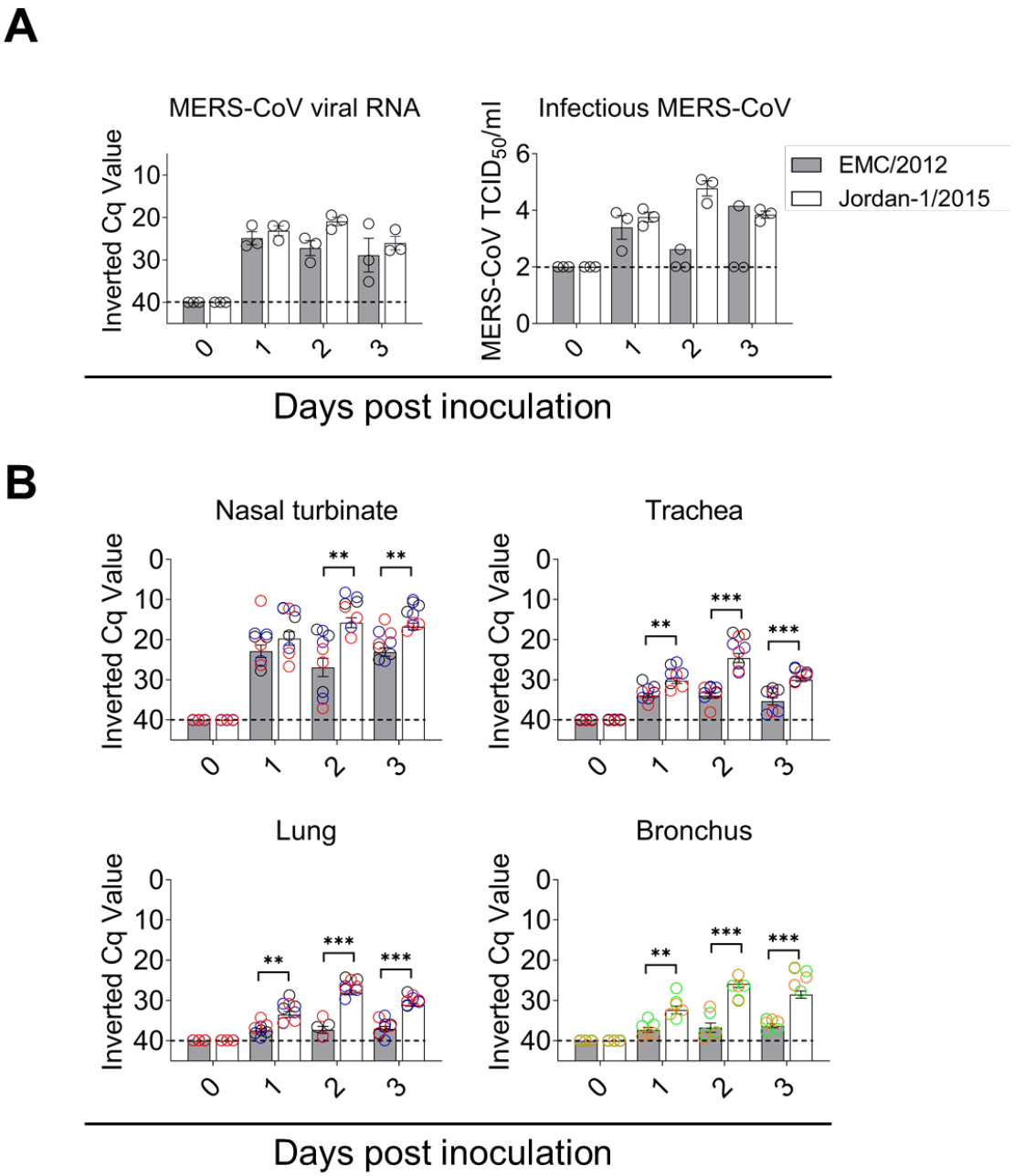

Figure 4-1. Viral loads in NS and respiratory tissues of MERS-CoV EMC/2012 and Jordan-1 infected alpacas (A) Viral RNA (left) and infectious MERS-CoV (right) loads from NS samples collected at different days of euthanasia. (B) Viral RNA loads from respiratory tissues of alpacas obtained at 0, 1, 2 and 3 dpi. Black circles: frontal turbinate, apical trachea, and apical lung; blue circles: medial turbinate, medial trachea, and medial lung; red circles: caudal turbinate, caudal trachea, and caudal lung. Green and yellow circles represent values obtained from large and small bronchus, respectively. Viral loads were determined by the UpE real-time RT-qPCR (A and B). Each bar represents the mean Cq value ± SEM of infected tissues from 3 animals euthanized at 0, 1, 2 and 3 dpi, respectively. Statistical significance was determined by Tukey's multiple comparisons test. *$P < 0.05$; **$P < 0.01$; ***$P < 0.001$; ****$P < 0.0001$. Dashed lines depict the detection limit of the assays. Cq, quantification cycle; MERS-CoV, Middle East respiratory syndrome coronavirus; $TCID_{50}$, 50% tissue culture infective dose.

MERS-CoV Jordan-1/2015 strain possesses stronger epithelial tropism compared to EMC/2012 strain.

To gain further information on viral replication and tissue tropism we performed IHC along alpaca respiratory tracts infected with both MERS-CoV strains. Viral antigen was found multifocally located in the nasal turbinates of alpacas inoculated with the MERS-CoV EMC/2012 isolate (Figure 4-2A). At 1 and 3 dpi, MERS-CoV positive nasal epithelial cells were only detected in one out of three animals whereas at 2 dpi all three animals harbored viral antigen in their nose (table 2). By contrast, the virus was found in the nasal epithelium of all alpacas inoculated with the Jordan-1/2015 strain throughout the whole study (table 2). While a moderate number of pseudostratified columnar epithelial cells in the nose contained MERS-CoV Jordan-1/2015 antigen at 1 dpi, the number of positive epithelial cells became remarkably high at 2 dpi; such number steadily decreased in the alpacas necropsied on dpi 3 (Figure 4-2A and table 2).

MERS-CoV Jordan-1/2015 infected cells were unevenly detected within the tracheal and bronchial mucosa at 2 dpi by IHC. Also, viral antigen was only scarcely found in bronchiolar epithelial cells of a single animal at 3 dpi (Figure 4-2B and table 2). By contrast, MERS-CoV EMC/2012 antigen was not present in trachea or LRT tissues (Figure 4-2B and table 2)

Table 2. MERS-CoV N protein distribution in alpaca respiratory tracts in response to EMC/2012 and Jordan-1/2015 strains

	1 dpi						2 dpi						3 dpi					
	EMC/2012			**Jordan-1/2015**			**EMC/2012**			**Jordan-1/2015**			**EMC/2012**			**Jordan-1/2015**		
	A1	A2	A3	A10	A11	A12	A4	A5	A6	A13	AP14	AP15	A7	A8	A9	A16	AP17	A18
Frontal turbinate	–	+/–	–	+/–	–	+/++	–	–	+	+++	++/+++	+++	–	–	+/++	+	+	+/–
Medial turbinate	–	+/–	–	+/++	+/–	+/++	–	+	+	+++/+	++	+++/+	–	–	++	+	+/–	+/–
Caudal turbinate	–	+	–	–	+++/++++	+/++	+	–	+	+++ +	++/+++	+++ +	–	–	+/++	+	+/–	+
Apical trachea	–	–	–	–	–	+/–	–	–	–	–	+/–	+	–	–	–	–	–	–
Medial trachea	–	–	–	–	–	–	–	–	–	–	+/–	+	–	–	–	–	–	–
Caudal trachea	–	–	–	–	–	–	–	–	–	–	+	+	–	–	–	–	–	–
Large bronchus	–	–	–	–	–	–	–	–	–	–	+/–	+/++	–	–	–	–	–	–
Small bronchus	–	–	–	–	–	–	–	–	–	–	–	+/++	–	–	–	+/–	–	–
Apical lung	–	–	–	–	–	–	–	–	–	–	–	–	–	–	–	+/–	–	–
Medial lung	–	–	–	–	–	–	–	–	–	–	–	–	–	–	–	–	–	–
Caudal lung	–	–	–	–	–	–	–	–	–	–	–	–	–	–	–	–	–	–

Abbreviations: dpi, days post inoculation; AP, alpaca; day post inoculation; -, no positive cells detected; +/-, less than 10 positive cells per tissue section; +, 10 to 50 positive cells per tissue section; ++, 50 to 150 positive cells per tissue section; +++, 150 to 300 positive cells per tissue section; and ++++, more than 300 positive cells per tissue section.

Both MERS-CoV isolates led to similar degrees of histological lesions that were mainly limited to the nasal turbinate, being of multifocal distribution and mild. From 1 to 3 dpi, lesions in the nasal turbinates were characterized by mild rhinitis, segmental hyperplasia of the nasal epithelium, lymphocytic exocytosis and epithelial vacuolation. Additionally, small numbers of lymphocytes with fewer macrophages infiltrated the underlying submucosa (Figure 4-2A). No significant microscopic lesions were observed in the trachea and bronchus in response to both strains. Besides, lung lobes showed very mild multifocal perivascular and peribronchiolar infiltration by lymphocytes in few animals. Control animals euthanized on day 0 (AP19 to AP21) did not display any significant histological lesion in collected tissues and IHC resulted negative in all of them (table 2). Thus, the Jordan-1/2015 strain showed a much better replication competence than did EMC/2012 in the alpaca respiratory tract, despite similar histopathological alterations provoked by both strains.

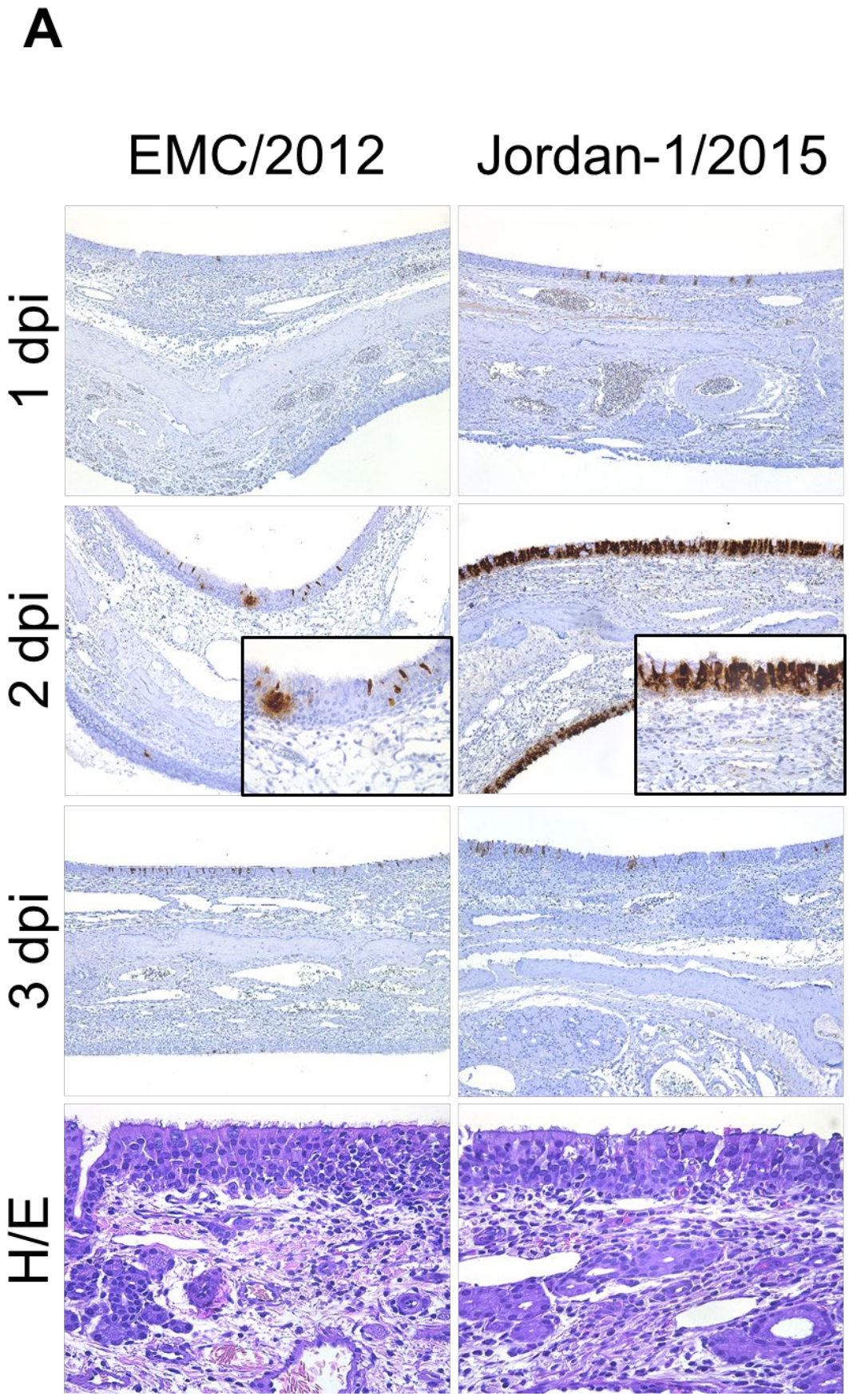
A
EMC/2012
Jordan-1/2015
1 dpi
2 dpi
3 dpi
H/E

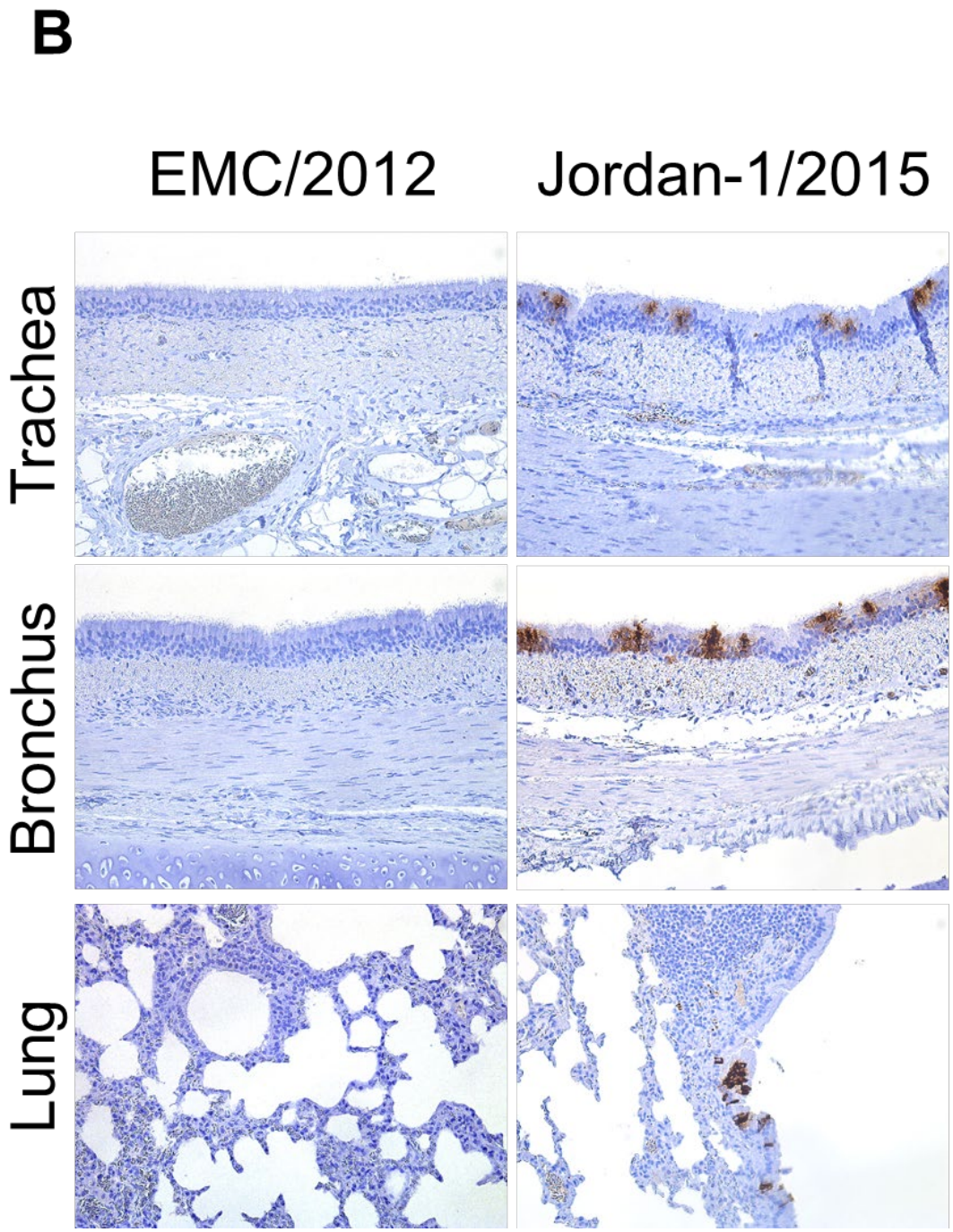

Figure 4-2. Histopathological changes and viral detection in respiratory tracts of alpacas inoculated with two MERS-CoV strains. Respiratory tissues (Nasal turbinate, trachea, bronchus, and lung) were harvested upon necropsy and immediately fixed in 10% neutral-buffered formalin. (A) Immunohistochemical (IHC) visualization of apical turbinate of alpacas infected with MERS-CoV EMC/2012 (left panel) and Jordan-1/2015 (right panel) necropsied on1 to 3 dpi. H/E staining of the apical nose collected at 2 dpi for both strains was displayed at the bottom. (B) IHC result of trachea, bronchus and lung of alpacas infected with MERS-CoV EMC/2012 (left panel) and Jordan-1/2015 (right panel) necropsied at 2 or 3 dpi. See table 2 for the detailed distribution of MERS-CoV antigen. Abbreviations: H/E, hematoxylin and eosin stain.

Viral loads in micro-dissected nasal tissues and whole tracheal and lung sections

To evaluate the loads of MERS-CoV genomic UpE and subgenomic M mRNA on individual MFPE respiratory tissue sections or micro-dissected mucosa that were used for cytokine quantification, we performed a microfluidic RT-qPCR assay. Since the nasal mucosa is the major driver of innate immune responses in MERS-CoV infected alpacas (Chapter 3), LCM was used to isolate MERS-CoV infected/non-infected nasal epithelial areas based on IHC examination. Also, MFPE trachea and lung sections were directly scrapped from the slide. The total surfaces obtained by LCM ranged from 0.055 to 0.095 cm^2 per specimen and 0.3 to 1 cm^2 were recovered from MFPE trachea and lung sections for RNA processing. Between 0.25 and 2.69 µg of total RNA were obtained for each LCM sample and scrapped tissue (Supplementary table 4-2). Due to the less infectivity of the EMC/2012 strain, nasal epithelial areas significantly labelled by IHC could only be harvested from two animals (AP4 on 2 dpi and AP9 on 3 dpi). Nasal specimens from animal AP14, infected with the Jordan-1/2015 strain, could not be examined due to autolysis before tissue fixation. All other nasal epithelia retrieved from animals inoculated by the Jordan-1/2015 strain could be processed as expected. As shown in Figure 4-3, UpE and M mRNA loads found in MERS-CoV IHC positive nasal epithelial (MPNE) areas were higher than those displayed by MERS-CoV IHC negative nasal epithelial (MNNE). In addition, MPNE micro-dissected areas of both strains showed comparable viral RNA loads while the Jordan-1/2015 strain had a slightly better replication in MNNE areas than that of EMC/2012. Like results obtained from tissue homogenates (Figure 4-1B), viral RNA was absent in trachea and lung of alpacas inoculated with EMC/2012 strain. Very little UpE (Figure 4-3A) and no M mRNA loads, except for one animal (AP14) on 3 dpi, were observed in the lung of animals infected with the Jordan-1/2015 strain (Figure 4-3B). MERS-CoV was replicating in the trachea of all group 2 animals.

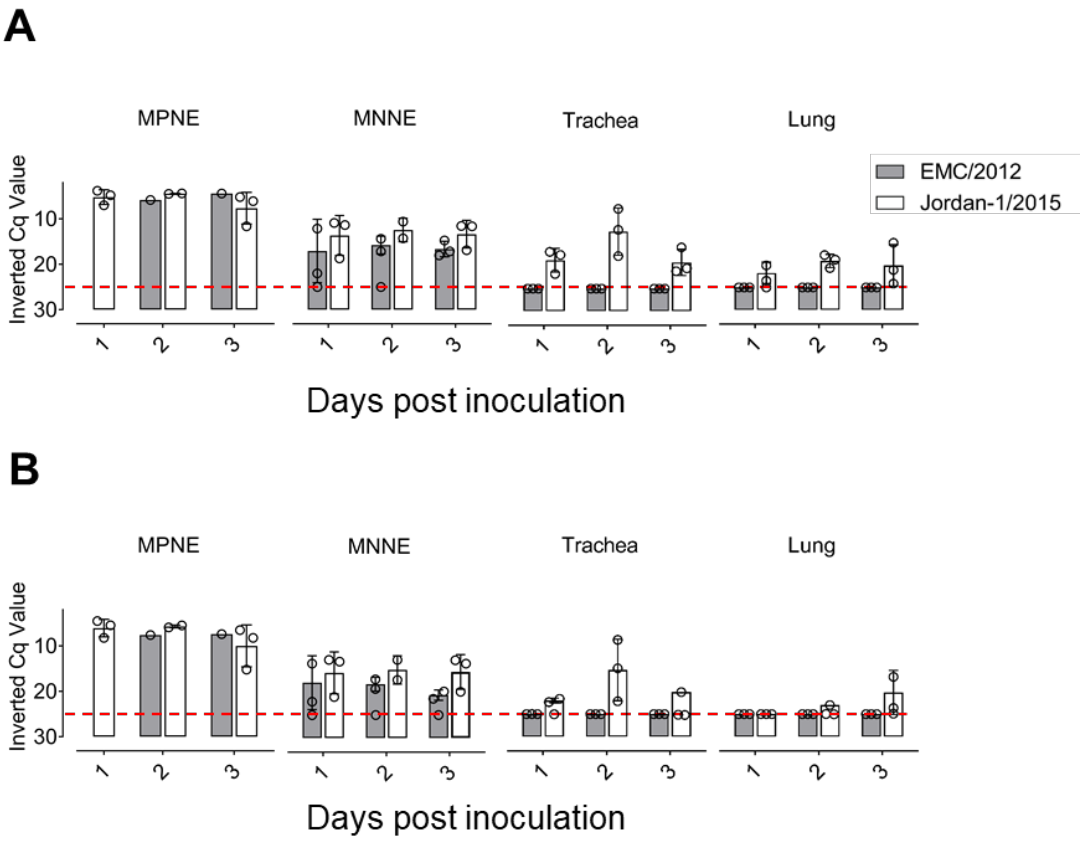

Figure 4-3. MERS-CoV UpE gene and M mRNA loads in MFPE samples. Tissue samples were collected during 3 consecutive days (1 to 3 dpi, n=3 per day and per strain) from alpacas inoculated with the MERS-CoV EMC/2012 and the Jordan-1/2015 strains. Nasal samples from AP14 sacrificed at 2 dpi could not be processed due autolysis. Micro-dissected MFPE nasal epithelia were prepared based on an overlapping template section stained by IHC to localize the MERS-CoV N protein. Only two IHC positive epithelial areas from two animals (AP13 and AP15) with significant labeling could be obtained. Trachea and lung were scrapped from MFPE tissue sections. RNA extracted from these samples were converted into cDNA and (A) the MERS-CoV UpE gene and (B) the M mRNA were amplified with a PCR microfluidic assay (Fluidigm Biomark). Error bars indicate SEM when results were positive in more than one animal. Abbreviations: MPNE, MERS-CoV IHC positive nasal epithelia; MNNE, MERS-CoV IHC negative nasal epithelia; MFPE, methacarn-fixed paraffin embedded-tissues; LCM, laser capture microdissection.

Expression of innate immune genes in the nasal epithelia of alpacas infected with the EMC/2012 and Jordan-1/2015 strains

Studies conducted *in vitro* have pointed to the antagonistic role of ORF4a in induction of IFNs as a key factor in the control of virus replication. Further, the EMC/2012 strain, which display a full length genome, has shown higher IFN inhibitory properties in Calu-3 cells than the clade B strain AH13 (Chu et al., 2018). To test this hypothesis *in vivo,* in a natural host, the Jordan-1/2015, which harbors a deletion in the ORF4a gene, was used along the prototype EMC/2012 strain to infect alpacas. To compare antiviral and

inflammatory pathways induced by both strains, relative mRNA expression levels for 37 innate immune response genes (Chapter 3) were assessed in the different respiratory tract tissues over the course of infection. After RNA conversion to cDNA, the samples were processed through a Fluidigm BioMark microfluidic assay. All the genes were detected at basal levels in micro-dissected samples of control non-infected animals.

In MPNE areas, type I and III IFNs were induced as early as 1 dpi in the group of alpacas inoculated with the Jordan-1/2015 isolate. However, MPNE areas could not be collected at 1 dpi due to the paucity of MERS-CoV EMC/2012 infected epithelial cells. On dpi 2 and 3, IFNs were upregulated in the MPNE areas infected by both strains. Of note, the Jordan-1/2015 strain induced much higher levels of IFNs (Figure 4-4A and B). Genes coding for PRRs including RIG1 and MDA5, antiviral ISGs (OAS1, CXCL10, MX1 and ISG15), chemokines (CCL2 and CCL3), the transcriptional factors IRF7 and the NLRP3 inflammasome component CASP1 were highly upregulated at 2 dpi and levels of expression decreased at 3 dpi. The same kinetic of mRNA transcription but with lower induction was observed for the pro-inflammatory cytokines (IL1β, IL6, IL8, IL15, TNFα and CXCL1) and the anti-inflammatory gene IL10 in MPNE areas infected by both strains. Nonetheless, levels of expression of these cytokines could drastically vary among animals (Figure 4-4A and B). Additionally, transcription levels of genes coding for the NLRP3 inflammasome components NLRP3 and PYCARD, downstream signaling adaptors (NFκBIA and CARD9), enzymes (CASP10, AZI2, PACT and TBK1) and the IFNLR1 receptor fluctuated around basal values independently of the animals, days of sample collection and the strain used for infection (Figure 4-4A and B).

Type I and III IFNs were not detected or marginally upregulated in MNNE areas from alpacas inoculated by both strains. On dpi 2, corresponding to the peak of infection, genes coding for ISGs, RLRs, STAT1, IRF7, IL8, CCL2, CCL3 and CASP1 were moderate to highly induced in MNNE areas infected by both strains while most of the remaining genes were unaltered or slightly downregulated upon infection (Figure 4-4A and C). Again, high variations of animals within groups were noticed.

In a previous study (Chapter 3), transcriptional levels of IFNs were found positively correlated with increased viral loads in the nasal mucosa of alpacas inoculated with the MERS-CoV Qatar15/2015 strain. To confirm this relation for the Jordan-1/2015 and the EMC/2012 strains, mRNA levels of IFNs, expressed in Fc, were plotted against Cq

values found for the MERS-CoV UpE gene in both MPNE and MNNE areas. As shown in the Figure 4-4D, MERS-CoV UpE loads in micro-dissected tissues were strongly or moderately correlated to the inductions of IFNβ (r = 0.72, $P = 0.0007$) and IFNλ1 (r = 0.8, $P < 0.0001$), or to IFNα (r = 0.65, $P = 0.0005$) and IFNλ3 (r = 0.66, $P = 0.004$), respectively. Despite similar viral loads (Figure 4-3A), the two MPNE areas infected with the EMC/2012 strain collected at 2 and 3 dpi had a comparable induction of IFNs than most of mucosal samples infected by the Jordan-1/2015 strain at 1 and 3 dpi. Thus, our previous finding that expression of IFNs depends on levels of viral replication was further confirmed. However, due to the limited number of heavily infected samples obtained from group 1, we could not definitely conclude that the Jordan-1/2015 strain is a better inducer of IFNs than the EMC/2012 strain.

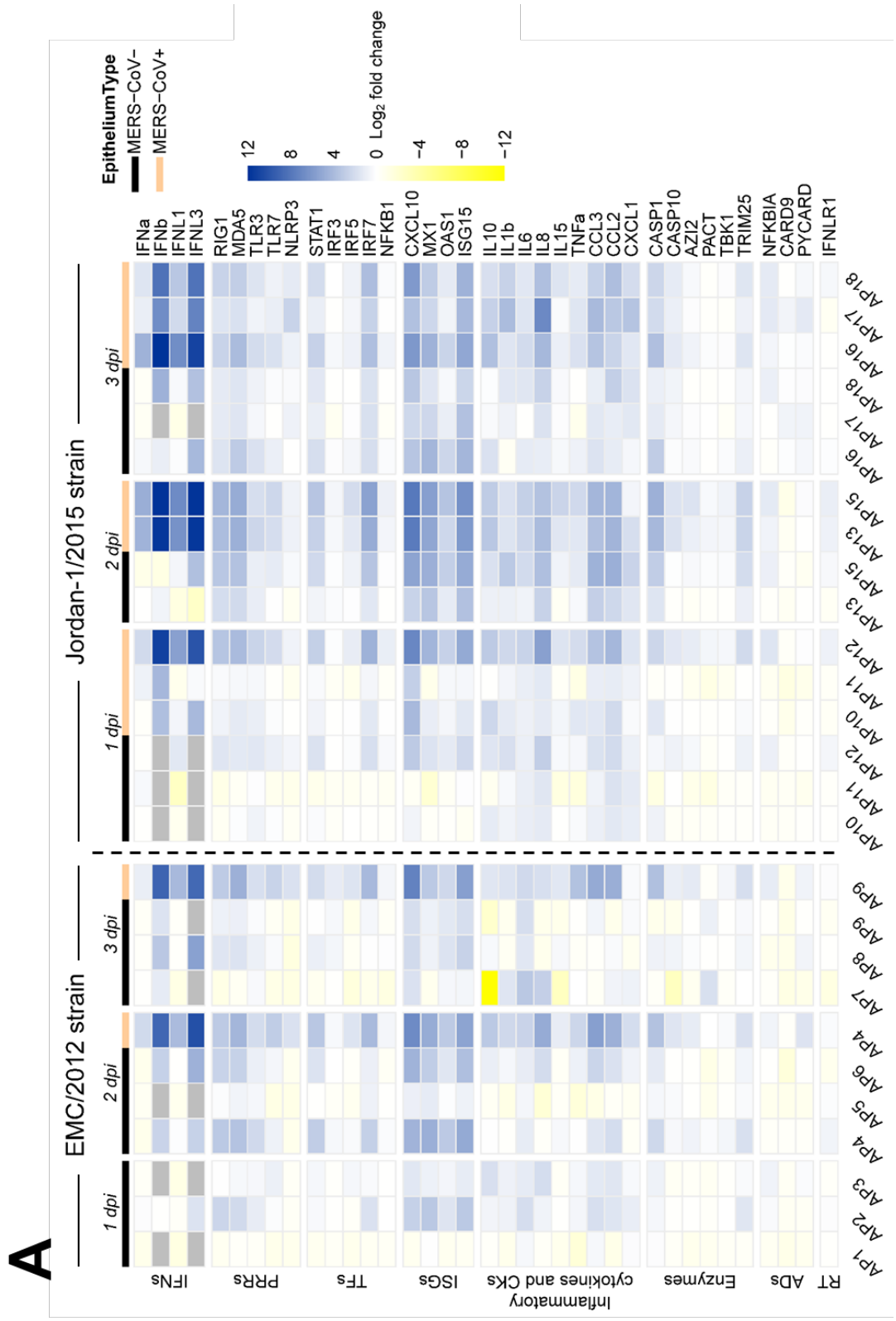
A
EMC/2012 strain
Jordan-1/2015 strain
1 dpi
2 dpi
3 dpi
EpitheliumType
MERS−CoV−
MERS−CoV+
12
8
4
0 Log2 fold change
−4
−8
−12
IFNa
IFNb
IFNL1
IFNL3
RIG1
MDA5
TLR3
TLR7
NLRP3
STAT1
IRF3
IRF5
IRF7
NFKB1
CXCL10
MX1
OAS1
ISG15
IL10
IL1b
IL6
IL8
IL15
TNFa
CCL3
CCL2
CXCL1
CASP1
CASP10
AZI2
PACT
TBK1
TRIM25
NFKBIA
CARD9
PYCARD
IFNLR1
IFNs
PRRs
TFs
ISGs
Inflammatory cytokines and CKs
Enzymes
ADs
RT
AP1
AP2
AP3
AP4
AP5
AP6
AP4
AP7
AP8
AP9
AP9
AP10
AP11
AP12
AP10
AP11
AP12
AP13
AP15
AP15
AP13
AP16
AP17
AP18
AP18
AP17
AP16

B

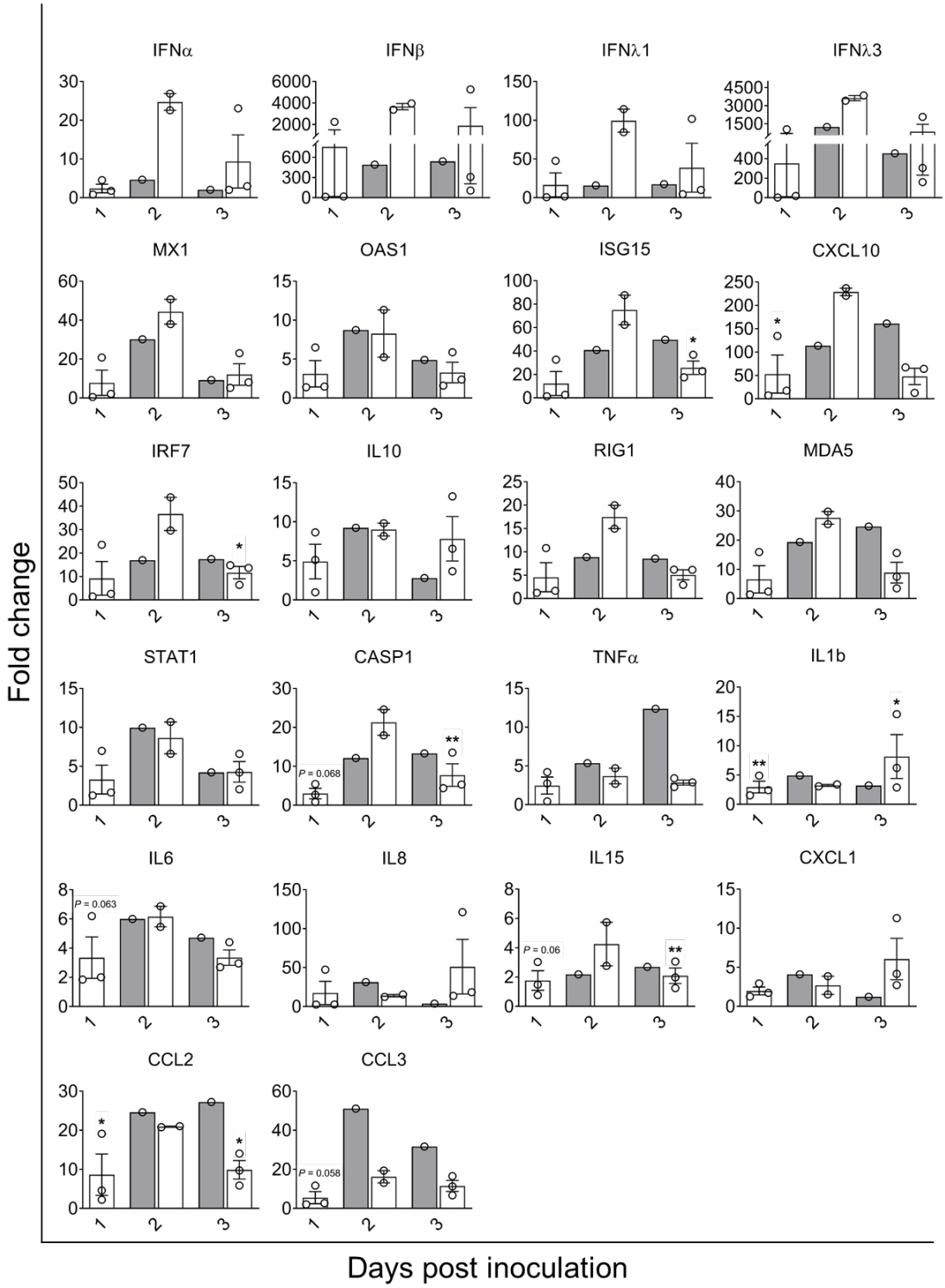
IFNα
IFNβ
IFNλ1
IFNλ3
MX1
OAS1
ISG15
CXCL10
IRF7
IL10
RIG1
MDA5
STAT1
CASP1
TNFα
IL1b
IL6
IL8
IL15
CXCL1
CCL2
CCL3
P = 0.063
P = 0.068
P = 0.06
P = 0.058
Fold change
Days post inoculation

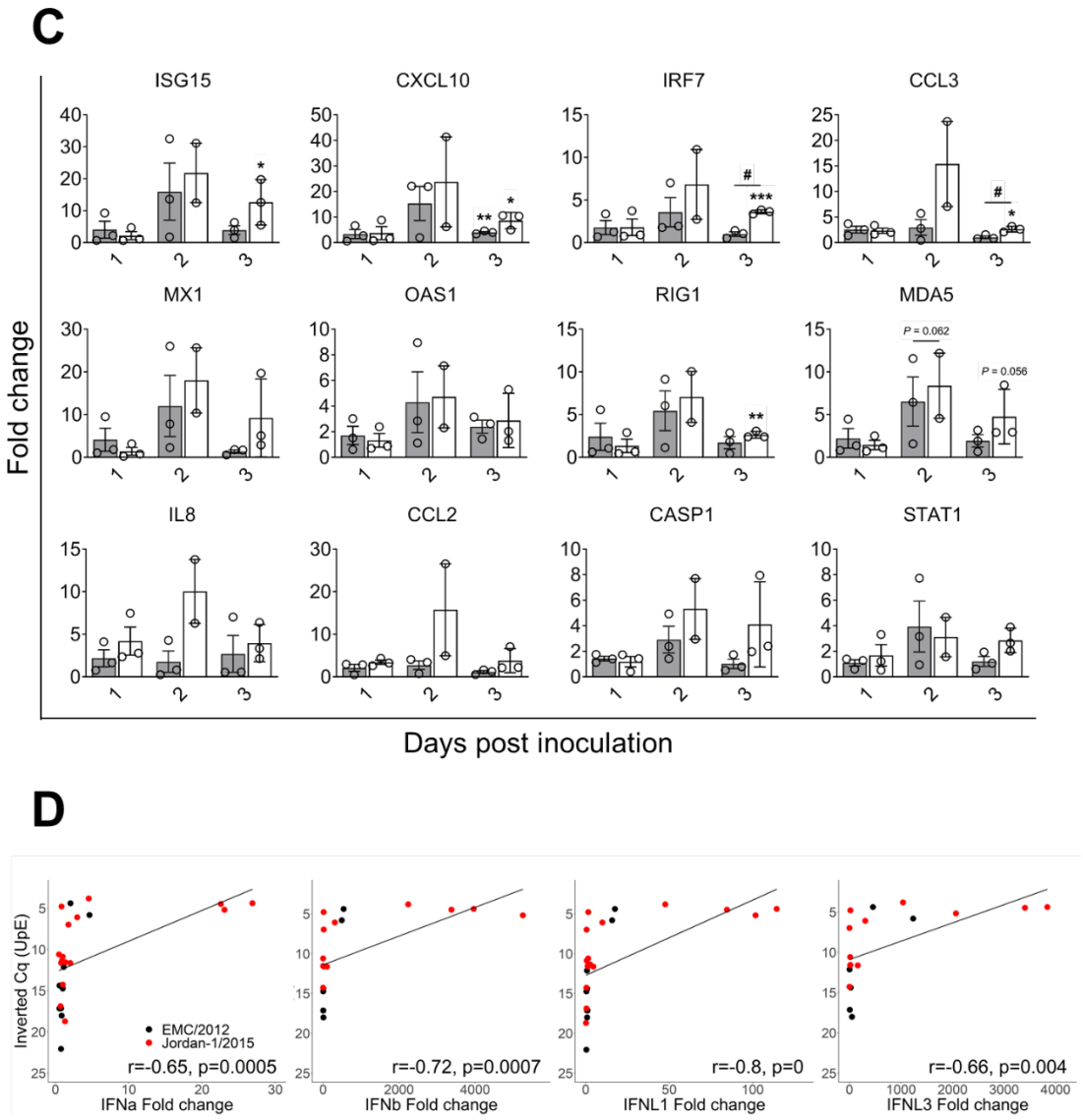

Figure 4-4. Kinetics of innate immune response genes and correlation coefficients between MERS-CoV UpE load and IFN induction in alpaca nasal epithelia. (**A**) The nasal epithelium of each alpaca (AP1 to AP21, except for AP14) was microdissected and infected (pink)/non-infected (black) areas, as assessed by IHC, were selected and isolated for RNA extraction and conversion to cDNA. However, we failed to obtain the RNA from AP14 since nasal turbinate of this animal showed heavy autolysis. The Fluidigm Biomark microfluidic assay was used to amplify and quantify transcripts of innate immune genes at different dpi (1 to 3 dpi). HPRT1, GAPDH and UbC genes were used as normalizer housekeeping genes and values obtained from the infected animals were compared to those obtained from non-infected alpacas. The resulting heatmap shows color variations corresponding to log2 fold change values; blue for increased and yellow for decreased gene expression, respectively. The grey rectangles indicate no expression of the corresponding gene. IFNs, interferons; PRRs, pattern recognition receptors; TFs, transcription factors; ISGs, interferon stimulated genes; CKs, chemokines; ADs, adaptors; RTs, receptors. MERS-CoV+ Epi and MERS-CoV- Epi, MERS-CoV positive andnegative epithelium areas as assessed by IHC, respectively. Average fold change of genes in (B) MPNE and (C) MNNE areas of EMC/2012 (gray bars) and Jordan-1/2015 (white bars) were shown. Data were displayed as means of ± SEM. Statistical significance was determined by Student's *t*-test. **P* < 0.05; ***P* < 0.01; ****P* < 0.001 (n = 3) compared with non-infected alpacas; #*P* < 0.05; ##*P* < 0.01; ###*P* < 0.001 (n = 3) compared between

(Continued)

groups on different dpi. (D) Cq values of MERS-CoV UpE of nasal epithelia were plotted against the relative expression levels of IFNα, IFNβ, IFNλ1 and IFNλ3. Correlation coefficients were established using the Spearman's correlation test.

Innate immune response genes follow the same kinetic of expression in trachea and lung upon infection with the EMC/2012 and Jordan-1/2015 strains.

Expression of innate immune response genes was further assessed along the URT and LRT. Except for IFNλ3, all other genes were detected at basal levels in the trachea and lung of control non-infected animals. Transcription of IFNα, IFNβ and IFNλ1 was not induced in the trachea and lungs of alpacas upon infection with any of the strains (Figure 4-5A and 6A). In trachea, genes coding for PRRs, ISGs, IRF7 and STAT1 were moderately expressed in both groups during the infection. (Figure 4-5A and B). Compared to non-infected controls, there was few alterations of mRNA transcription in the remaining genes tested during the infection period.

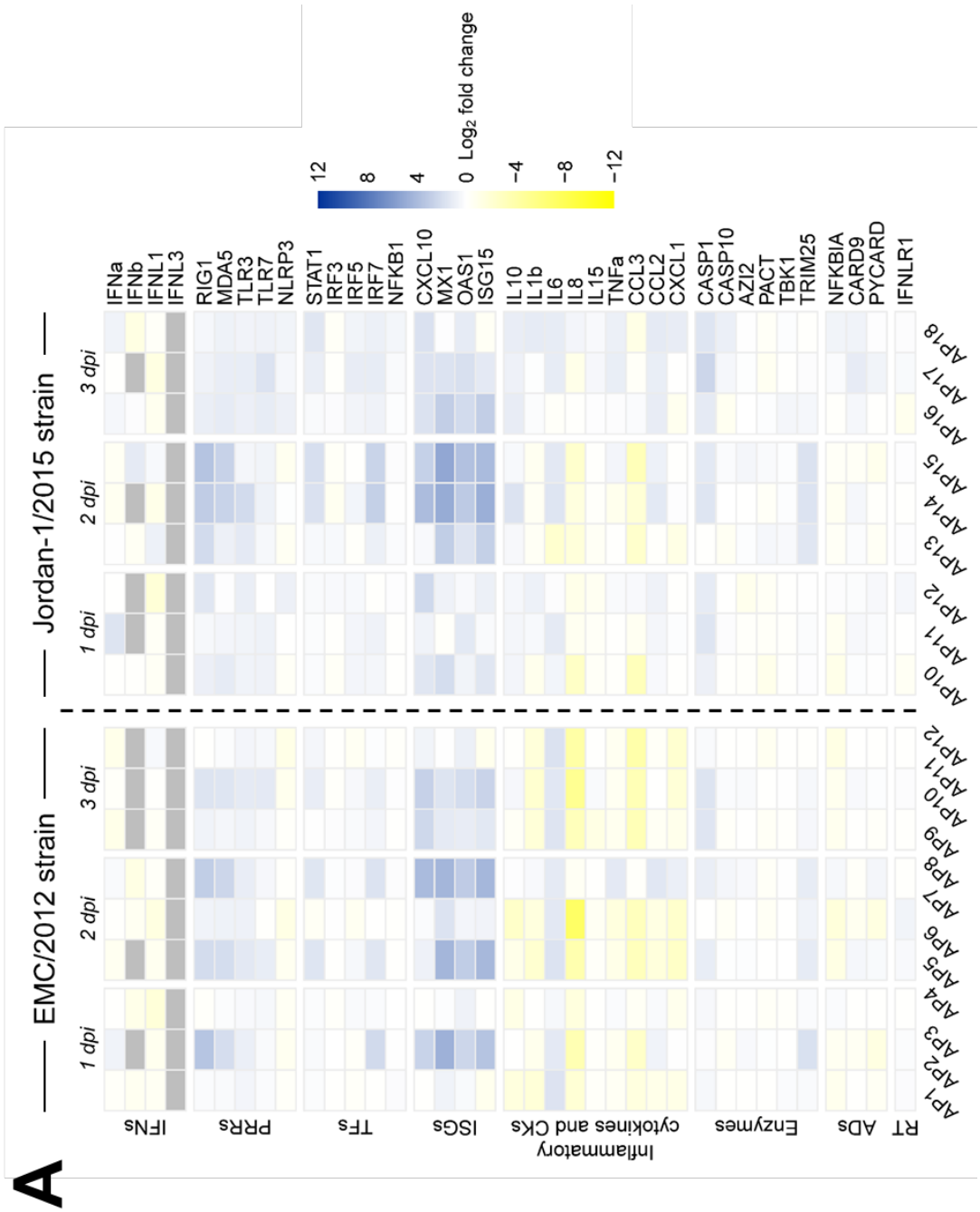
A
EMC/2012 strain
Jordan-1/2015 strain
1 dpi
2 dpi
3 dpi
AP1
AP2
AP3
AP4
AP5
AP6
AP7
AP8
AP9
AP10
AP11
AP12
AP10
AP11
AP12
AP13
AP14
AP15
AP16
AP17
AP18
RT
ADs
Enzymes
Inflammatory cytokines and CKs
ISGs
TFs
PRRs
IFNs
IFNLR1
PYCARD
CARD9
NFKBIA
TRIM25
TBK1
PACT
AZI2
CASP10
CASP1
CXCL1
CCL2
CCL3
TNFa
IL15
IL8
IL6
IL1b
IL10
ISG15
OAS1
MX1
CXCL10
NFKB1
IRF7
IRF5
IRF3
STAT1
NLRP3
TLR7
TLR3
MDA5
RIG1
IFNL3
IFNL1
IFNb
IFNa
12
8
4
0 Log2 fold change
−4
−8
−12

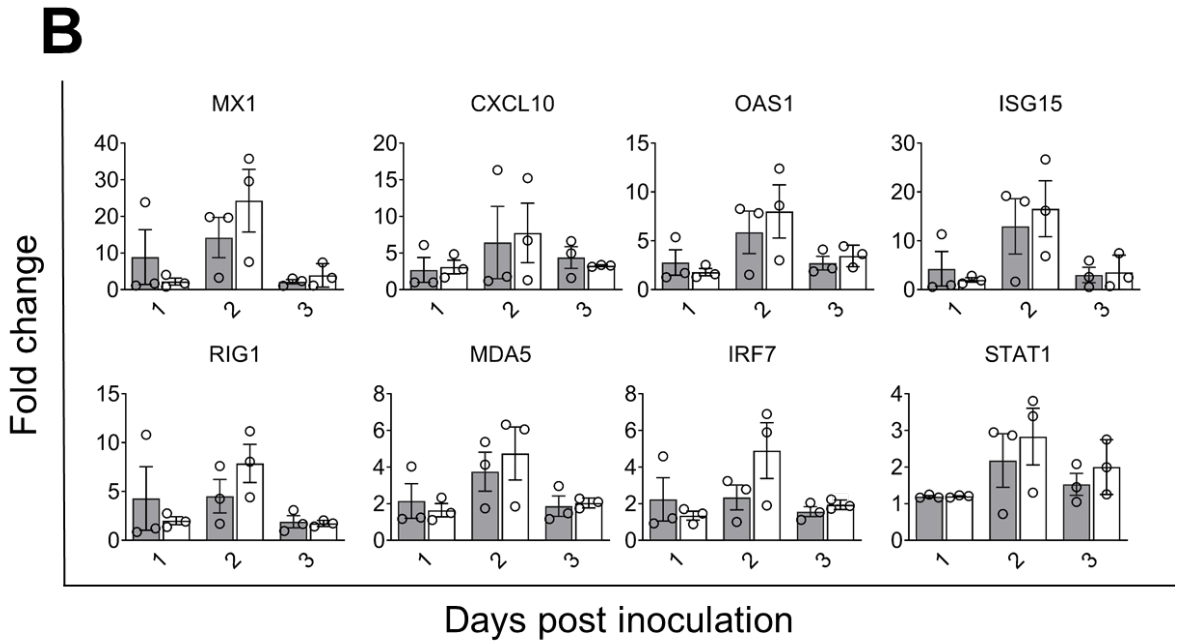

Figure 4-5. Kinetics of innate immune response genes in the trachea of alpacas upon infection with MERS-CoV EMC/2012 and Jordan-1/2015 strains. Trachea samples were obtained by scraping MFPE sections from control and infected alpacas (AP1 to AP21). After RNA extraction and conversion to cDNA, a Fluidigm Biomark microfluidic assay was used to amplify and quantify transcripts of innate immune genes at different dpi (1 to 3 dpi). HPRT1, GAPDH and UbC genes were used as normalizers and values obtained from the infected animals were compared to those obtained from noninfected alpacas. (A) The resulting heatmaps show color variations corresponding to log2 fold change values; blue for increased and yellow for decreased gene expression, respectively. IFNs, interferons; PRRs, pattern recognition receptors; TFs, transcription factors; ISGs, interferon stimulated genes; CKs, chemokines; ADs, adaptors. (B) Average fold change of upregulated genes in the trachea of alpacas infected with EMC/2012 (gray bars) and Jordan-1/2015 (white bars) were shown. Data were displayed as means of ± SEM. Statistical significance was determined by Student's *t*-test. **P* < 0.05; ***P* < 0.01; ****P* < 0.001 (n = 3) compared with non-infected alpacas.

In the lung, the EMC/2012 and Jordan-1/2015 strains induced the same pattern of gene transcription in the two groups. For both strains, ISGs, RLRs (RIG1 and MDA5), IRF7, IL8, CXCL1, CCL2, CCL3 and CASP10 were slightly to moderately upregulated from 1 dpi, reaching a peak at 2 dpi to further decay at 3 dpi (Figure 4-6A and B). However, as in trachea, one or two animals from group 2 showed higher induction of the abovementioned cytokines. The rest of the genes fluctuated around basal levels independently of the animals and days of sample collection (Figure 4-6A and B).

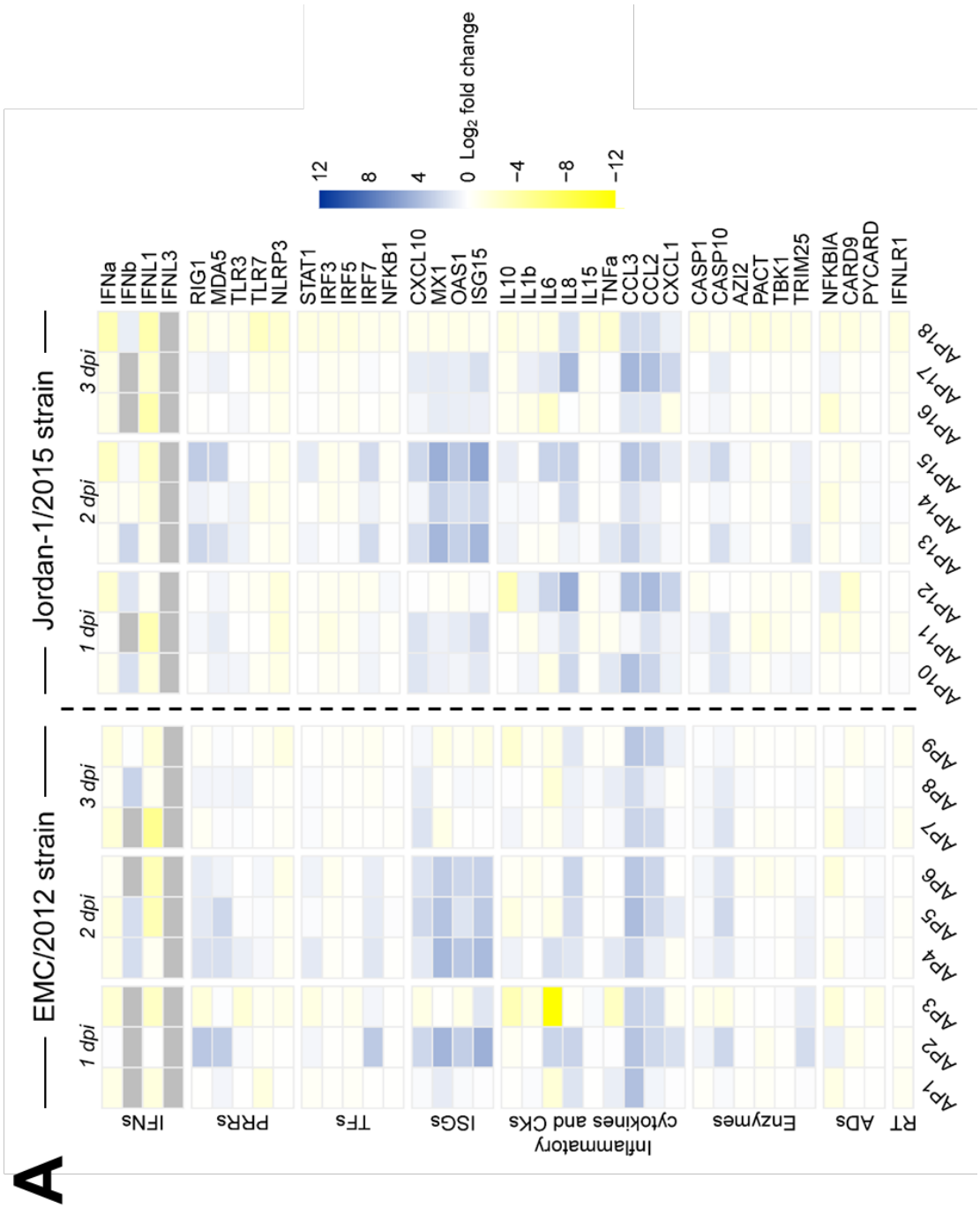
A
EMC/2012 strain
Jordan-1/2015 strain
1 dpi
2 dpi
3 dpi
AP1
AP2
AP3
AP4
AP5
AP6
AP7
AP8
AP9
AP10
AP11
AP12
AP13
AP14
AP15
AP16
AP17
AP18
RT
ADs
Enzymes
Inflammatory cytokines and CKs
ISGs
TFs
PRRs
IFNs
IFNLR1
PYCARD
CARD9
NFKBIA
TRIM25
TBK1
PACT
AZI2
CASP10
CASP1
CXCL1
CCL2
CCL3
TNFa
IL15
IL8
IL6
IL1b
IL10
ISG15
OAS1
MX1
CXCL10
NFKB1
IRF7
IRF5
IRF3
STAT1
NLRP3
TLR7
TLR3
MDA5
RIG1
IFNL3
IFNL1
IFNb
IFNa
12
8
4
0 Log2 fold change
−4
−8
−12

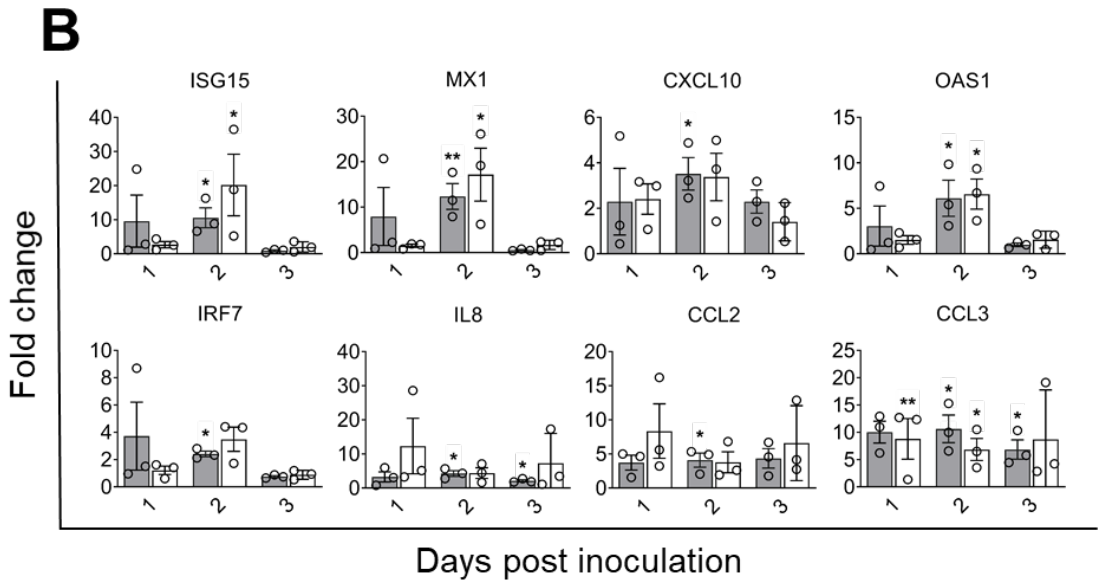

Figure 4-6. Kinetics of innate immune response genes in the lung of alpacas upon infection with MERS-CoV EMC/2012 and Jordan-1/2015 strains. Lung samples were obtained by scraping MFPE sections from control and infected alpacas (AP1 to AP21). After RNA extraction and conversion to cDNA, a Fluidigm Biomark microfluidic assay was used to amplify and quantify transcripts of innate immune genes at different dpi (1 to 3 dpi). HPRT1, GAPDH and UbC genes were used as normalizers and values obtained from the infected animals were compared to those obtained from noninfected alpacas. (A) The resulting heatmaps show color variations corresponding to log2 fold change values; blue for increased and yellow for decreased gene expression, respectively. IFNs, interferons; PRRs, pattern recognition receptors; TFs, transcription factors; ISGs, interferon stimulated genes; CKs, chemokines; ADs, adaptors. (B) Average fold change of upregulated genes in the lung of alpacas infected with EMC/2012 (gray bars) and Jordan-1/2015 (white bars) were shown. Data were displayed as means of ± SEM. Statistical significance was determined by Student's *t*-test. **P* < 0.05; ***P* < 0.01; ****P* < 0.001 (n = 3) compared with non-infected alpacas.

Protein alignment of selected clade A and B MERS-CoV strains

To explore whether the increased replication competence of the Jordan-1/2015 strain could be due to clade B specific mutations, all protein coding genes of four clade A and nine clade B strains, encompassing linages 1 to 6 (table 1), were aligned using the UniProt alignment tool. All clade B MERS-CoV strains tested in this study share 5 specific aa mutations in the replicase genes of ORF1ab. Of note, a L864I substitution occurred in the catalytic domain (palm and fingers subdomains) of PLpro that cleaves the viral replicase polyproteins at three sites releasing viral nsp1, nsp2, and nsp3. Further, all MERS-CoV clade B strains show a Q1020Rchange in the heptad repeat (HR) 1 of the S protein (Figure 4-7). Except for the residue at position 1261 of the nsp3 protein, remaining aa sequences of clade A strains were highly conserved in the nsp2, nsp3, nsp4 and S proteins where all 5 clade B specific mutations occurred. Moreover,

compared with the EMC/2012 strain, the two clade B viruses (Qatar15/2015 and Jordan-1/2015) used so far to infect alpacas share 36 specific aa mutations mostly in the ORF1ab gene and to a lesser extent, in ORF3, M, ORF4a, N and the S gene products. The Jordan-1/2015 harbored a unique 16 aa deletions in ORF4a not found in all clade A and B strains analyzed. The deleted region contains a predicted β-sheet belonging to the classical double-stranded RNA binding αββββα fold of this protein (Figure 4-7, boxed in blue). Overall, genomic analysis revealed that clade B viruses have several mutations that could affect the fusion of the virus with endosomal membranes, replication and the IFN cascade.

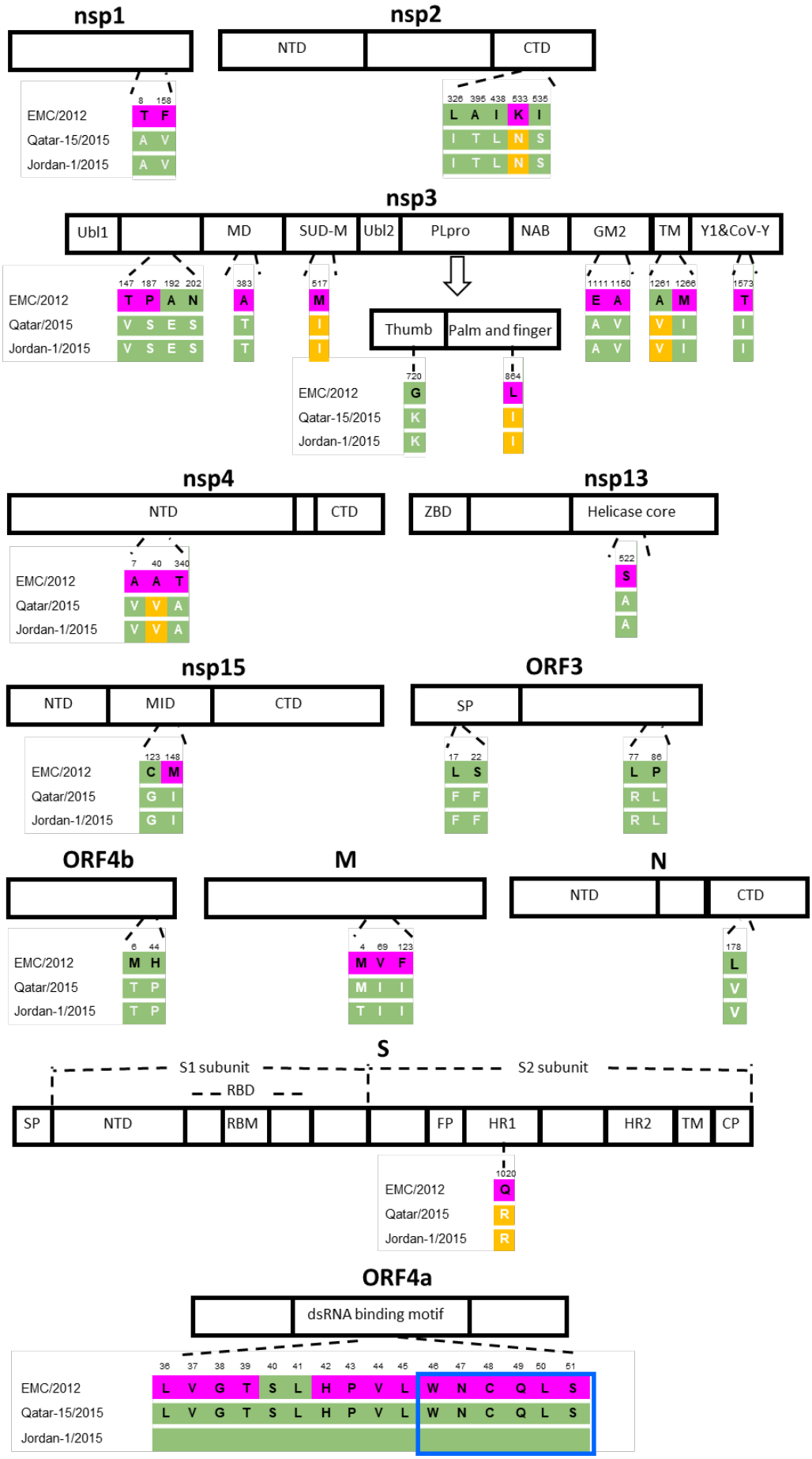
nsp1
8 158
EMC/2012 T F
Qatar-15/2015 A V
Jordan-1/2015 A V
nsp2
NTD
CTD
326 395 438 533 535
L A I K I
I T L N S
I T L N S
nsp3
Ubl1
MD
SUD-M
Ubl2
PLpro
NAB
GM2
TM
Y1&CoV-Y
147 187 192 202
EMC/2012 T P A N
Qatar/2015 V S E S
Jordan-1/2015 V S E S
383
A
T
T
517
M
I
I
Thumb
Palm and finger
720
G
K
K
864
L
I
I
1111 1150
E A
A V
A V
1261 1266
A M
V I
V I
1573
T
I
I
nsp4
NTD
CTD
7 40 340
EMC/2012 A A T
Qatar/2015 V V A
Jordan-1/2015 V V A
nsp13
ZBD
Helicase core
522
S
A
A
nsp15
NTD
MID
CTD
123 148
EMC/2012 C M
Qatar/2015 G I
Jordan-1/2015 G I
ORF3
SP
17 22
L S
F F
F F
77 86
L P
R L
R L
ORF4b
6 44
EMC/2012 M H
Qatar/2015 T P
Jordan-1/2015 T P
M
4 69 123
M V F
M I I
T I I
N
NTD
CTD
178
L
V
V
S
S1 subunit
S2 subunit
RBD
SP
NTD
RBM
FP
HR1
HR2
TM
CP
1020
EMC/2012 Q
Qatar/2015 R
Jordan-1/2015 R
ORF4a
dsRNA binding motif
36 37 38 39 40 41 42 43 44 45 46 47 48 49 50 51
EMC/2012 L V G T S L H P V L W N C Q L S
Qatar-15/2015 L V G T S L H P V L W N C Q L S
Jordan-1/2015

Figure 4-7. Schematic diagram of divergent amino acids found in proteins of clade A and B MERS-CoV strains. Full aa sequences of thirteen MERS-CoV strains were aligned by the UniProt alignment tool. Differences in aa residues affecting each protein are indicated by single-letter aa codes with positions indicated at the top of the diagram. The black and white letters indicate the aa of the prototype strain EMC/2012 and the clade B strains (Qatar15/2015 and Jordan-1/2015), respectively. The conserved aa sequences within clade A and B strains were highlighted by purple and yellow, respectively. The predicted β-sheet belonging to the classical double-stranded RNA binding αββββα fold of ORF4a is blue boxed. Abbreviations: nsp, non-structural protein; NTD, N terminal domain; CTD, C terminal domain; Ubl, ubiquitin-like domain; MD, Macro domain; SUD-M, middle region of SARS-CoV unique domain; PLpro, papain like protease; NAB, nucleic-acid binding domain; GM2, betacoronavirus-specific marker; TM, transmembrane domain; ZBD, Zinc binding domain; MID, middle domain; SP, signal peptidase; RBD, receptor binding domain; RBM, receptor binding motif; FP, fusion peptide; HR, heptad repeat; CP, cytoplasmic domain.

Discussion

Despite the worldwide reduction of MERS cases and deaths since 2016 (Donnelly et al., 2019), MERS-CoV is nowadays still circulating among dromedary camels (Al-Shomrani et al., 2020) and sporadic cases of human infection have continuously been reported (National Events et al.; WHO, 2020). In the Arabian Peninsula, all contemporary zoonotic MERS-CoVs belong to clade B. Hence, the evolution of clade B viruses throughout the epidemic must be an advantage over early epidemic clade A strains in the reservoir host. Here, our study provides a rational explanation on why B strains substituted clade A strains in the field. We compared the viral replication competence, tissue tropism and induced innate host immune responses of the prototype MERS-CoV strain EMC/2012 (clade A) to the Jordan-1/2015 strain (clade B), all isolated from humans. None of the inoculated alpacas had clinical signs at any time, and no macroscopic or significant histopathological lesions were observed upon infection with both strains. Nonetheless, MERS-CoV EMC/2012 and Jordan-1/2015 strains exhibited sharp contrasts in viral nasal shedding, tissue tropism and replication competence. Alpacas challenged with the Jordan-1/2015 strain had higher titers of infectious virus in their nasal cavity than those receiving the EMC/2012 strain, suggesting a higher transmission capability of clade B strains by camelids. Indeed, a higher replication capacity of the Jordan-1/2015 strain was observed in the nasal epithelia of infected alpacas. Moreover, compared to the EMC/2012 strain, the Jordan-1/2015 strain exhibited a broader tissue tropism, showing productive infection in tracheal, bronchial, and bronchiolar epithelial cells. In fact, Qatar15/2015, another

MERS-CoV clade B strain used in a previous study, had comparable replication competences in the nasal mucosa as observed with the Jordan-1/2015 strain (Chapter 3). Thus, clade B viral strains are apparently displaying a better replicative fitness in camelids than the EMC/2012 strain (a clade A strain).

At the first 24 h of infection, type I or III IFNs were moderate to highly (see Supplementary table 4-1) induced in nasal tissues of alpacas in response to the Jordan-1/2015 strain, but not to the EMC/2012 strain. Our previous results with the Qatar15/2015 strain showed that only IFNβ started to be transcribed on 1 dpi (Chapter 3). Thus, such an early IFN response is likely due to the partial aa deletion in the ORF4a protein affecting the Jordan-1/2015 strain. ORF4a strongly antagonizes the dsRNA-binding protein PACT, thereby inhibiting PACT-induced activation of RIG1 and further suppressing the induction of IFNβ (Siu et al., 2014). Of note, the deleted region of the Jordan-1/2015 ORF4a contains a predicted β-sheet that is suspected to affect the binding of dsRNA (Lamers et al., 2016). By contrast, the EMC/2012 and the Qatar15/2015 strains harbor intact ORF4a genomes. Therefore, ORF4a is not implicated in the early replication of MERS-CoV. In addition, the peaks of MERS-CoV replication and IFN transcription coincided in all three strains at 2 dpi. We confirmed that the levels of IFNs transcription correlated with tissue viral replication; however, despite similar viral loads were found in MPNE areas collected at 2 and 3 dpi, the Jordan-1/2015 strain elicited a much higher transcription of IFNs than did the EMC/2012 strain. Nevertheless, it cannot definitely be concluded that the Jordan-1/2015 strain is a better inducer of IFNs because of the small number of MPNE samples collected in group 1 animals. A more adequate technology, such as single cell RNAseq on camelid primary epithelial cells could answer this question.

Despite an enhanced replication competence and early IFN induction in the nasal mucosa, the Jordan-1/2015 strain led to very similar moderate pro-inflammatory gene responses as the one caused by the EMC/2012 strain along alpaca respiratory tracts. Of interest, and contrary to ISGs, IFNs were not induced at any time of the infection in trachea and lungs as observed in a previous study performed with the Qatar15/2015 strain (Chapter 3), supporting the hypothesis that IFNs produced in the nasal mucosa can act in an endocrine manner. Additionally, the same microscopic histopathological alterations were noted in nasal turbinates of alpacas infected by strains used in the present study and were like those provoked by the Qatar15/2015 strain (Chapter 3

manuscript). These tissue alterations were characterized by very mild lesions, with infiltration of a low number of macrophages and lymphocytes. Nevertheless, differences found between Qatar15/2015 and Jordan-1/2015 strains resided in higher numbers of IHC MERS-CoV positive epithelial cells in the LRT and infiltration of leukocytes in the lungs of alpacas undergoing an infection with the Qatar15/2015. By contrast, the EMC/2012 strains did not replicate within the alpaca lungs, suggesting that Qatar15/2015 strain might be the most pathogenic virus used so far in camelids. These observations translated at the transcriptional level in Qatar15/2015 infected animals by an upregulation of pro-inflammatory genes such as NLRP3, TNFa and IL15 (Chapter 3). By contrast, in lungs of hDPP4 transduced mice infected with the clade B strain, ChinaGD01, only IRF3, IRF5 and IL15 were significantly upregulated in relation to the EMC/2012 strain. A more severe inflammation was reported in the lung of mice infected with the ChinaGD01 strain, but no differences in transcription of IFNs were observed between the two strains (Wang et al., 2020).

Based on the comparison of coding sequences between all clade A and representative clade B strains, it appears that multiple punctual aa mutations are mostly distributed along the replicase gene. One of the most striking changes differentiating clade A and B strains is the L864I substitution at the palm and fingers subdomain of PLpro but this mutation does not occur at the catalytic core of PLpro. Of note, CoV PLpros have a dual functionality, as they not only cleave three sites in the polyproteins to release nsp1, nsp2 and nsp3, but can also deconjugate ubiquitine (Ub) and ISG15 which play an important role in antiviral innate immunity (Mielech et al., 2014b). Further work is required to determine whether this mutation or others affect viral replication capacities, as observed in this study, or antiviral mechanisms. Another key clade B specific mutation (Q1020R) happened in HR1, which is an essential component of the fusion mechanism of the CoV S protein allowing passage of the virus across the endosomal membrane (Gao et al., 2013b). In fact, Arginine at position 1020 of the S protein was believed to be the hallmark of the clade B strains (Lau et al., 2017) and was positively selected during the virus evolution (Naeem et al., 2020). Despite the fact that the Q1020R mutation is not predicted to alter its alpha helical structure, the arginine provides an endosomal protonated residue and a potential endosomal protease cleavage site that may affect the S protein membrane fusion function (Cotten et al., 2014). Further studies are required to demonstrate the role of this motif in the survival of

lineage B strains over lineage A. The remaining three clade B specific mutations affecting nsp2 (K533N), nsp3 (M517I) and nsp4 (A40V) occurred at sites of undetermined biological functions. Together, all these clade specific mutations could contribute to an enhanced replication competence of clade B strains. Overall, we show experimental evidence that early epidemic clade A strains could be outcompeted by contemporary viruses due to a higher reproductive fitness in camelid populations. Nonetheless, none of the strains tested so far in camelids caused disease but rather elicited an effective innate immune response based on an early recruitment of antiviral mechanisms and a controlled inflammation. Further reverse genetic studies are needed to unravel the consequences of mutations differentiating different MERS-CoV clades and influencing increased replication capacity as their interaction with host components of innate immune pathways.

Supplementary tables 4-1 and 4-2 are available online at:

https://drive.google.com/drive/folders/1CqA0ynYq-BQXqKhpLnqg_FTuVFWqUqZO?usp=sharing

PART III

General discussion and conclusions

Chapter 5

General discussion

SARS and MERS outbreaks, which have caused major public concern in the last two decades, and the ongoing COVID-19 pandemic urge the need to be fully prepared for emerging pathogenic CoVs of zoonotic origin. Among all these life-threatening viruses, MERS-CoV infection exhibits the highest case fatality rate of 35% among patients. The severe pathogenic features of MERS-CoV infection, including diffuse alveolar damage and ARDS or even death, is mainly due to complex and dynamic processes characterized by high levels of inflammatory cytokines and chemokines and massive infiltration of inflammatory cells towards the lungs (Alosaimi et al., 2020). By contrast, the infection in dromedary camels, the natural intermediate/reservoir host for MERS-CoV (Corman et al., 2014a; Reusken et al., 2013b), is only manifested as asymptomatic, accompanied by a quick viral clearance in about 1 week post-infection (Adney et al., 2014). Since MERS-CoV main acquisition in humans is by close contact with dromedary camels (Azhar et al., 2014), it was of major interest to gain insights into how this reservoir/intermediate host control MERS-CoV infection. In our study, we selected alpacas as the animal model since this new world camelid is also an important surrogate for dromedaries under experimental conditions (Adney et al., 2016a; Crameri et al., 2016b). However, information in camelids on aspects such as innate immune responses and susceptibility to different MERS-CoV strains has not been addressed in the existing literature before starting of this PhD Thesis. For these reasons, two experimental infections with clade A and B MERS-CoV strains were performed in the alpaca model.

Firstly, we unraveled the mechanistic features underlying asymptomatic clinical manifestations of alpacas in response to the Qatar15/2015 MERS-CoV clade B strain. These animals elicited a strong type I/III IFN response concomitant with the peak of viral infection and induction of the anti-inflammatory cytokine IL10. This was associated with a mild to moderate upregulation of pro-inflammatory cytokines in the respiratory mucosa, which eventually led to the rapid clearance of the virus (Chapter 3). Secondly, we studied two viral strains, the EMC/2012 and the Jordan-1/2015 belonging to MERS-CoV clade A and B strains, respectively. Comparative pathogenesis of both strains at the early stages of infection revealed a better replicative capacity of the Jordan-1/2015 strain than did the EMC/2012 strain in alpaca respiratory tracts, providing a rationale for the substitution of clade A over clade B strains in host reservoirs as observed in the Arabian Peninsula (Chapter 4). Furthermore, unlike the EMC/2012 strain and its clade B counterpart (Qatar15/2015), the Jordan-1/2015 strain,

exhibiting a deletion in ORF4a, induced an earlier type I and III IFN transcription on 1 dpi.

Robust, well-timed, and localized type I and III IFN responses in counteracting early MERS-CoV infection in camelids are the most noteworthy findings of the present PhD Thesis. Existing literature reported that IFNs were either inhibited or delayed in humans cells and *ex vivo* respiratory tissues (Chan et al., 2013b; Comar et al., 2019; Zhao et al., 2019; Zhou 2, 3) et al., 2014; Zielecki et al., 2013). Such an impaired IFN response seems to be also a hallmark of other highly pathogenic CoV infections, as described in SARS-CoV and SARS-CoV-2 related studies. Aged macaques developed a far more severe lung pathology than young adult animals in response to SARS-CoV (Smits et al., 2010). Cytokine transcriptional profiles indicated that aged macaques had a stronger activation of pro-inflammatory pathways, such as upregulation of IL6, IP10, MCP1 and IL8, and significantly lower levels of IFNβ mRNA than did young adult macaques on 4 dpi. Thus, differential regulation of IFNs and pro-inflammatory cytokine responses between young and aged macaques can determine disease outcome (Smits et al., 2010). Apparently, young adult macaques avoided lung immunopathology due to both optimal IFNβ and probably anti-inflammatory effector responses, like what has been observed for MERS-CoV infected alpacas. In that respect, our studies in this camelid species highlights the possible role of type III IFNs and IL10 as negative regulators of the inflammatory response. By contrast, exacerbated innate immune responses to SARS-CoV in aged macaques resembles that affecting patients severely affected by SARS, MERS and COVID-19 in which the disease progression may lead to widespread immune dysregulation and severe pathology such as ARDS (Franks et al., 2003; Ksiazek et al., 2003; Nicholls et al., 2003; PY et al., 2004; Yang et al., 2020; Zumla et al., 2015). Notably, delayed or dysregulated expression of IFNβ is also known to be the major cause for exuberant inflammatory host responses with consequences of severe lung injury described in murine models of SARS and MERS (Channappanavar et al., 2016, 2019a). These latter authors observed that administration of IFNβ after the peak of infection promotes a robust pro-inflammatory cytokine response and accumulation of activated monocyte–macrophages, resulting in fatal pneumonia in an otherwise sublethal illness in SARS-CoV and MERS-CoV infected BALB/c mice. By contrast, type I IFNs administered prior to the peak of infection in mice promoted viral clearance and protected animals from lethal SARS-CoV and MERS-CoV infections

(Channappanavar et al., 2016, 2019a; Kumaki et al., 2011; Zhao et al., 2014). In addition, impaired type I and III IFN induction and high expression levels of pro-inflammatory cytokines and chemokines, such as IL6, CXCL8, CCL8, CXCL9, CXCL16 and CCL2, in lungs of critically ill COVID-19 patients have been described (Blanco-Melo et al., 2020). In that respect, MERS-CoV induced early and transient type I and III IFN transcription simultaneous to the peak of the viral infection in alpacas, most likely resulting in protective mucosal immunity and dampened deleterious inflammatory responses. Thus, it appears that robust and well-timed (prior or concomitant to maximal viral replication) type I/III IFN mucosal responses can effectively control viral disease.

In our studies, we have highlighted the importance of the nasal mucosa, the privileged tissue for MERS-CoV replication, as the key location for triggering IFN responses and modulating the strong antiviral effect along the respiratory tract. We speculate that the cross talk between the viral activated mucosa and infiltrating leukocytes prevent exacerbation of inflammatory cell infiltration in intermediary/reservoir hosts leading to asymptomatic disease. Most, if not all, studies performed in fully susceptible hosts indicate a paralysis of mucosal epithelial cell responses, which could inhibit effector mechanisms aimed to modulate the recruitment and activation of inflammatory cells.

Upregulation of antiviral ISGs elicited by MERS-CoV are key findings of IFN - mediated protective innate immune responses in alpacas. Despite tight IFN responses localized only at the nasal mucosa, antiviral ISGs were induced along the whole respiratory tract, suggesting a potential paracrine/endocrine mode of action. In contrast, global ISG responses are mostly suppressed in Calu-3 human epithelial cells due to the altered histone modification caused by MERS-CoV (Menachery et al., 2014). In addition, MERS-CoV accessory and structural proteins also inhibit the production of ISGs. For instance, MERS-CoV ORF 4a and 4b antagonize Protein kinase R and OAS1 respectively, thereby evading infection by limiting antiviral host responses (Rabouw et al., 2016; Thornbrough et al., 2016). The MERS-CoV N protein also impedes RIG1 ubiquitination by interacting with TRIM25, eventually blocking the production of IFNs and thus, various antiviral ISGs. In alpaca nasal mucosa, by contrast, MX1, ISG15, OAS1, CXCL10 and TRIM25 followed the same transcriptional kinetics as type I and III IFNs, starting at 1 dpi, peaking at 2 dpi and dimming from 3 dpi onwards. Such a timely induction of ISGs mRNAs was previously reported to be an important

mechanism for clearance of RNA viruses (Malterer et al., 2014; Schoggins et al., 2011). As a given ISG hardly inhibits virus infection when expressed individually, antiviral effects increase once various ISGs are expressed in combination (Malterer et al., 2014; Schoggins et al., 2011). Accordingly, in the alpaca mucosa, simultaneous upregulation of several antiviral ISGs potentially acting at different stages of the MERS-CoV life cycle and survival, such as genomic viral replication (OAS1), ubiquitination of RIG1 (TRIM 25), protein viral assembly (MX1) or viral translation, replication and egress (ISG15), suggests a potential cross talk between all these antiviral effectors. Importantly, except for TRIM25, no functional studies have been performed to assess the exact role of antiviral ISGs in counteracting highly pathogenic CoVs. In that respect, interactions of camelid ISGs at the molecular level with MERS-CoV compounds should provide important indications on an effective innate immune response. Therefore, further studies and development of specific reagents will be needed to ascertain the role of each ISG against MERS-CoV pathogenesis.

The main manifestation characterizing disease of pathogenic CoVs is an acute inflammation occurring in the LRT. This finding sharply contrasts with reservoir/intermediary hosts. The NLRP3 inflammasome, an essential cause of activation of pro-inflammatory cytokines, is composed of a sensor NLRP3, an adapter component ASC (PYCARD), and an effector CASP1 which cleaves pro IL1β to a mature IL1β form (Elliott and Sutterwala, 2015; Latz et al., 2013). It has been reported that highly pathogenic CoVs initiates the NLRP3 inflammasome cascade (Ahn et al., 2019; Conti et al., 2020; Shi et al., 2019) with IL1β acting via mechanisms such as formation of pores with ion-redistribution and lysosomal disruption (Mangan et al., 2018; Shah, 2020). SARS-CoV activates the NLRP3 inflammasome in both human macrophages and human lung epithelial cells, thereby releasing mature IL1β, a potent mediator of pulmonary inflammation and fever (Shi et al., 2019). In humans or mice, MERS-CoV and SARS-CoV-2 are also suggested to promote overactivation of the NLRP3 inflammasome cascades by eventually triggering an IL1β driven cytokine storm (Ahn et al., 2019; Conti et al., 2020). By contrast, reduced activation of pro-inflammatory pathways in bat cells following MERS-CoV infection is due to a dampened NLRP3 inflammasome, being the hallmark of an enhanced innate immune tolerance (Ahn et al., 2019). In the alpaca respiratory mucosa, MERS-CoV infection did not cause an upregulation of all NLRP3 inflammasome components. Indeed, the

transcription of NLRP3 remained at basal levels in the UTR mucosa and was slightly upregulated in the lung. Therefore, camelids and bats may control acute inflammatory responses caused by MERS-CoV infection via a controlled regulation of the NLRP3 inflammasome. However, initiation of the inflammatory cascade is not known in fully susceptible hosts. Here again, in depth studies in reservoir/intermediary hosts will shed insights on how the NLRP3 inflammasome is not fully activated, either by transcriptional control or deprivation of compounds (reactive oxygen species or cathepsins B for example) initiating the cascade. In all, the NLRP3 inflammasome cascade appears to be an interesting druggable target to reduce acute inflammation in COVID-19 patients, or in other diseases caused by CoVs (Shah, 2020).

Taking into account the relatively mild disease manifestation in young people and severe or even lethal outcome in elderly patients (Alghamdi et al., 2014; Hon et al., 2003; Leung and Chiu, 2004; Peiris et al., 2003; Zhou et al., 2020), it is likely that aging is also a predisposing factor determining CoV prognosis. It has been shown that significant differences of host immune responses between aged and young adult macaques infected with SARS-CoV were a result of aging only (Smits et al., 2010). This observation was largely in line with studies performed in the murine model. Aged mice displayed more severe histopathologic lesions in the lungs and a robust pro-inflammatory cytokine response to SARS-CoV and SARS-CoV-2 than in young adult mice, suggesting an exacerbated and dysregulated host response (Baas et al., 2008; Sun et al., 2020). Young adult mice, however, were able to clear the virus as pro-inflammatory cytokine regressed to basal levels (Baas et al., 2008). It has been hypothesized that age-related accumulated oxidative damage can be an essential mechanism for disease progression (Chung et al., 2006; Imai et al., 2008; Smits et al., 2010). Since all our experiments were performed using young adult alpacas (6 to 8 months age), it is rather difficult to conclude whether aging significantly affects disease outcome in camelids. In that respect, comparative pathogenesis of MERS-CoV in young and aged alpacas will answer this question although clinical signs have never been reported in camelids suggesting mild differences in immunopathogenic mechanisms.

Future directions

A more detailed understanding of the MERS-CoV pathogenesis would probably require establishing *in vitro* explant/organoid models in which main innate immune pathways (PRRs, NF-κB, JAK-STAT and NLRP3 inflammasome) could be easily manipulated by the use of specific agonists/antagonist drugs or compounds. Such a model will definitively allow identifying the exact signaling pathways through which MERS-CoV can replicate during the first days of infection and camelids mount latter an efficient innate immune response. These pathways could be common to highly pathogenic CoVs, leading to a more rational search for curative drugs.

MERS-CoV clade C strains, which form a separate group from those currently circulating in the Arabian Peninsula (Chan et al., 2014; Chu et al., 2015, 2014a, 2018), are endemic in dromedaries across Africa. However, locally acquired zoonotic MERS has not been reported so far in the African continent (Kandeil et al., 2019). Thus, one would speculate that genetic or phenotypic differences in these viruses may explain differences in zoonotic potential. Despite frequent imports of MERS-CoV infected camels from Africa, clade C strains were not found in dromedary herds in Saudi Arabia (El-Kafrawy et al., 2019). Considering that clade B strains successfully substituted clade A strains in the Arabian Peninsula due to an enhanced replicative fitness in camelids, it would be of interest to compare and contrast the pathogenesis of clade C African strains with Arabian strains in a camelid model. Such a study will definitively help addressing the question on how MERS-CoV strains are evolving and acquiring transmissibility and virulence.

Chapter 6

Conclusions

1. Efficient MERS-CoV replication in the respiratory tract indicate that alpacas represent a good experimental model to recapitulate the subclinical MERS-CoV infection observed in the reservoir host, the dromedary camel.

2. In response to MERS-CoV, and concomitant to the peak of infection occurring at 2 dpi, type I and III IFNs were induced only in the nasal mucosa of alpacas where virus replication was most abundant. Consequently, ISGs were upregulated along the whole respiratory tract via a paracrine/endocrine manner. Infection was resolved in tissues from 3 dpi onwards.

3. Concomitant to the mild and focal infiltration of some leucocytes in the nasal mucosa and submucosa, the anti-inflammatory gene IL10 was upregulated along a dampened transcription of pro-inflammatory cytokines and NLRP3 inflammasome components under NF-κB control restricting an eventual cytokine storm.

4. Induction of chemokines (CCL2 and CCL3) in the lung correlated with a transient accumulation of leukocytes in the absence of IRF5 transcription, suggesting low abundance of M1 macrophages and thus, controlled inflammation. Besides, upregulation of IL15 could activate of NK cells contributing to virus clearance.

5. Alpacas inoculated with MERS-CoV Qatar15/2015 and Jordan-1/2015 strains had higher viral replication in respiratory tissues and higher viral shedding than did the clade A EMC/2012 strain, confirming an enhanced replicative fitness of clade B MERS-CoV strains in a camelid host. Indeed, clade B strains carry specific, non-synonymous mutations particularly in the replicase and the S protein. Such characteristics provide a rational for the dominance of clade B strains in the Arabian Peninsula.

6. The Jordan-1/2015 strain exhibits a 16 aa deletion in ORF4a and was able to induce earlier type I and III IFN transcripts than the EMC/2012 and Qatar15/2015 strains in the nasal epithelia, proving the IFN antagonistic role of ORF4a *in vivo*. This early IFN induction accompanied by an early transcription of ISGs did not preclude high viral replication in the first 2 days of infection.

7. All three MERS-CoV strains used in this PhD Thesis (EMC/2012, Qatar15/2015 and Jordan-1/2015) led to very similar histopathological changes, except that alpacas infected by the Qatar15/2015 strain displayed a higher infiltration of leukocytes within the alveoli. Apparently, pro-inflammatory responses differed only by their intensity and not by the timing of induction and the categories of genes involved.

References

Aboagye, J.O., Yew, C.W., Ng, O.-W., Monteil, V.M., Mirazimi, A., and Tan, Y.-J. (2018). Overexpression of the nucleocapsid protein of Middle East respiratory syndrome coronavirus up-regulates CXCL10. Biosci. Rep. *38*, BSR20181059.

Adney, D.R., van Doremalen, N., Brown, V.R., Bushmaker, T., Scott, D., de Wit, E., Bowen, R.A., and Munster, V.J. (2014). Replication and shedding of MERS-CoV in upper respiratory tract of inoculated droamedary camels. Emerg. Infect. Dis. *20*, 1999–2005.

Adney, D.R., Bielefeldt-Ohmann, H., Hartwig, A.E., and Bowen, R.A. (2016a). Infection, replication, and transmission of Middle East respiratory syndrome coronavirus in alpacas. Emerg. Infect. Dis. *22*, 1031–1037.

Adney, D.R., Brown, V.R., Porter, S.M., Bielefeldt-Ohmann, H., Hartwig, A.E., and Bowen, R.A. (2016b). Inoculation of goats, sheep, and horses with MERS-CoV does not result in productive viral shedding. Viruses *8*.

Adney, D.R., Letko, M., Ragan, I.K., Scott, D., van Doremalen, N., Bowen, R.A., and Munster, V.J. (2019). Bactrian camels shed large quantities of Middle East respiratory syndrome coronavirus (MERS-CoV) after experimental infection*. Emerg. Microbes Infect. *8*, 717–723.

Agrawal, A.S., Garron, T., Tao, X., Peng, B.-H., Wakamiya, M., Chan, T.-S., Couch, R.B., and Tseng, C.-T.K. (2015). Generation of a Transgenic Mouse Model of Middle East Respiratory Syndrome Coronavirus Infection and Disease. J. Virol. *89*, 3659–3670.

Ahn, M., Anderson, D.E., Zhang, Q., Tan, C.W., Lim, B.L., Luko, K., Wen, M., Chia, W.N., Mani, S., Wang, L.C., et al. (2019). Dampened NLRP3-mediated inflammation in bats and implications for a special viral reservoir host. Nat. Microbiol. *4*, 789–799.

Akira, S., Takeda, K., and Kaisho, T. (2001). Toll-like receptors: Critical proteins linking innate and acquired immunity. Nat. Immunol.

Akira, S., Uematsu, S., and Takeuchi, O. (2006). Pathogen recognition and innate immunity. Cell.

Al-Abdallat, M.M., Payne, D.C., Alqasrawi, S., Rha, B., Tohme, R.A., Abedi, G.R., Nsour, M. Al, Iblan, I., Jarour, N., Farag, N.H., et al. (2014). Hospital-associated outbreak of middle east respiratory syndrome coronavirus: A serologic, epidemiologic, and clinical description. Clin. Infect. Dis.

Al-Shomrani, B.M., Manee, M.M., Manee, M.M., Alharbi, S.N., Altammami, M.A., Alshehri, M.A., Nassar, M.S., Bakhrebah, M.A., and Al-Fageeh, M.B. (2020). Genomic sequencing and analysis of eight camel-derived middle east respiratory syndrome coronavirus (MERS-CoV) isolates in Saudi Arabia. Viruses *12*.

Al-Tawfiq, J.A., and Auwaerter, P.G. (2019). Healthcare-associated infections: the hallmark of Middle East respiratory syndrome coronavirus with review of the literature. J. Hosp. Infect.

Alenazi, T.H., Al Arbash, H., El-Saed, A., Alshamrani, M.M., Baffoe-Bonnie, H., Arabi, Y.M., Al Johani, S.M., Hijazi, R., Alothman, A., and Balkhy, H.H. (2017). Identified Transmission Dynamics of Middle East Respiratory Syndrome Coronavirus

Infection during an Outbreak: Implications of an Overcrowded Emergency Department. Clin. Infect. Dis. *65*, 675–679.

Alfaraj, S.H., Al-Tawfiq, J.A., Altuwaijri, T.A., Alanazi, M., Alzahrani, N., and Memish, Z.A. (2018). Middle East respiratory syndrome coronavirus transmission among health care workers: Implication for infection control. Am. J. Infect. Control.

Alghamdi, I.G., Hussain, I.I., Almalki, S.S., Alghamdi, M.S., Alghamdi, M.M., and El-Sheemy, M.A. (2014). The pattern of Middle east respiratory syndrome coronavirus in Saudi Arabia: A descriptive epidemiological analysis of data from the Saudi Ministry of Health. Int. J. Gen. Med. *7*, 417–423.

Alharbi, N.S., Guan, Y., Alsulaimany, F.A.S., Li, L., Abu-Zeid, M., E. M. Abo-Aba, S., Zhou, B., Sabir, J.S.M., Zhang, Y., Qureshi, M.I., et al. (2015). Co-circulation of three camel coronavirus species and recombination of MERS-CoVs in Saudi Arabia. Science (80-.). *351*, 81–84.

Ali, S., Mann-Nüttel, R., Schulze, A., Richter, L., Alferink, J., and Scheu, S. (2019). Sources of type I interferons in infectious immunity: Plasmacytoid dendritic cells not always in the driver's seat. Front. Immunol. *10*.

Alosaimi, B., Hamed, M.E., Naeem, A., Alsharef, A.A., AlQahtani, S.Y., AlDosari, K.M., Alamri, A.A., Al-Eisa, K., Khojah, T., Assiri, A.M., et al. (2020). MERS-CoV infection is associated with downregulation of genes encoding Th1 and Th2 cytokines/chemokines and elevated inflammatory innate immune response in the lower respiratory tract. Cytokine *126*, 154895.

Alsaad, K.O., Hajeer, A.H., Al Balwi, M., Al Moaiqel, M., Al Oudah, N., Al Ajlan, A., AlJohani, S., Alsolamy, S., Gmati, G.E., Balkhy, H., et al. (2018). Histopathology of Middle East respiratory syndrome coronovirus (MERS-CoV) infection - clinicopathological and ultrastructural study. Histopathology *72*, 516–524.

Arabi, Y.M., Shalhoub, S., Mandourah, Y., Al-Hameed, F., Al-Omari, A., Qasim, E. Al, Jose, J., Alraddadi, B., Almotairi, A., Khatib, K. Al, et al. (2020). Ribavirin and Interferon Therapy for Critically Ill Patients with Middle East Respiratory Syndrome: A Multicenter Observational Study. Clin. Infect. Dis.

Azhar, E.I., El-Kafrawy, S.A., Farraj, S.A., Hassan, A.M., Al-Saeed, M.S., Hashem, A.M., and Madani, T.A. (2014). Evidence for camel-to-human transmission of MERS coronavirus. N. Engl. J. Med. *370*, 2499–2505.

Baas, T., Roberts, A., Teal, T.H., Vogel, L., Chen, J., Tumpey, T.M., Katze, M.G., and Subbarao, K. (2008). Genomic Analysis Reveals Age-Dependent Innate Immune Responses to Severe Acute Respiratory Syndrome Coronavirus. J. Virol. *82*, 9465–9476.

Bailey-Elkin, B.A., Knaap, R.C.M., Johnson, G.G., Dalebout, T.J., Ninaber, D.K., Van Kasteren, P.B., Bredenbeek, P.J., Snijder, E.J., Kikkert, M., and Mark, B.L. (2014). Crystal structure of the middle east respiratory syndrome coronavirus (MERS-CoV) papain-like protease bound to ubiquitin facilitates targeted disruption of deubiquitinating activity to demonstrate its role in innate immune suppression. J. Biol. Chem. *289*, 34667–34682.

Ballester, M., Cordón, R., and Folch, J.M. (2013). DAG expression: High-throughput gene expression analysis of real-time PCR data using standard curves for relative quantification. PLoS One *8*.

Bart L. Haagmans, 1, * Judith M. A. van den Brand, 1 V. Stalin Raj, 1 Asisa Volz, 2, Peter Wohlsein, 3 Saskia L. Smits, 1 Debby Schipper, 1 Theo M. Bestebroer, 1, Nisreen Okba, 1 Robert Fux, 2 Albert Bensaid, 4 David Solanes Foz, 4 Thijs Kuiken, 1, Wolfgang Baumgärtner, 3 Joaquim Segalés, 5, 6 Gerd Sutter, 2, and * Albert D. M. E. Osterhaus1, 7, 8* (2016). An orthopoxvirus-based vaccine reduces virus excretion after MERS-CoV infection in dromedary camels. Science (80-.). *351*, 77–82.

Baseler, L.J., Falzarano, D., Scott, D.P., Rosenke, R., Thomas, T., Munster, V.J., Feldmann, H., and De Wit, E. (2016). An acute immune response to middle east respiratory syndrome coronavirus replication contributes to viral pathogenicity. Am. J. Pathol. *186*, 630–638.

Bermingham, A., Chand, M.A., Brown, C.S., Aarons, E., Tong, C., Langrish, C., Hoschler, K., Brown, K., Galiano, M., Myers, R., et al. (2012). Severe respiratory illness caused by a novel coronavirus, in a patient transferred to the United Kingdom from the Middle East, September 2012. Eurosurveillance.

Blanco-Melo, D., Nilsson-Payant, B.E., Liu, W.C., Uhl, S., Hoagland, D., Møller, R., Jordan, T.X., Oishi, K., Panis, M., Sachs, D., et al. (2020). Imbalanced Host Response to SARS-CoV-2 Drives Development of COVID-19. Cell *181*, 1036-1045.e9.

van Boheemen, S., de Graaf, M., Lauber, C., Bestebroer, T.M., Raj, V.S., Zaki, A.M., Osterhaus, A.D.M.E., Haagmans, B.L., Gorbalenya, A.E., Snijder, E.J., et al. (2012). Genomic characterization of a newly discovered coronavirus associated with acute respiratory distress syndrome in humans. MBio *3*.

Bohmwald, K., Gálvez, N.M.S., Canedo-Marroquín, G., Pizarro-Ortega, M.S., Andrade-Parra, C., Gómez-Santander, F., and Kalergis, A.M. (2019). Contribution of cytokines to tissue damage during human respiratory syncytial virus infection. Front. Immunol. *10*, 452.

Caì, Y., Yú, S.Q., Postnikova, E.N., Mazur, S., Bernbaum, J.G., Burk, R., Zhāng, T., Radoshitzky, S.R., Müller, M.A., Jordan, I., et al. (2014). CD26/DPP4 cell-surface expression in bat cells correlates with bat cell susceptibility to Middle East respiratory syndrome coronavirus (MERS-CoV) infection and evolution of persistent infection. PLoS One *9*, e112060.

Chan, J.F.W., Lau, S.K.P., and Woo, P.C.Y. (2013a). The emerging novel Middle East respiratory syndrome coronavirus: The “knowns” and “unknowns.” J. Formos. Med. Assoc.

Chan, J.F.W., Choi, G.K.Y., Tsang, A.K.L., Tee, K.M., Lam, H.Y., Yip, C.C.Y., To, K.K.W., Cheng, V.C.C., Yeung, M.L., Lau, S.K.P., et al. (2015a). Development and evaluation of novel real-time reverse transcription-PCR assays with locked nucleic acid probes targeting leader sequences of human-pathogenic coronaviruses. J. Clin. Microbiol.

Chan, J.F.W., Yao, Y., Yeung, M.L., Deng, W., Bao, L., Jia, L., Li, F., Xiao, C., Gao, H., Yu, P., et al. (2015b). Treatment with lopinavir/ritonavir or interferon-β1b improves outcome of MERSCoV infection in a nonhuman primate model of common marmoset. J. Infect. Dis. *212*, 1904–1913.

Chan, R.W.Y., Chan, M.C.W., Agnihothram, S., Chan, L.L.Y., Kuok, D.I.T., Fong, J.H.M., Guan, Y., Poon, L.L.M., Baric, R.S., Nicholls, J.M., et al. (2013b). Tropism of and Innate Immune Responses to the Novel Human Betacoronavirus Lineage C Virus in Human Ex Vivo Respiratory Organ Cultures. J. Virol. *87*, 6604–6614.

Chan, R.W.Y., Chu, D.K.W., Poon, L.L.M., Tao, K.P., Ng, H.Y., Chan, M.C.W., Guan, Y., Peiris, J.S.M., Nicholls, J.M., Hemida, M.G., et al. (2014). Tropism and replication of Middle East respiratory syndrome coronavirus from dromedary camels in the human respiratory tract: An in-vitro and ex-vivo study. Lancet Respir. Med. *2*, 813–822.

Chang, C.-Y., Liu, H.M., Chang, M.-F., and Chang, S.C. (2020). Middle East respiratory syndrome coronavirus nucleocapsid protein suppresses type I and type III interferon induction by targeting RIG-I signaling. J. Virol.

Channappanavar, R., Fehr, A.R., Vijay, R., Mack, M., Zhao, J., Meyerholz, D.K., and Perlman, S. (2016). Dysregulated Type I Interferon and Inflammatory Monocyte-Macrophage Responses Cause Lethal Pneumonia in SARS-CoV-Infected Mice. Cell Host Microbe *19*, 181–193.

Channappanavar, R., Fehr, A.R., Zheng, J., Wohlford-Lenane, C., Abrahante, J.E., Mack, M., Sompallae, R., McCray, P.B., Meyerholz, D.K., and Perlman, S. (2019a). IFN-I response timing relative to virus replication determines MERS coronavirus infection outcomes. J. Clin. Invest. *129*, 3625–3639.

Channappanavar, R., Fehr, A.R., Zheng, J., Wohlford-Lenane, C., Abrahante, J.E., Mack, M., Sompallae, R., McCray, P.B., Meyerholz, D.K., and Perlman, S. (2019b). IFN-I response timing relative to virus replication determines MERS coronavirus infection outcomes. J. Clin. Invest. *129*, 3625–3639.

Chowell, G., Abdirizak, F., Lee, S., Lee, J., Jung, E., Nishiura, H., and Viboud, C. (2015). Transmission characteristics of MERS and SARS in the healthcare setting: A comparative study. BMC Med.

Chu, D.K., Oladipo, J.O., Perera, R.A., Kuranga, S.A., Chan, S.M., Poon, L.L., and Peiris, M. (2015). Middle east respiratory syndrome coronavirus (MERSCoV) in dromedary camels in nigeria, 2015. Eurosurveillance *20*, 1–7.

Chu, D.K.W., Poon, L.L.M., Gomaa, M.M., Shehata, M.M., Perera, R.A.P.M., Zeid, D.A., El Rifay, A.S., Siu, L.Y., Guan, Y., Webby, R.J., et al. (2014a). MERS coronaviruses in dromedary camels, Egypt. Emerg. Infect. Dis.

Chu, D.K.W., Hui, K.P.Y., Perera, R.A.P.M., Miguel, E., Niemeyer, D., Zhao, J., Channappanavar, R., Dudas, G., Oladipo, J.O., Traoré, A., et al. (2018). MERS coronaviruses from camels in Africa exhibit region-dependent genetic diversity. Proc. Natl. Acad. Sci. *115*, 3144–3149.

Chu, H., Zhou, J., Ho-Yin Wong, B., Li, C., Cheng, Z.S., Lin, X., Kwok-Man Poon, V., Sun, T., Choi-Yi Lau, C., Fuk-Woo Chan, J., et al. (2014b). Productive replication of Middle East respiratory syndrome coronavirus in monocyte-derived dendritic cells modulates innate immune response. Virology *454–455*, 197–205.

Chung, H.Y., Sung, B., Jung, K.J., Zou, Y., and Yu, B.P. (2006). The molecular inflammatory process in aging. Antioxidants Redox Signal.

Clementz, M.A., Chen, Z., Banach, B.S., Wang, Y., Sun, L., Ratia, K., Baez-Santos, Y.M., Wang, J., Takayama, J., Ghosh, A.K., et al. (2010). Deubiquitinating and Interferon Antagonism Activities of Coronavirus Papain-Like Proteases. J. Virol.

Cockrell, A.S., Peck, K.M., Yount, B.L., Agnihothram, S.S., Scobey, T., Curnes, N.R., Baric, R.S., and Heise, M.T. (2014). Mouse Dipeptidyl Peptidase 4 Is Not a Functional Receptor for Middle East Respiratory Syndrome Coronavirus Infection. J. Virol. *88*, 5195–5199.

Cockrell, A.S., Yount, B.L., Scobey, T., Jensen, K., Douglas, M., Beall, A., Tang, X.-C., Marasco, W.A., Heise, M.T., and Baric, R.S. (2017). A Mouse Model for MERS Coronavirus Induced Acute Respiratory Distress Syndrome Introductory Paragraph HHS Public Access.

Comar, C.E., Goldstein, S.A., Li, Y., Yount, B., Baric, R.S., and Weiss, S.R. (2019). Antagonism of dsRNA-Induced Innate Immune Pathways by NS4a and NS4b Accessory Proteins during MERS Coronavirus Infection. MBio *10*.

Conti, P., Ronconi, G., Caraffa, A., Gallenga, C.E., Ross, R., Frydas, I., and Kritas, S.K. (2020). Induction of pro-inflammatory cytokines (IL-1 and IL-6) and lung inflammation by Coronavirus-19 (COVI-19 or SARS-CoV-2): anti-inflammatory strategies. J. Biol. Regul. Homeost. Agents *34*, 327–331.

Corman, V.M., Eckerle, I., Bleicker, T., Zaki, A., Landt, O., Eschbach-Bludau, M., van Boheemen, S., Gopal, R., Ballhause, M., Bestebroer, T.M., et al. (2012). Detection of a novel human coronavirus by real-time reverse-transcription polymerase chain reaction. Eurosurveillance.

Corman, V.M., Jores, J., Meyer, B., Younan, M., Liljander, A., Said, M.Y., Gluecks, I., Lattwein, E., Bosch, B.J., Drexler, J.F., et al. (2014a). Antibodies against MERS coronavirus in dromedary camels, Kenya, 1992-2013. Emerg. Infect. Dis. *20*, 1319–1322.

Corman, V.M., Ithete, N.L., Richards, L.R., Schoeman, M.C., Preiser, W., Drosten, C., and Drexler, J.F. (2014b). Rooting the Phylogenetic Tree of Middle East Respiratory Syndrome Coronavirus by Characterization of a Conspecific Virus from an African Bat. J. Virol.

Cotten, M., Watson, S.J., Kellam, P., Al-Rabeeah, A.A., Makhdoom, H.Q., Assiri, A., Aal-Tawfiq, J., Alhakeem, R.F., Madani, H., AlRabiah, F.A., et al. (2013). Transmission and evolution of the Middle East respiratory syndrome coronavirus in Saudi Arabia: A descriptive genomic study. Lancet *382*, 1993–2002.

Cotten, M., Watson, S.J., Zumla, A.I., Makhdoom, H.Q., Palser, A.L., Ong, S.H., Al Rabeeah, A.A., Alhakeem, R.F., Assiri, A., Al-Tawfiq, J.A., et al. (2014). Spread, circulation, and evolution of the Middle East respiratory syndrome coronavirus. MBio *5*, 1062–1075.

Crameri, G., Durr, P.A., Klein, R., Foord, A., Yu, M., Riddell, S., Haining, J., Johnson, D., Hemida, M.G., Barr, J., et al. (2016a). Experimental infection and response to rechallenge of alpacas with middle east respiratory syndrome coronavirus. Emerg. Infect. Dis.

Crameri, G., Durr, P.A., Klein, R., Foord, A., Yu, M., Riddell, S., Haining, J., Johnson, D., Hemida, M.G., Barr, J., et al. (2016b). Experimental infection and response to rechallenge of alpacas with middle east respiratory syndrome coronavirus. Emerg. Infect. Dis. *22*, 1071–1074.

Cui, J., Eden, J.-S., Holmes, E.C., and Wang, L.-F. (2013). Adaptive evolution of bat dipeptidyl peptidase 4 (dpp4): implications for the origin and emergence of Middle East respiratory syndrome coronavirus. Virol. J. *10*, 304.

David, D., Rotenberg, D., Khinich, E., Erster, O., Bardenstein, S., van Straten, M., Okba, N.M.A., Raj, S. V., Haagmans, B.L., Miculitzki, M., et al. (2018). Middle East

respiratory syndrome coronavirus specific antibodies in naturally exposed Israeli llamas, alpacas and camels. One Heal. *5*, 65–68.

Davis, W.C., Heirman, L.R., Hamilton, M.J., Parish, S.M., Barrington, G.M., Loftis, A., and Rogers, M. (2000). Flow cytometric analysis of an immunodeficiency disorder affecting juvenile llamas. Vet. Immunol. Immunopathol. *74*, 103–120.

Donnelly, C.A., Malik, M.R., Elkholy, A., Cauchemez, S., and Van Kerkhove, M.D. (2019). Worldwide reduction in MERS cases and deaths since 2016. Emerg. Infect. Dis. *25*, 1758–1760.

van Doremalen, N., Bushmaker, T., and Munster, V.J. (2013). Stability of middle east respiratory syndrome coronavirus (MERS-CoV) under different environmental conditions. Eurosurveillance.

van Doremalen, N., Miazgowicz, K.L., Milne-Price, S., Bushmaker, T., Robertson, S., Scott, D., Kinne, J., McLellan, J.S., Zhu, J., and Munster, V.J. (2014). Host Species Restriction of Middle East Respiratory Syndrome Coronavirus through Its Receptor, Dipeptidyl Peptidase 4. J. Virol. *88*, 9220–9232.

Dotti, I., Bonin, S., Basili, G., Nardon, E., Balani, A., Siracusano, S., Zanconati, F., Palmisano, S., De Manzini, N., and Stanta, G. (2010). Effects of formalin, methacarn, and finefix fixatives on RNA preservation. Diagnostic Mol. Pathol.

Drosten, C., Meyer, B., Müller, M.A., Corman, V.M., Al-Masri, M., Hossain, R., Madani, H., Sieberg, A., Bosch, B.J., Lattwein, E., et al. (2014). Transmission of MERS-coronavirus in household contacts. N. Engl. J. Med.

Drosten, C., Muth, D., Corman, V.M., Hussain, R., Al Masri, M., HajOmar, W., Landt, O., Assiri, A., Eckerle, I., Al Shangiti, A., et al. (2015). An observational, laboratory-based study of outbreaks of middle east respiratory syndrome coronavirus in Jeddah and Riyadh, Kingdom of Saudi Arabia, 2014. Clin. Infect. Dis.

Du, L., Yang, Y., Zhou, Y., Lu, L., Li, F., and Jiang, S. (2017). MERS-CoV spike protein: a key target for antivirals. Expert Opin. Ther. Targets *21*, 131–143.

Dumoutier, L., Lejeune, D., Hor, S., Fickenscher, H., and Renauld, J.C. (2003). Cloning of a new type II cytokine receptor activating signal transducer and activator of transcription (STAT)1, STAT2 and STAT3. Biochem. J.

Durai, P., Batool, M., Shah, M., and Choi, S. (2015). Middle East respiratory syndrome coronavirus: transmission, virology and therapeutic targeting to aid in outbreak control. Exp. Mol. Med. *47*, e181.

El-Kafrawy, S.A., Corman, V.M., Tolah, A.M., Al Masaudi, S.B., Hassan, A.M., Müller, M.A., Bleicker, T., Harakeh, S.M., Alzahrani, A.A., Alsaaidi, G.A., et al. (2019). Enzootic patterns of Middle East respiratory syndrome coronavirus in imported African and local Arabian dromedary camels: a prospective genomic study. Lancet Planet. Heal. *3*, e521–e528.

Elliott, E.I., and Sutterwala, F.S. (2015). Initiation and perpetuation of NLRP3 inflammasome activation and assembly. Immunol. Rev.

Falzarano, D., de Wit, E., Rasmussen, A.L., Feldmann, F., Okumura, A., Scott, D.P., Brining, D., Bushmaker, T., Martellaro, C., Baseler, L., et al. (2013). Treatment with interferon-α2b and ribavirin improves outcome in MERS-CoV-infected rhesus macaques. Nat. Med. *19*, 1313–1317.

Falzarano, D., de Wit, E., Feldmann, F., Rasmussen, A.L., Okumura, A., Peng, X., Thomas, M.J., van Doremalen, N., Haddock, E., Nagy, L., et al. (2014). Infection with MERS-CoV Causes Lethal Pneumonia in the Common Marmoset. PLoS Pathog. *10*.

Fan, J., Ye, R.D., and Malik, A.B. (2001). Transcriptional mechanisms of acute lung injury. Am. J. Physiol. - Lung Cell. Mol. Physiol.

Farag, E.A.B.A., Reusken, C.B.E.M., Haagmans, B.L., Mohran, K.A., Raj, V.S., Pas, S.D., Voermans, J., Smits, S.L., Godeke, G.-J., Al-Hajri, M.M., et al. (2015). High proportion of MERS-CoV shedding dromedaries at slaughterhouse with a potential epidemiological link to human cases, Qatar 2014. Infect. Ecol. Epidemiol. *5*, 28305.

Faure, E., Poissy, J., Goffard, A., Fournier, C., Kipnis, E., Titecat, M., Bortolotti, P., Martinez, L., Dubucquoi, S., Dessein, R., et al. (2014). Distinct immune response in two MERS-CoV-infected patients: Can we go from bench to bedside? PLoS One *9*.

Fehr, A.R., and Perlman, S. (2015). Coronaviruses: An overview of their replication and pathogenesis. In Coronaviruses: Methods and Protocols, p.

Franks, T.J., Chong, P.Y., Chui, P., Galvin, J.R., Lourens, R.M., Reid, A.H., Selbs, E., McEvoy, P.L., Hayden, D.L., Fukuoka, J., et al. (2003). Lung pathology of severe acute respiratory syndrome (SARS): A study of 8 autopsy cases from Singapore. Hum. Pathol. *34*, 743–748.

Gao, J., Lu, G., Qi, J., Li, Y., Wu, Y., Deng, Y., Geng, H., Li, H., Wang, Q., Xiao, H., et al. (2013a). Structure of the fusion core and inhibition of fusion by a heptad repeat peptide derived from the S protein of Middle East respiratory syndrome coronavirus. J. Virol. *87*, 13134–13140.

Gao, J., Lu, G., Qi, J., Li, Y., Wu, Y., Deng, Y., Geng, H., Li, H., Wang, Q., Xiao, H., et al. (2013b). Structure of the Fusion Core and Inhibition of Fusion by a Heptad Repeat Peptide Derived from the S Protein of Middle East Respiratory Syndrome Coronavirus. J. Virol. *87*, 13134–13140.

Gossner, C., Danielson, N., Gervelmeyer, A., Berthe, F., Faye, B., Kaasik Aaslav, K., Adlhoch, C., Zeller, H., Penttinen, P., and Coulombier, D. (2016). Human-Dromedary Camel Interactions and the Risk of Acquiring Zoonotic Middle East Respiratory Syndrome Coronavirus Infection. Zoonoses Public Health.

de Groot, R.J., Baker, S.C., Baric, R.S., Brown, C.S., Drosten, C., Enjuanes, L., Fouchier, R.A.M., Galiano, M., Gorbalenya, A.E., Memish, Z.A., et al. (2013). Middle East Respiratory Syndrome Coronavirus (MERS-CoV): Announcement of the Coronavirus Study Group. J. Virol. *87*, 7790–7792.

Guarda, G., Zenger, M., Yazdi, A.S., Schroder, K., Ferrero, I., Menu, P., Tardivel, A., Mattmann, C., and Tschopp, J. (2011). Differential Expression of NLRP3 among Hematopoietic Cells. J. Immunol.

Haagmans, B.L., Al Dhahiry, S.H.S., Reusken, C.B.E.M., Raj, V.S., Galiano, M., Myers, R., Godeke, G.J., Jonges, M., Farag, E., Diab, A., et al. (2014). Middle East respiratory syndrome coronavirus in dromedary camels: An outbreak investigation. Lancet Infect. Dis.

Haagmans, B.L., van den Brand, J.M.A., Provacia, L.B., Raj, V.S., Stittelaar, K.J., Getu, S., de Waal, L., Bestebroer, T.M., van Amerongen, G., Verjans, G.M.G.M., et al. (2015). Asymptomatic Middle East Respiratory Syndrome Coronavirus Infection in Rabbits. J. Virol. *89*, 6131–6135.

Hartl, D., Tirouvanziam, R., Laval, J., Greene, C.M., Habiel, D., Sharma, L., Yildirim, A.Ö., Dela Cruz, C.S., and Hogaboam, C.M. (2018). Innate Immunity of the Lung: From Basic Mechanisms to Translational Medicine. J. Innate Immun.

Hastings, D.L., Tokars, J.I., Abdel Aziz, I.Z.A.M., Alkhaldi, K.Z., Bensadek, A.T., Alraddadi, B.M., Jokhdar, H., Jernigan, J.A., Garout, M.A., Tomczyk, S.M., et al. (2016). Outbreak of Middle East Respiratory Syndrome at Tertiary Care Hospital, Jeddah, Saudi Arabia, 2014. Emerg. Infect. Dis. *22*, 794–801.

Hayden, M.S., and Ghosh, S. (2004). Signaling to NF-κB. Genes Dev. *18*, 2195–2224.

Hemann, E.A., Green, R., Turnbull, J.B., Langlois, R.A., Savan, R., and Gale, M. (2019). Interferon-λ modulates dendritic cells to facilitate T cell immunity during infection with influenza A virus. Nat. Immunol.

Hemida, M.G., Perera, R.A., Wang, P., Alhammadi, M.A., Siu, L.Y., Li, M., Poon, L.L., Saif, L., Alnaeem, A., and Peiris, M. (2013). Middle east respiratory syndrome (MERS) coronavirus seroprevalence in domestic livestock in Saudi Arabia, 2010 to 2013. Eurosurveillance *18*.

Hemida, M.G., Chu, D.K.W., Poon, L.L.M., Perera, R.A.P.M., Alhammadi, M.A., Ng, H.Y., Siu, L.Y., Guan, Y., Alnaeem, A., and Peiris, M. (2014). Mers coronavirus in dromedary camel herd, Saudi Arabia. Emerg. Infect. Dis.

Hoffmann, H.H., Schneider, W.M., and Rice, C.M. (2015). Interferons and viruses: An evolutionary arms race of molecular interactions. Trends Immunol.

Hon, K.L.E., Leung, C.W., Cheng, W.T.F., Chan, P.K.S., Chu, W.C.W., Kwan, Y.W., Li, A.M., Fong, N.C., Ng, P.C., Chiu, M.C., et al. (2003). Clinical presentations and outcome of severe acute respiratory syndrome in children. Lancet.

Hsieh, Y.H. (2015). 2015 Middle East Respiratory Syndrome Coronavirus (MERS-CoV) nosocomial outbreak in South Korea: Insights from modeling. PeerJ.

Imai, Y., Kuba, K., Neely, G.G., Yaghubian-Malhami, R., Perkmann, T., van Loo, G., Ermolaeva, M., Veldhuizen, R., Leung, Y.H.C., Wang, H., et al. (2008). Identification of Oxidative Stress and Toll-like Receptor 4 Signaling as a Key Pathway of Acute Lung Injury. Cell.

Ithete, N.L., Stoffberg, S., Corman, V.M., Cottontail, V.M., Richards, L.R., Schoeman, M.C., Drosten, C., Drexler, J.F., and Preiser, W. (2013). Close relative of human middle east respiratory syndrome coronavirus in bat, South Africa. Emerg. Infect. Dis.

Kandeil, Gomaa, Nageh, Shehata, Kayed, Sabir, Abiadh, Jrijer, Amr, Said, et al. (2019). Middle East Respiratory Syndrome Coronavirus (MERS-CoV) in Dromedary Camels in Africa and Middle East. Viruses *11*, 717.

Katze, M.G., He, Y., and Gale, M. (2002). Viruses and interferon: A fight for supremacy. Nat. Rev. Immunol.

Kawai, T., and Akira, S. (2010). The role of pattern-recognition receptors in innate immunity: Update on toll-like receptors. Nat. Immunol.

Kawasaki, T., and Kawai, T. (2014). Toll-Like Receptor Signaling Pathways. Front. Immunol. *5*, 124–128.

Kiambi, S., Corman, V.M., Sitawa, R., Githinji, J., Ngoci, J., Ozomata, A.S., Gardner, E., von Dobschuetz, S., Morzaria, S., Kimutai, J., et al. (2018). Detection of distinct

MERS-Coronavirus strains in dromedary camels from Kenya, 2017. Emerg. Microbes Infect. *7*.

Killerby, M.E., Biggs, H.M., Midgley, C.M., Gerber, S.I., and Watson, J.T. (2020). Middle east respiratory syndrome coronavirus transmission. Emerg. Infect. Dis. *26*, 191–198.

Kim, E.S., Choe, P.G., Park, W.B., Oh, H.S., Kim, E.J., Nam, E.Y., Na, S.H., Kim, M., Song, K.H., Bang, J.H., et al. (2016a). Clinical progression and cytokine profiles of middle east respiratory syndrome coronavirus infection. J. Korean Med. Sci. *31*, 1717–1725.

Kim, K.H., Tandi, T.E., Choi, J.W., Moon, J.M., and Kim, M.S. (2017). Middle East respiratory syndrome coronavirus (MERS-CoV) outbreak in South Korea, 2015: epidemiology, characteristics and public health implications. J. Hosp. Infect. *95*, 207–213.

Kim, Y., Lee, S., Chu, C., Choe, S., Hong, S., and Shin, Y. (2016b). The Characteristics of Middle Eastern Respiratory Syndrome Coronavirus Transmission Dynamics in South Korea. Osong Public Heal. Res. Perspect.

Kindler, E., and Thiel, V. (2016). SARS-CoV and IFN: Too Little, Too Late. Cell Host Microbe *19*, 139–141.

Kindler, E., Jónsdóttir, H.R., Muth, D., Hamming, O.J., Hartmann, R., Rodriguez, R., Geffers, R., Fouchier, R.A.M., Drosten, C., Müller, M.A., et al. (2013). Efficient replication of the novel human betacoronavirus EMC on primary human epithelium highlights its zoonotic potential. MBio *4*.

Klinkhammer, J., Schnepf, D., Ye, L., Schwaderlapp, M., Gad, H.H., Hartmann, R., Garcin, D., Mahlakõiv, T., and Staeheli, P. (2018). IFN-λ prevents influenza virus spread from the upper airways to the lungs and limits virus transmission. Elife.

Kok, K.H., Lui, P.Y., Ng, M.H.J., Siu, K.L., Au, S.W.N., and Jin, D.Y. (2011). The double-stranded RNA-binding protein PACT functions as a cellular activator of RIG-I to facilitate innate antiviral response. Cell Host Microbe *9*, 299–309.

Kotenko, S. V. (2011). IFN-λs. Curr. Opin. Immunol. *23*, 583–590.

Kotenko, S. V., Gallagher, G., Baurin, V. V., Lewis-Antes, A., Shen, M., Shah, N.K., Langer, J.A., Sheikh, F., Dickensheets, H., and Donnelly, R.P. (2003). IFN-λs mediate antiviral protection through a distinct class II cytokine receptor complex. Nat. Immunol.

Kotenko, S. V., Rivera, A., Parker, D., and Durbin, J.E. (2019). Type III IFNs: Beyond antiviral protection. Semin. Immunol. *43*.

Krausgruber, T., Blazek, K., Smallie, T., Alzabin, S., Lockstone, H., Sahgal, N., Hussell, T., Feldmann, M., and Udalova, I.A. (2011). IRF5 promotes inflammatory macrophage polarization and T H1-TH17 responses. Nat. Immunol.

Ksiazek, T.G., Erdman, D., Goldsmith, C.S., Zaki, S.R., Peret, T., Emery, S., Tong, S., Urbani, C., Comer, J.A., Lim, W., et al. (2003). A Novel Coronavirus Associated with Severe Acute Respiratory Syndrome. N. Engl. J. Med. *348*, 1953–1966.

Kumaki, Y., Ennis, J., Rahbar, R., Turner, J.D., Wandersee, M.K., Smith, A.J., Bailey, K.W., Vest, Z.G., Madsen, J.R., Li, J.K.K., et al. (2011). Single-dose intranasal administration with mDEF201 (adenovirus vectored mouse interferon-alpha) confers protection from mortality in a lethal SARS-CoV BALB/c mouse model. Antiviral Res.

L. Ferreira, V., H.L. Borba, H., de F. Bonetti, A., P. Leonart, L., and Pontarolo, R. (2019). Cytokines and Interferons: Types and Functions. In Autoantibodies and Cytokines, (IntechOpen), p.

Lamers, M.M., Raj, S. V., Shafei, M., Ali, S.S., Abdallh, S.M., Gazo, M., Nofal, S., Lu, X., Erdman, D.D., Koopmans, M.P., et al. (2016). Deletion variants of middle east respiratory syndrome coronavirus from humans, Jordan, 2015. Emerg. Infect. Dis. *22*, 716–719.

Latz, E., Xiao, T.S., and Stutz, A. (2013). Activation and regulation of the inflammasomes. Nat. Rev. Immunol.

Lau, S.K.P., Lau, C.C.Y., Chan, K.H., Li, C.P.Y., Chen, H., Jin, D.Y., Chan, J.F.W., Woo, P.C.Y., and Yuen, K.Y. (2013). Delayed induction of proinflammatory cytokines and suppression of innate antiviral response by the novel Middle East respiratory syndrome coronavirus: Implications for pathogenesis and treatment. J. Gen. Virol. *94*, 2679–2690.

Lau, S.K.P., Wernery, R., Wong, E.Y.M., Joseph, S., Tsang, A.K.L., Patteril, N.A.G., Elizabeth, S.K., Chan, K.H., Muhammed, R., Kinne, J., et al. (2016). Polyphyletic origin of MERS coronaviruses and isolation of a novel clade A strain from dromedary camels in the United Arab Emirates. Emerg. Microbes Infect. *5*, e128.

Lau, S.K.P., Wong, A.C.P., Lau, T.C.K., and Woo, P.C.Y. (2017). Molecular evolution of MERS coronavirus: Dromedaries as a recent intermediate host or long-time animal reservoir? Int. J. Mol. Sci. *18*.

Lazear, H.M., Schoggins, J.W., and Diamond, M.S. (2019). Shared and Distinct Functions of Type I and Type III Interferons. Immunity *50*, 907–923.

Lee, J.Y., Bae, S., and Myoung, J. (2019). Middle East Respiratory Syndrome Coronavirus-Encoded Accessory Proteins Impair MDA5-and TBK1-Mediated Activation of NF-κB. J. Microbiol. Biotechnol. *29*, 1316–1323.

Leung, C.W., and Chiu, W.K. (2004). Clinical picture, diagnosis, treatment and outcome of severe acute respiratory syndrome (SARS) in children. Paediatr. Respir. Rev.

Li, F. (2015). Receptor recognition mechanisms of coronaviruses: a decade of structural studies. J. Virol. *89*, 1954–1964.

Lindner, H.A., Fotouhi-Ardakani, N., Lytvyn, V., Lachance, P., Sulea, T., and Menard, R. (2005). The Papain-Like Protease from the Severe Acute Respiratory Syndrome Coronavirus Is a Deubiquitinating Enzyme. J. Virol.

Lindner, H.A., Lytvyn, V., Qi, H., Lachance, P., Ziomek, E., and Ménard, R. (2007). Selectivity in ISG15 and ubiquitin recognition by the SARS coronavirus papain-like protease. Arch. Biochem. Biophys.

Liu, H.M., Loo, Y.M., Horner, S.M., Zornetzer, G.A., Katze, M.G., and Gale, M. (2012). The mitochondrial targeting chaperone 14-3-3ε regulates a RIG-I translocon that mediates membrane association and innate antiviral immunity. Cell Host Microbe.

Liu, L., Botos, I., Wang, Y., Leonard, J.N., Shiloach, J., Segal, D.M., and Davies, D.R. (2008). Structural basis of toll-like receptor 3 signaling with double-stranded RNA. Science (80-.).

Lokugamage, K.G., Narayanan, K., Nakagawa, K., Terasaki, K., Ramirez, S.I., Tseng, C.-T.K., and Makino, S. (2015). Middle East Respiratory Syndrome Coronavirus nsp1 Inhibits Host Gene Expression by Selectively Targeting mRNAs Transcribed in the Nucleus while Sparing mRNAs of Cytoplasmic Origin. J. Virol. *89*, 10970–10981.

Lu, G., Hu, Y., Wang, Q., Qi, J., Gao, F., Li, Y., Zhang, Y., Zhang, W., Yuan, Y., Bao, J., et al. (2013). Molecular basis of binding between novel human coronavirus MERS-CoV and its receptor CD26. Nature *500*, 227–231.

Lu, L., Liu, Q., Zhu, Y., Chan, K.H., Qin, L., Li, Y., Wang, Q., Chan, J.F.W., Du, L., Yu, F., et al. (2014). Structure-based discovery of Middle East respiratory syndrome coronavirus fusion inhibitor. Nat. Commun.

Lui, P.Y., Wong, L.Y.R., Fung, C.L., Siu, K.L., Yeung, M.L., Yuen, K.S., Chan, C.P., Woo, P.C.Y., Yuen, K.Y., and Jin, D.Y. (2016). Middle East respiratory syndrome coronavirus M protein suppresses type I interferon expression through the inhibition of TBK1-dependent phosphorylation of IRF3. Emerg. Microbes Infect. *5*, e39.

Mackay, I.M., and Arden, K.E. (2015a). Middle East respiratory syndrome: An emerging coronavirus infection tracked by the crowd. Virus Res. *202*, 60–88.

Mackay, I.M., and Arden, K.E. (2015b). MERS coronavirus: Diagnostics, epidemiology and transmission. Virol. J. *12*, 1–21.

Malterer, M.B., Glass, S.J., and Newman, J.P. (2014). Interferon-stimulated genes: A complex web of host defenses. Annu. Rev. Immunol. *44*, 735–745.

Mangan, M.S.J., Olhava, E.J., Roush, W.R., Seidel, H.M., Glick, G.D., and Latz, E. (2018). Targeting the NLRP3 inflammasome in inflammatory diseases. Nat. Rev. Drug Discov.

Mascarell, L., Lombardi, V., Louise, A., Saint-Lu, N., Chabre, H., Moussu, H., Betbeder, D., Balazuc, A.M., Van Overtvelt, L., and Moingeon, P. (2008). Oral dendritic cells mediate antigen-specific tolerance by stimulating TH1 and regulatory CD4+ T cells. J. Allergy Clin. Immunol. *122*, 603-609.e5.

Matthews, K.L., Coleman, C.M., van der Meer, Y., Snijder, E.J., and Frieman, M.B. (2014). The ORF4b-encoded accessory proteins of Middle East respiratory syndrome coronavirus and two related bat coronaviruses localize to the nucleus and inhibit innate immune signalling. J. Gen. Virol. *95*, 874–882.

Memish, Z.A., Mishra, N., Olival, K.J., Fagbo, S.F., Kapoor, V., Epstein, J.H., AlHakeem, R., Al Asmari, M., Islam, A., Kapoor, A., et al. (2013). Middle East respiratory syndrome coronavirus in Bats, Saudi Arabia. Emerg. Infect. Dis.

Memish, Z.A., Perlman, S., Van Kerkhove, M.D., and Zumla, A. (2020). Middle East respiratory syndrome. Lancet *395*, 1063–1077.

Menachery, V.D., Schäfer, A., Sims, A.C., Gralinski, L.E., Long, C., Webb-Robertson, B.-J., Baric, R.S., Eisfeld, A.J., Fan, S., Li, C., et al. (2014). Pathogenic influenza viruses and coronaviruses utilize similar and contrasting approaches to control interferon-stimulated gene responses. MBio *5*, 1–11.

Menachery, V.D., Mitchell, H.D., Cockrell, A.S., Gralinski, L.E., Yount, B.L., Graham, R.L., McAnarney, E.T., Douglas, M.G., Scobey, T., Beall, A., et al. (2017). MERS-CoV Accessory ORFs Play Key Role for Infection and Pathogenesis. MBio *8*.

Mendoza, J.L., Schneider, W.M., Hoffmann, H.H., Vercauteren, K., Jude, K.M., Xiong, A., Moraga, I., Horton, T.M., Glenn, J.S., de Jong, Y.P., et al. (2017a). The IFN-λ-IFN-λR1-IL-10Rβ Complex Reveals Structural Features Underlying Type III IFN Functional Plasticity. Immunity.

Mendoza, J.L., Schneider, W.M., Hoffmann, H.-H., Vercauteren, K., Jude, K.M., Xiong, A., Moraga, I., Horton, T.M., Glenn, J.S., de Jong, Y.P., et al. (2017b). The IFN-λ-IFN-λR1-IL-10Rβ Complex Reveals Structural Features Underlying Type III IFN Functional Plasticity. Immunity *46*, 379–392.

Mielech, A.M., Kilianski, A., Baez-Santos, Y.M., Mesecar, A.D., and Baker, S.C. (2014a). MERS-CoV papain-like protease has deISGylating and deubiquitinating activities. Virology *450–451*, 64–70.

Mielech, A.M., Chen, Y., Mesecar, A.D., and Baker, S.C. (2014b). Nidovirus papain-like proteases: Multifunctional enzymes with protease, deubiquitinating and deISGylating activities. Virus Res.

Mogensen, T.H., and Paludan, S.R. (2001). Molecular Pathways in Virus-Induced Cytokine Production. Microbiol. Mol. Biol. Rev. *65*, 131–150.

Mou, H., Raj, V.S., van Kuppeveld, F.J.M., Rottier, P.J.M., Haagmans, B.L., and Bosch, B.J. (2013). The Receptor Binding Domain of the New Middle East Respiratory Syndrome Coronavirus Maps to a 231-Residue Region in the Spike Protein That Efficiently Elicits Neutralizing Antibodies. J. Virol. *87*, 9379–9383.

Müller, M.A., Corman, V.M., Jores, J., Meyer, B., Younan, M., Liljander, A., Bosch, B.-J., Lattwein, E., Hilali, M., Musa, B.E., et al. (2014). MERS coronavirus neutralizing antibodies in camels, Eastern Africa, 1983-1997. Emerg. Infect. Dis. *20*, 2093–2095.

Munster, V.J., De Wit, E., and Feldmann, H. (2013). Pneumonia from human coronavirus in a macaque model. N. Engl. J. Med.

Munster, V.J., Adney, D.R., Van Doremalen, N., Brown, V.R., Miazgowicz, K.L., Milne-Price, S., Bushmaker, T., Rosenke, R., Scott, D., Hawkinson, A., et al. (2016). Replication and shedding of MERS-CoV in Jamaican fruit bats (Artibeus jamaicensis). Sci. Rep. *6*.

Naeem, A., Hamed, M.E., Alghoribi, M.F., Aljabr, W., Alsaran, H., Enani, M.A., and Alosaimi, B. (2020). Molecular evolution and structural mapping of N-terminal domain in spike gene of middle east respiratory syndrome coronavirus (MERS-CoV). Viruses *12*.

Nal, B., Chan, C., Kien, F., Siu, L., Tse, J., Chu, K., Kam, J., Staropoli, sabelle, Crescenzo-Chaigne, B., Escriou, N., et al. (2005). Differential maturation and subcellular localization of severe acute respiratory syndrome coronavirus surface proteins S, M and E. J. Gen. Virol.

Napetschnig, J., and Wu, H. (2013). Molecular Basis of NF-κB Signaling. Annu. Rev. Biophys.

De Nardo, D. (2015). Toll-like receptors: Activation, signalling and transcriptional modulation. Cytokine.

National Events et al., 2020 National Events et al., 2020.

Ng, D.L., Al Hosani, F., Keating, M.K., Gerber, S.I., Jones, T.L., Metcalfe, M.G., Tong, S., Tao, Y., Alami, N.N., Haynes, L.M., et al. (2016). Clinicopathologic,

immunohistochemical, and ultrastructural findings of a fatal case of middle east respiratory syndrome coronavirus infection in the United Arab Emirates, April 2014. Am. J. Pathol. *186*, 652–658.

Nicholls, J.M., Poon, L.L.M., Lee, K.C., Ng, W.F., Lai, S.T., Leung, C.Y., Chu, C.M., Hui, P.K., Mak, K.L., Lim, W., et al. (2003). Lung pathology of fatal severe acute respiratory syndrome. Lancet *361*, 1773–1778.

Nicholson, L.B. (2016). The immune system. Essays Biochem.

Niemeyer, D., Zillinger, T., Muth, D., Zielecki, F., Horvath, G., Suliman, T., Barchet, W., Weber, F., Drosten, C., and Muller, M.A. (2013). Middle East Respiratory Syndrome Coronavirus Accessory Protein 4a Is a Type I Interferon Antagonist. J. Virol. *87*, 12489–12495.

Oh, M.D., Park, W.B., Park, S.W., Choe, P.G., Bang, J.H., Song, K.H., Kim, E.S., Kim, H. Bin, and Kim, N.J. (2018). Middle east respiratory syndrome: What we learned from the 2015 outbreak in the republic of Korea. Korean J. Intern. Med.

Omrani, A.S., Matin, M.A., Haddad, Q., Al-Nakhli, D., Memish, Z.A., and Albarrak, A.M. (2013). A family cluster of middle east respiratory syndrome coronavirus infections related to a likely unrecognized asymptomatic or mild case. Int. J. Infect. Dis.

Ouyang, W., Rutz, S., Crellin, N.K., Valdez, P.A., and Hymowitz, S.G. (2011). Regulation and Functions of the IL-10 Family of Cytokines in Inflammation and Disease. Annu. Rev. Immunol.

Pascal, K.E., Coleman, C.M., Mujica, A.O., Kamat, V., Badithe, A., Fairhurst, J., Hunt, C., Strein, J., Berrebi, A., Sisk, J.M., et al. (2015). Pre- and postexposure efficacy of fully human antibodies against Spike protein in a novel humanized mouse model of MERS-CoV infection. Proc. Natl. Acad. Sci. *112*, 8738–8743.

Peiris, J.S.M., Chu, C.M., Cheng, V.C.C., Chan, K.S., Hung, I.F.N., Poon, L.L.M., Law, K.I., Tang, B.S.F., Hon, T.Y.W., Chan, C.S., et al. (2003). Clinical progression and viral load in a community outbreak of coronavirus-associated SARS pneumonia: A prospective study. Lancet.

Perlman, S., and Netland, J. (2009). Coronaviruses post-SARS: Update on replication and pathogenesis. Nat. Rev. Microbiol.

Petrosillo, N., Viceconte, G., Ergonul, O., Ippolito, G., and Petersen, E. (2020). COVID-19, SARS and MERS: are they closely related? Clin. Microbiol. Infect. *26*, 729–734.

PY, C., P, C., AE, L., TJ, F., DY, T., YS, L., GJ, K., G, W., KP, C., LL, E.O., et al. (2004). Analysis of deaths during the severe acute respiratory syndrome (SARS) epidemic in Singapore: challenges in determining a SARS diagnosis. Arch. Pathol. Lab. Med. *128*.

Rabouw, H.H., Langereis, M.A., Knaap, R.C.M., Dalebout, T.J., Canton, J., Sola, I., Enjuanes, L., Bredenbeek, P.J., Kikkert, M., de Groot, R.J., et al. (2016). Middle East Respiratory Coronavirus Accessory Protein 4a Inhibits PKR-Mediated Antiviral Stress Responses. PLoS Pathog. *12*.

Raj, V.S., Dijkman, R., Muth, D., Mou, H., Smits, S.L., Dekkers, D.H.W., Mu, M.A., Demmers, J.A.A., Zaki, A., Fouchier, R.A.M., et al. (2013). Dipeptidyl peptidase 4 is a functional receptor for the emerging human coronavirus-EMC. Nature *495*, 251–255.

Raj, V.S., Osterhaus, A.D.M.E., Fouchier, R.A.M., and Haagmans, B.L. (2014a). MERS: Emergence of a novel human coronavirus. Curr. Opin. Virol.

Raj, V.S., Smits, S.L., Provacia, L.B., van den Brand, J.M.A., Wiersma, L., Ouwendijk, W.J.D., Bestebroer, T.M., Spronken, M.I., van Amerongen, G., Rottier, P.J.M., et al. (2014b). Adenosine Deaminase Acts as a Natural Antagonist for Dipeptidyl Peptidase 4-Mediated Entry of the Middle East Respiratory Syndrome Coronavirus. J. Virol. *88*, 1834–1838.

Randall, R.E., and Goodbourn, S. (2008). Interferons and viruses: An interplay between induction, signalling, antiviral responses and virus countermeasures. J. Gen. Virol.

Rawling, D.C., and Pyle, A.M. (2014). Parts, assembly and operation of the RIG-I family of motors. Curr. Opin. Struct. Biol.

Reusken, C.B., Ababneh, M., Raj, V.S., Meyer, B., Eljarah, A., Abutarbush, S., Godeke, G.J., Bestebroer, T.M., Zutt, I., Müller, M.A., et al. (2013a). Middle east respiratory syndrome coronavirus (MERS-CoV) serology in major livestock species in an affected region in Jordan, june to September 2013. Eurosurveillance.

Reusken, C.B., Farag, E.A., Jonges, M., Godeke, G.J., El-Sayed, A.M., Pas, S.D., Raj, V.S., Mohran, K.A., Moussa, H.A., Ghobashy, H., et al. (2014). Middle east respiratory syndrome coronavirus (MERS-CoV) RNA and neutralising antibodies in milk collected according to local customs from dromedary camels, Qatar, April 2014. Eurosurveillance *19*.

Reusken, C.B.E.M., Haagmans, B.L., Müller, M.A., Gutierrez, C., Godeke, G.J., Meyer, B., Muth, D., Raj, V.S., Vries, L.S. De, Corman, V.M., et al. (2013b). Middle East respiratory syndrome coronavirus neutralising serum antibodies in dromedary camels: A comparative serological study. Lancet Infect. Dis. *13*, 859–866.

Reusken, C.B.E.M., Haagmans, B.L., Müller, M.A., Gutierrez, C., Godeke, G.J., Meyer, B., Muth, D., Raj, V.S., Vries, L.S. De, Corman, V.M., et al. (2013c). Middle East respiratory syndrome coronavirus neutralising serum antibodies in dromedary camels: A comparative serological study. Lancet Infect. Dis.

Reusken, C.B.E.M., Schilp, C., Raj, V.S., De Bruin, E., Kohl, R.H.G., Farag, E.A.B.A., Haagmans, B.L., Al-Romaihi, H., Le Grange, F., Bosch, B.-J., et al. (2016). MERS-CoV Infection of Alpaca in a Region Where MERS-CoV is Endemic. Emerg. Infect. Dis. *22*, 1129–1131.

Rodon, J., Okba, N.M.A., Te, N., van Dieren, B., Bosch, B.J., Bensaid, A., Segalés, J., Haagmans, B.L., and Vergara-Alert, J. (2019). Blocking transmission of Middle East respiratory syndrome coronavirus (MERS-CoV) in llamas by vaccination with a recombinant spike protein. Emerg. Microbes Infect. *8*, 1593–1603.

Scheuplein, V.A., Seifried, J., Malczyk, A.H., Miller, L., Höcker, L., Vergara-Alert, J., Dolnik, O., Zielecki, F., Becker, B., Spreitzer, I., et al. (2015). High Secretion of Interferons by Human Plasmacytoid Dendritic Cells upon Recognition of Middle East Respiratory Syndrome Coronavirus. J. Virol. *89*, 3859–3869.

Schoggins, J.W., Wilson, S.J., Panis, M., Murphy, M.Y., Jones, C.T., Bieniasz, P., and Rice, C.M. (2011). A diverse range of gene products are effectors of the type i interferon antiviral response. Nature.

Shah, A. (2020). Novel Coronavirus-Induced NLRP3 Inflammasome Activation: A Potential Drug Target in the Treatment of COVID-19. Front. Immunol. *11*.

Shao, B.Z., Xu, Z.Q., Han, B.Z., Su, D.F., and Liu, C. (2015). NLRP3 inflammasome and its inhibitors: A review. Front. Pharmacol.

Sheppard, P., Kindsvogel, W., Xu, W., Henderson, K., Schlutsmeyer, S., Whitmore, T.E., Kuestner, R., Garrigues, U., Birks, C., Roraback, J., et al. (2003). IL-28, IL-29 and their class II cytokine receptor IL-28R. Nat. Immunol.

Shi, Z.L. (2013). Emerging infectious diseases associated with bat viruses. Sci. China Life Sci.

Shi, C.S., Nabar, N.R., Huang, N.N., and Kehrl, J.H. (2019). SARS-Coronavirus Open Reading Frame-8b triggers intracellular stress pathways and activates NLRP3 inflammasomes. Cell Death Discov. *5*, 101.

Shokri, S., Mahmoudvand, S., Taherkhani, R., and Farshadpour, F. (2019). Modulation of the immune response by Middle East respiratory syndrome coronavirus. J. Cell. Physiol. *234*, 2143–2151.

Siu, K.-L., Yeung, M.L., Kok, K.-H., Yuen, K.-S., Kew, C., Lui, P.-Y., Chan, C.-P., Tse, H., Woo, P.C.Y., Yuen, K.-Y., et al. (2014). Middle East Respiratory Syndrome Coronavirus 4a Protein Is a Double-Stranded RNA-Binding Protein That Suppresses PACT-Induced Activation of RIG-I and MDA5 in the Innate Antiviral Response. J. Virol. *88*, 4866–4876.

Smith, I., and Wang, L.F. (2013). Bats and their virome: An important source of emerging viruses capable of infecting humans. Curr. Opin. Virol.

Smits, S.L., De Lang, A., Van Den Brand, J.M.A., Leijten, L.M., Van Ijcken, W.F., Eijkemans, M.J.C., Van Amerongen, G., Kuiken, T., Andeweg, A.C., Osterhaus, A.D.M.E., et al. (2010). Exacerbated innate host response to SARS-CoV in aged non-human primates. PLoS Pathog. *6*.

Snijder, E.J., van der Meer, Y., Zevenhoven-Dobbe, J., Onderwater, J.J.M., van der Meulen, J., Koerten, H.K., and Mommaas, A.M. (2006). Ultrastructure and Origin of Membrane Vesicles Associated with the Severe Acute Respiratory Syndrome Coronavirus Replication Complex. J. Virol.

Stalin Raj, V., Farag, E.A.B.A., Reusken, C.B.E.M., Lamers, M.M., Pas, S.D., Voermans, J., Smits, S.L., Osterhaus, A.D.M.E., Al-Mawlawi, N., Al-Romaihi, H.E., et al. (2014). Isolation of MERS coronavirus from dromedary camel, Qatar, 2014. Emerg. Infect. Dis.

Stark, G.R., Kerr, I.M., Williams, B.R.G., Silverman, R.H., and Schreiber, R.D. (1998). HOW CELLS RESPOND. Annu. Rev. Biochem.

Sun, S.H., Chen, Q., Gu, H.J., Yang, G., Wang, Y.X., Huang, X.Y., Liu, S.S., Zhang, N.N., Li, X.F., Xiong, R., et al. (2020). A Mouse Model of SARS-CoV-2 Infection and Pathogenesis. Cell Host Microbe *28*, 124-133.e4.

Takeuchi, O., and Akira, S. (2009). Innate immunity to virus infection. Immunol. Rev.

Tamin, A., Queen, K., Paden, C.R., Lu, X., Andres, E., Sakthivel, S.K., Li, Y., Tao, Y., Zhang, J., Kamili, S., et al. (2019). Isolation and growth characterization of novel full length and deletion mutant human MERS-CoV strains from clinical specimens collected during 2015. J. Gen. Virol. *100*, 1523–1529.

Te, N., Vergara-Alert, J., Lehmbecker, A., Pérez, M., Haagmans, B.L., Baumgärtner, W., Bensaid, A., and Segalés, J. (2019). Co-localization of Middle East respiratory

syndrome coronavirus (MERS-CoV) and dipeptidyl peptidase-4 in the respiratory tract and lymphoid tissues of pigs and llamas. Transbound. Emerg. Dis. *66*, 831–841.

Thornbrough, J.M., Jha, B.K., Yount, B., Goldstein, S.A., Li, Y., Elliott, R., Sims, A.C., Baric, R.S., Silverman, R.H., and Weissa, S.R. (2016). Middle east respiratory syndrome coronavirus NS4b protein inhibits host RNase L activation. MBio *7*.

Tsiodras, S., Baka, A., Mentis, A., Iliopoulos, D., Dedoukou, X., Papamavrou, G., Karadima, S., Emmanouil, M., Kossyvakis, A., Spanakis, N., et al. (2014). A case of imported Middle East Respiratory Syndrome coronavirus infection and public health response, Greece, April 2014. Eurosurveillance.

Tsushima, K., King, L.S., Aggarwal, N.R., De Gorordo, A., D'Alessio, F.R., and Kubo, K. (2009). Acute lung injury review. Intern. Med.

Verbist, K.C., and Klonowski, K.D. (2012). Functions of IL-15 in anti-viral immunity: Multiplicity and variety. Cytokine.

Vergara-Alert, J., van den Brand, J.M.A., Widagdo, W., Muñoz, M., Raj, V.S., Schipper, D., Solanes, D., Cordón, I., Bensaid, A., Haagmans, B.L., et al. (2017a). Livestock susceptibility to infection with middle east respiratory syndrome coronavirus. Emerg. Infect. Dis. *23*, 232–240.

Vergara-Alert, J., Raj, V.S., Muñoz, M., Abad, F.X., Cordón, I., Haagmans, B.L., Bensaid, A., and Segalés, J. (2017b). Middle East respiratory syndrome coronavirus experimental transmission using a pig model. Transbound. Emerg. Dis. *64*, 1342–1345.

Wang, N., Shi, X., Jiang, L., Zhang, S., Wang, D., Tong, P., Guo, D., Fu, L., Cui, Y., Liu, X., et al. (2013). Structure of MERS-CoV spike receptor-binding domain complexed with human receptor DPP4. Cell Res. *23*, 986–993.

Wang, Q., Qi, J., Yuan, Y., Xuan, Y., Han, P., Wan, Y., Ji, W., Li, Y., Wu, Y., Wang, J., et al. (2014). Bat origins of MERS-CoV supported by bat Coronavirus HKU4 usage of human receptor CD26. Cell Host Microbe.

Wang, Y., Sun, J., Li, X., Zhu, A., Guan, W., Sun, D.-Q., Gan, M., Niu, X., Dai, J., Zhang, L., et al. (2020). Increased Pathogenicity and Virulence of Virus in Middle East Respiratory Syndrome Coronavirus Clade B in Vitro and in Vivo. J. Virol.

Ware, L.B., and Matthay, M.A. (2000). The acute respiratory distress syndrome. N. Engl. J. Med.

Weiss, M., Blazek, K., Byrne, A.J., Perocheau, D.P., and Udalova, I.A. (2013). IRF5 is a specific marker of inflammatory macrophages in vivo. Mediators Inflamm.

WHO (2015). WHO | Summary and risk assessment of current situation in Republic of Korea and China. WHO.

WHO (2020). WHO | Middle East respiratory syndrome coronavirus (MERS-CoV). WHO.

Widagdo, W., Raj, V.S., Schipper, D., Kolijn, K., van Leenders, G.J.L.H., Bosch, B.J., Bensaid, A., Segalés, J., Baumgärtner, W., Osterhaus, A.D.M.E., et al. (2016a). Differential Expression of the Middle East Respiratory Syndrome Coronavirus Receptor in the Upper Respiratory Tracts of Humans and Dromedary Camels. J. Virol. *90*, 4838–4842.

Widagdo, W., Raj, V.S., Schipper, D., Kolijn, K., van Leenders, G.J.L.H., Bosch, B.J., Bensaid, A., Segalés, J., Baumgärtner, W., Osterhaus, A.D.M.E., et al. (2016b).

Differential Expression of the Middle East Respiratory Syndrome Coronavirus Receptor in the Upper Respiratory Tracts of Humans and Dromedary Camels. J. Virol. *90*, 4838–4842.

Widagdo, W., Begeman, L., Schipper, D., Van Run, P.R., Cunningham, A.A., Kley, N., Reusken, C.B., Haagmans, B.L., and Van Den Brand, J.M.A. (2017). Tissue Distribution of the MERS-Coronavirus Receptor in Bats. Sci. Rep. *7*.

Widagdo, W., Okba, N.M.A., Richard, M., de Meulder, D., Bestebroer, T.M., Lexmond, P., Farag, E.A.B.A., Al-Hajri, M., Stittelaar, K.J., de Waal, L., et al. (2019). Lack of Middle East Respiratory Syndrome Coronavirus Transmission in Rabbits. Viruses *11*.

de Wit, E., Prescott, J., Baseler, L., Bushmaker, T., Thomas, T., Lackemeyer, M.G., Martellaro, C., Milne-Price, S., Haddock, E., Haagmans, B.L., et al. (2013). The Middle East Respiratory Syndrome Coronavirus (MERS-CoV) Does Not Replicate in Syrian Hamsters. PLoS One.

de Wit, E., Feldmann, F., Cronin, J., Jordan, R., Okumura, A., Thomas, T., Scott, D., Cihlar, T., and Feldmann, H. (2020). Prophylactic and therapeutic remdesivir (GS-5734) treatment in the rhesus macaque model of MERS-CoV infection. Proc. Natl. Acad. Sci. U. S. A. 1–6.

De Wit, E., Rasmussen, A.L., Falzarano, D., Bushmaker, T., Feldmann, F., Brining, D.L., Fischer, E.R., Martellaro, C., Okumura, A., Chang, J., et al. (2013). Middle East respiratory syndrome coronavirus (MERSCoV) causes transient lower respiratory tract infection in rhesus macaques. Proc. Natl. Acad. Sci. U. S. A. *110*, 16598–16603.

De Wit, E., Van Doremalen, N., Falzarano, D., and Munster, V.J. (2016). SARS and MERS: Recent insights into emerging coronaviruses. Nat. Rev. Microbiol. *14*, 523–534.

De Wit, E., Feldmann, F., Horne, E., Martellaro, C., Haddock, E., Bushmaker, T., Rosenke, K., Okumura, A., Rosenke, R., Saturday, G., et al. (2017). Domestic pig unlikely reservoir for MERS-COV. Emerg. Infect. Dis. *23*, 985–988.

Wu, A., Peng, Y., Huang, B., Ding, X., Wang, X., Niu, P., Meng, J., Zhu, Z., Zhang, Z., Wang, J., et al. (2020). Genome Composition and Divergence of the Novel Coronavirus (2019-nCoV) Originating in China. Cell Host Microbe.

Wu, H., Guang, X., Al-Fageeh, M.B., Cao, J., Pan, S., Zhou, H., Zhang, L., Abutarboush, M.H., Xing, Y., Xie, Z., et al. (2014). Camelid genomes reveal evolution and adaptation to desert environments. Nat. Commun.

Yang, X., Chen, X., Bian, G., Tu, J., Xing, Y., Wang, Y., and Chen, Z. (2014). Proteolytic processing, deubiquitinase and interferon antagonist activities of Middle East respiratory syndrome coronavirus papain-like protease. J. Gen. Virol.

Yang, X., Yu, Y., Xu, J., Shu, H., Xia, J., Liu, H., Wu, Y., Zhang, L., Yu, Z., Fang, M., et al. (2020). Clinical course and outcomes of critically ill patients with SARS-CoV-2 pneumonia in Wuhan, China: a single-centered, retrospective, observational study. Lancet Respir. Med. *8*, 475–481.

Yang, Y., Zhang, L., Geng, H., Deng, Y., Huang, B., Guo, Y., Zhao, Z., and Tan, W. (2013). The structural and accessory proteins M, ORF 4a, ORF 4b, and ORF 5 of Middle East respiratory syndrome coronavirus (MERS-CoV) are potent interferon antagonists. Protein Cell *4*, 951–961.

Yang, Y., Ye, F., Zhu, N., Wang, W., Deng, Y., Zhao, Z., and Tan, W. (2015). Middle East respiratory syndrome coronavirus ORF4b protein inhibits type i interferon production through both cytoplasmic and nuclear targets. Sci. Rep. *5*.

Yao, Y., Bao, L., Deng, W., Xu, L., Li, F., Lv, Q., Yu, P., Chen, T., Xu, Y., Zhu, H., et al. (2014). An animal model of mers produced by infection of rhesus macaques with MERS coronavirus. J. Infect. Dis.

Yoneyama, M., Kikuchi, M., Natsukawa, T., Shinobu, N., Imaizumi, T., Miyagishi, M., Taira, K., Akira, S., and Fujita, T. (2004). The RNA helicase RIG-I has an essential function in double-stranded RNA-induced innate antiviral responses. Nat. Immunol.

Yu, P., Xu, Y., Deng, W., Bao, L., Huang, L., Xu, Y., Yao, Y., and Qin, C. (2017). Comparative pathology of rhesus macaque and common marmoset animal models with Middle East respiratory syndrome coronavirus. PLoS One *12*.

Yusof, M.F., Queen, K., Eltahir, Y.M., Paden, C.R., Al Hammadi, Z.M.A.H., Tao, Y., Li, Y., Khalafalla, A.I., Shi, M., Zhang, J., et al. (2017). Diversity of Middle East respiratory syndrome coronaviruses in 109 dromedary camels based on full-genome sequencing, Abu Dhabi, United Arab Emirates. Emerg. Microbes Infect. *6*, e101.

Zaki, A.M., van Boheemen, S., Bestebroer, T.M., Osterhaus, A.D.M.E., and Fouchier, R.A.M. (2012a). Isolation of a Novel Coronavirus from a Man with Pneumonia in Saudi Arabia. N. Engl. J. Med. *367*, 1814–1820.

Zaki, A.M., van Boheemen, S., Bestebroer, T.M., Osterhaus, A.D.M.E., and Fouchier, R.A.M. (2012b). Isolation of a Novel Coronavirus from a Man with Pneumonia in Saudi Arabia. N. Engl. J. Med. *367*, 1814–1820.

Zanoni, I., Granucci, F., and Broggi, A. (2017). Interferon (IFN)-λ takes the helm: Immunomodulatory roles of type III IFNs. Front. Immunol. *8*, 1–8.

Zhao, J., Li, K., Wohlford-Lenane, C., Agnihothram, S.S., Fett, C., Zhao, J., Gale, M.J., Baric, R.S., Enjuanes, L., Gallagher, T., et al. (2014). Rapid generation of a mouse model for Middle East respiratory syndrome. Proc. Natl. Acad. Sci. U. S. A. *111*, 4970–4975.

Zhao, J., Alshukairi, A.N., Baharoon, S.A., Ahmed, W.A., Bokhari, A.A., Nehdi, A.M., Layqah, L.A., Alghamdi, M.G., Al Gethamy, M.M., Dada, A.M., et al. (2017). Recovery from the Middle East respiratory syndrome is associated with antibody and T cell responses. Sci. Immunol. *2*.

Zhao, X., Chu, H., Wong, B.H.-Y., Chiu, M.C., Wang, D., Li, C., Liu, X., Yang, D., Poon, V.K.-M., Cai, J., et al. (2019). Activation of C-Type Lectin Receptor and (RIG)-I-Like Receptors Contributes to Proinflammatory Response in Middle East Respiratory Syndrome Coronavirus-Infected Macrophages. J. Infect. Dis. 1–39.

Zhao, X., Chu, H., Wong, B.H.Y., Chiu, M.C., Wang, D., Li, C., Liu, X., Yang, D., Poon, V.K.M., Cai, J., et al. (2020). Activation of C-Type Lectin Receptor and (RIG)-I-Like Receptors Contributes to Proinflammatory Response in Middle East Respiratory Syndrome Coronavirus-Infected Macrophages. J. Infect. Dis. *221*, 647–659.

Zhou, F., Yu, T., Du, R., Fan, G., Liu, Y., Liu, Z., Xiang, J., Wang, Y., Song, B., Gu, X., et al. (2020). Clinical course and risk factors for mortality of adult inpatients with COVID-19 in Wuhan, China: a retrospective cohort study. Lancet *395*, 1054–1062.

Zhou, J., Chu, H., Li, C., Wong, B.H.Y., Cheng, Z.S., Poon, V.K.M., Sun, T., Lau, C.C.Y., Wong, K.K.Y., Chan, J.Y.W., et al. (2014). Active replication of middle east respiratory syndrome coronavirus and aberrant induction of inflammatory cytokines and chemokines in human macrophages: Implications for pathogenesis. J. Infect. Dis. *209*, 1331–1342.

Zhou, J., Chu, H., Chan, J.F.W., and Yuen, K.Y. (2015). Middle East respiratory syndrome coronavirus infection: Virus-host cell interactions and implications on pathogenesis. Virol. J. *12*.

Zhou 2, 3), J.(1, Chan 2, 3, 4), J.F.-W.(1, To 2, 3, 4), K.K.-W.(1, Zheng 2, 3, 4), B.-J.(1, Yuen 2, 3, 4, 5), K.-Y.(1, Chu, H.(2), Li, C.(2), Wong, B.H.-Y.(2), Cheng, Z.-S.(2), Poon, V.K.-M.(2), et al. (2014). Active Replication ofMiddle East Respiratory of Inflammatory Cytokines and Chemokines Syndrome Coronavirus and Aberrant Induction in Human Macrophages: Implications for Pathogenesis. J. Infect. Dis. *209*, 1331–1342.

Zielecki, F., Weber, M., Eickmann, M., Spiegelberg, L., Zaki, A.M., Matrosovich, M., Becker, S., and Weber, F. (2013). Human Cell Tropism and Innate Immune System Interactions of Human Respiratory Coronavirus EMC Compared to Those of Severe Acute Respiratory Syndrome Coronavirus. J. Virol. *87*, 5300–5304.

Zumla, A., Hui, D.S., and Perlman, S. (2015). Middle East respiratory syndrome. Lancet *386*, 995–1007.